4
Two-Link Flexible Manipulators

4.1 INTRODUCTION

In present chapter a noteworthy attempt to demonstrate the detailed mathematical modeling and subsequent modal characterization along with the determination of static deflection of a two-link flexible manipulator with a payload has been made. In addition, investigation of nonlinear phenomena of dynamic responses under external, parametric and internal resonance has also been accomplished. An appropriate and realistic dynamic modeling of the two-link manipulator that takes into accounts for the inertial coupling and geometry compatibility between equations of motion and boundary conditions incorporating both link and joint flexibilities subjected to a harmonic motions has been derived using the extended Hamilton's principle. The Cartesian actuator and revolute joint flexibilities have been modeled as a combination of linear spring-mass and torsional spring-inertia elements, respectively. The effect of parametric variation on system eigenfrequencies is well tabulated, and the corresponding eigenspectrums are illustrated graphically for different models of the two-link flexible manipulator. Also, from the literature review, it is evident that the studies demonstrating the influence of system parameters on the eigenspectrums, especially mode-shapes of the two-manipulator is trivial. Hence, here the eigenfrequency equation and mode-shapes has been derived for different types of manipulator driven by different types of joints and also incorporating the generic payload condition. The system has been analyzed for the vibration attributes of steady-state responses and their stability under various resonance conditions. The effect of geometric and inertial coupling existing between the flexible arms on bifurcation states and stability of the obtained solutions has been thoroughly investigated. The significant influence of generic payload parameters on the eigen-parameters and nonlinear dynamics are studied and compared with those of point payload. Analytically obtained results have been verified numerically and found to be in good agreement.

Further, the assumed mode method is explored to derive the coupled nonlinear second order equivalent temporal equations of motion of the links and the joints. The simulation of the resulting computationally efficient nonlinear model with smooth sinusoidal input torques at the joint actuators is investigated and graphically presented. In addition, the control problem for the trajectory tracking of a flexible two-link manipulator incorporating a payload described by a nonlinear model is addressed in the present work. The comparative mode shapes, bifurcation diagrams and control characteristics those describe the vibrating system have been illustrated to demonstrate the dynamics of the flexible manipulator. The outcome of the present work enables new understanding into the design criterion and performance limitation of multilink flexible robots. The present theoretical results deliver a useful insight into the attributes of vibration characteristics along with the nonlinear dynamic behavior and operational stability of two-link flexible manipulator under joint motion.

4.2 MATHEMATICAL MODELING

A schematic diagram of a flexible two-link manipulator incorporating payload has been shown in Fig. 4.1. A brief procedure to model the manipulator is presented considering stretching effect and gravitational forces acting on the beam and masses in addition to bending deformation of the system. Here, the first link is fixed at one end and attached to the motor on other end while the second link is attached to the first motor from one end with a payload mass at the end of the second link. The motor and the payload mass at the end of the link are considered as

concentrated mass. Let *(X,Y)* and *(x,y)* represent the global and local co-ordinate system with $(\hat{X},\hat{Y})$ and $(\hat{x},\hat{y})$ as the unit vectors, respectively. The links are modelled based on Euler-Bernoulli beam theory which ignores rotary inertia and shear deformation. The elastic deformation w(x,t) is assumed to be small compared to the length of the links.

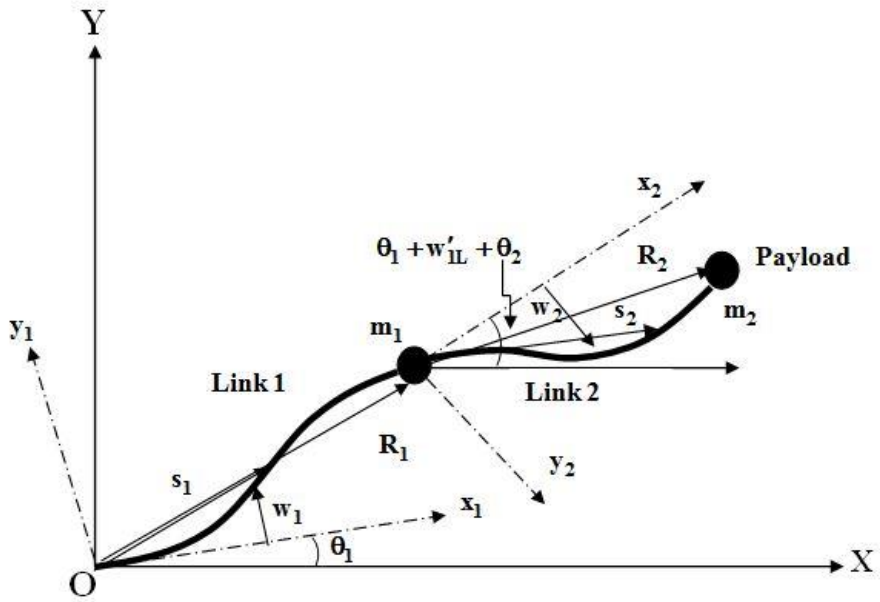

Fig. 4.1: Schematic diagram of deflected planar two-link flexible manipulator.

The relations between the unit vectors of inertial and moving co-ordinate system for the both the links are given as.

$$\begin{bmatrix}\hat{x}_1\\ \hat{y}_1\end{bmatrix}=\begin{bmatrix}\cos(\theta_1) & \sin(\theta_1)\\ -\sin(\theta_1) & \cos(\theta_1)\end{bmatrix}\begin{bmatrix}\hat{X}\\ \hat{Y}\end{bmatrix},\quad \begin{bmatrix}\hat{x}_2\\ \hat{y}_2\end{bmatrix}=\begin{bmatrix}\cos(\theta_1+w'_{1L}+\theta_2) & \sin(\theta_1+w'_{1L}+\theta_2)\\ -\sin(\theta_1+w'_{1L}+\theta_2) & \cos(\theta_1+w'_{1L}+\theta_2)\end{bmatrix}\begin{bmatrix}\hat{X}\\ \hat{Y}\end{bmatrix}.$$

The end point (*R*) and the general point (*s*) on the flexible links are given, respectively as:

$$R_1=L_1\hat{x}_1+w_{1L}\hat{y}_1,\ R_2=R_1+L_2\hat{x}_2+w_{2L}\hat{y}_2. \tag{4.1}$$

$$s_1=(x)\hat{x}_1+(y+w_1)\hat{y}_1,\ s_2=R_1+(x)\hat{x}_2+(y+w_2)\hat{y}_2. \tag{4.2}$$

Here, *(x,y)* denotes the undeformed position of an arbitrary point on the link. The total kinetic energy (T_{total}) of the system composed of the translational energy of mass of links, joint and payload is given by:

$$T_{total}=(1/2)\sum_{i=1}^{2}\left(m_i\dot{R}_i^T\dot{R}_i+\int_0^{L_i}\rho_i\dot{s}_i^T\dot{s}_i dx\right). \tag{4.3}$$

Total potential energy (U_{total}) of the system is given by:

$$U_{total}=U_1+U_2+U_3+U_4. \tag{4.4}$$

$$U_1=(1/2)\sum_{i=1}^{2}\int_0^{L_i}E_iI_i\left(w_i''\right)^2dx, U_2=(1/2)\sum_{i=1}^{2}\int_0^{L_i}E_iA_i\left((1/2)w_i'^2\right)^2dx,$$

$$U_3=\sum_{i=1}^{2}\int_0^{L_i}\rho_i g\left(w_{(i-1)L}+x\cos\left(\sum_{j=1}^{i}\left(\theta_j+w'_{(j-1)L}\right)\right)+(y+w_i)\sin\left(\sum_{j=1}^{i}\left(\theta_j+w'_{(j-1)L}\right)\right)\right)dx,$$

$$U_4=\sum_{i=1}^{2}m_i g\left(w_{(i-1)L}+L_i\cos\left(\sum_{j=1}^{i}\left(\theta_j+w'_{(j-1)L}\right)\right)+w_{iL}\sin\left(\sum_{j=1}^{i}\left(\theta_j+w'_{(j-1)L}\right)\right)\right)$$

Here, U_1, U_2, U_3 and U_4 represent the elastic strain energy, energy due to axial stretching, potential energy of the link and potential energy of masses at the end of the link, respectively.

4.3 FLEXIBLE MANIPULATOR WITH POINT PAYLOAD

The equations of motion and associated boundary conditions for the two-link flexible manipulator are modelled in this section from Eqs. (4.1)-(4.4) by exploiting Hamilton's principle.
Governing equation of first link in transverse direction:

$$\{w_1\}:\ \rho_1 A_1\left(\ddot{w}_1 + x\ddot{\theta}_1 - w_1\dot{\theta}_1^{\,2} + g\right) + E_1 I_1 w_1'''' - E_1 A_1\left((3/2)w_1'^{\,2}w_1''\right) = 0. \tag{4.5}$$

The associated boundary conditions of the first link:

$$\{E_1 I_1 w_1\}_{(0,t)} = 0,\ \{E_1 I_1 w_1'\}_{(0,t)} = 0,$$

$$\int_0^{L_2}\rho_2 A_2\begin{pmatrix} x\ddot{w}_2 + x^2\ddot{w}_{1L}' + x^2\ddot{\theta}_1 + x^2\ddot{\theta}_2 + g\left(x\sin(\theta_2 + w_{1L}') + w_2\cos(\theta_2 + w_{1L}')\right) \\ +2w_2\dot{w}_2\dot{\theta}_1 + 2w_2\dot{w}_2\dot{\theta}_2 + 2w_2\dot{w}_2\dot{w}_{1L}' - w_2^{\,2}\ddot{\theta}_1 + w_2^{\,2}\ddot{\theta}_2 + w_2^{\,2}\ddot{w}_{1L}' \end{pmatrix} dx + E_1 I_1 w_{1L}''$$

$$+m_2\left(L_2\ddot{w}_{2L} + L_2^{\,2}\ddot{w}_{1L}' + L_2^{\,2}\ddot{\theta}_2 + L_2^{\,2}\ddot{\theta}_1 - 2w_{2L}\dot{w}_{2L} + g\left(L_2\sin(\theta_2 + w_{1L}') - w_{2L}\cos(\theta_2 + w_{1L}')\right)\right) = 0$$

$$(m_1 + m_2)\left(\ddot{w}_{1L} + L_1\ddot{\theta}_1 + g - w_{1L}\dot{\theta}_1^{\,2}\right) + \int_0^{L_2}\rho_2 A_2\left(\ddot{w}_{1L} + L_1\ddot{\theta}_1 + g - w_{1L}\dot{\theta}_1^{\,2}\right)dx - E_1 I_1 w_{1L}''' + \tag{4.6}$$

$$E_2 I_2 w_2'''(0,t) + E_1 A_1\left((1/2)w_{1L}'^{\,3}\right) = 0.$$

Governing equation of second link in transverse direction:

$$\{w_2\}:\ \begin{aligned} &\rho_2 A_2(\ddot{w}_2 + x\ddot{w}_{1L}' + x\ddot{\theta}_1 + x\ddot{\theta}_2 + g\sin(\theta_2 + w_{1L}') - w_2\dot{\theta}_1^{\,2} - w_2\dot{\theta}_2^{\,2} - w_2\dot{w}_{1L}'^{\,2} - \\ &2\dot{\theta}_1\dot{\theta}_2 v_2 - 2\dot{\theta}_2 w_2\dot{w}_{2L}' + 2\dot{\theta}_1 w_2\dot{w}_{2L}') + E_2 I_2 w_2'''' - E_2 A_2\left((3/2)w_2'^{\,2}w_2''\right) = 0. \end{aligned} \tag{4.7}$$

The associated boundary conditions of the second link:

$$\{E_2 I_2 w_2\}_{(0,t)} = 0,\ \{E_2 I_2 w_2'\}_{(0,t)} = 0,\ \{E_2 I_2 w_2''\}_{(L_2,t)} = 0,$$

$$\begin{aligned} &m_2(\ddot{w}_{2L} + L_2\ddot{w}_{1L}' + L_2\ddot{\theta}_1 + L_2\ddot{\theta}_2 - 2w_{2L}\dot{\theta}_2\dot{w}_{1L}' - w_{2L}\dot{w}_{1L}'^{\,2} - w_{2L}\dot{\theta}_1^{\,2} - w_{2L}\dot{\theta}_2^{\,2} - 2w_{2L}\dot{\theta}_1\dot{\theta}_2 \\ &-g\sin(\theta_2 + w_{1L}') - 2w_{2L}\dot{\theta}_1\dot{w}_{1L}') - E_2 I_2 w_{2L}''' + E_2 A_2\left((1/2)w_{2L}'^{\,3}\right) = 0. \end{aligned} \tag{4.8}$$

After neglecting the gravitational terms, the governing equation of motion and the boundary condtions obtained in Eqs. (4.5-4.8) are similar to those obtained by [Fung and Chang, 1998] for un-constrained manipulator with no revolute joints.

4.3.1 Free vibration analysis

Variable separation method has been used to discretize the deflection functions which are the explicit function of space and time and expressed as $w_1(x,t) = W_1^n(x)\cos(\omega_m t)$ and $w_2(x,t) = W_2^n(x)\cos(\omega_m t)$. Here, $W_1^n(x)$, $W_2^n(x)$ are the corresponding nth mode of eigenfunction for the first and second link, respectively and $\cos\left(\omega_m^n t\right)$ is the time modulation for a unknown nth mode of eigenfrequency $\left(\omega_m^n\right)$ of the whole system. Substituting these expressions in the linearized Eqs. (4.5) & (4.7), the solution of the equations of motion gives the eigenfunction for both the links in the following form:

$$W_1^n(x) = B_1^n\sin\left(\delta^n x\right) + B_2^n\cos\left(\delta^n x\right) + B_3^n\sinh\left(\delta^n x\right) + B_4^n\cosh\left(\delta^n x\right). \tag{4.9}$$

$$W_2^n(x) = C^n{}_1\sin\left(\mu\delta^n x\right) + C^n{}_2\cos\left(\mu\delta^n x\right) + C^n{}_3\sinh\left(\mu\delta^n x\right) + C^n{}_4\cosh\left(\mu\delta^n x\right) - W_1^{n\prime}(L_1)x. \tag{4.10}$$

Here, unknown $\left(B^n{}_1\cdots B^n{}_4, C^n{}_1\cdots C^n{}_4,\right)$ are the integration constants for n^{th} mode of vibration and can be obtained by substituting Eq. (4.9) and Eq. (4.10) into the boundary conditions that

result a set of five algebraic equations in five unknown in terms of characteristics exponent (δ) and following nondimensional parameters.

$\delta^4 = \rho_1 A_1 \omega_m^2 / E_1 I_1$, $\chi = E_2 I_2 / E_1 I_1$, $\alpha_M = \rho_2 A_2 / \rho_1 A_1$, $\mu^4 = \alpha_M / \chi$, $\bar{\delta} = \delta L_1$, $\alpha_L = L_2 / L_1$, $\alpha_{m_1} = m_1 / \rho_1 A_1 L_1$, $\alpha_{m2} = m_2 / \rho_1 A_1 L_1$, and $\lambda = \mu \alpha_L$. (4.11)

$$\left[K\left(\bar{\delta}^n\right)\right] \Rightarrow \begin{bmatrix} 0 & 0 & K^n{}_{13} & K^n{}_{14} & K^n{}_{15} \\ 0 & 0 & K^n{}_{23} & K^n{}_{24} & K^n{}_{25} \\ K^n{}_{31} & K^n{}_{32} & K^n{}_{33} & 0 & K^n{}_{35} \\ K^n{}_{41} & K^n{}_{42} & K^n{}_{43} & 0 & K^n{}_{45} \\ K^n{}_{51} & K^n{}_{52} & K^n{}_{53} & K^n{}_{54} & K^n{}_{55} \end{bmatrix} \begin{bmatrix} B^n{}_1 \\ B^n{}_2 \\ C^n{}_1 \\ C^n{}_2 \\ C^n{}_3 \end{bmatrix} = \begin{bmatrix} 0 \\ 0 \\ 0 \\ 0 \\ 0 \end{bmatrix} \tag{4.12}$$

Here $B_1^n = -B_3^n$, $B_2^n = -B_4^n$, and $C_2^n = -C_4^n$.

The elements of the above matrix are expressed below:

$K_{13} = \alpha_{m2} \bar{\delta}^n \sin\left(\lambda \bar{\delta}^n\right) - \chi \mu^3 \cos\left(\lambda \bar{\delta}^n\right)$, $K_{15} = \alpha_{m2} \bar{\delta}^n \sinh\left(\lambda \bar{\delta}^n\right) + \chi \mu^3 \cosh\left(\lambda \bar{\delta}^n\right)$,

$K_{14} = \alpha_{m2} \bar{\delta}^n \left(\cos\left(\lambda \bar{\delta}^n\right) - \cosh\left(\lambda \bar{\delta}^n\right)\right) + \chi \mu^3 \left(\sin\left(\lambda \bar{\delta}^n\right) - \sinh\left(\lambda \bar{\delta}^n\right)\right)$, $K_{23} = \sin\left(\lambda \bar{\delta}^n\right)$,

$K_{24} = \cos\left(\lambda \bar{\delta}^n\right) + \cosh\left(\lambda \bar{\delta}^n\right)$, $K_{25} = -\sinh\left(\lambda \bar{\delta}^n\right)$,

$K_{31} = \left(\alpha_{m1} + \alpha_{m2} + \alpha_M \alpha_L\right) \bar{\delta}^n \left(\sin\left(\bar{\delta}^n\right) - \sinh\left(\bar{\delta}^n\right)\right) - \left(\cos\left(\bar{\delta}^n\right) + \cosh\left(\bar{\delta}^n\right)\right)$,

$K_{32} = \left(\alpha_{m1} + \alpha_{m2} + \alpha_M \alpha_L\right) \bar{\delta}^n \left(\cos\left(\bar{\delta}^n\right) - \cosh\left(\bar{\delta}^n\right)\right) + \left(\sin\left(\bar{\delta}^n\right) - \sinh\left(\bar{\delta}^n\right)\right)$, $K_{33} = \alpha_M / \mu$,

$K_{35} = -\alpha_M / \mu$, $K_{41} = -\cos\left(\bar{\delta}^n\right) + \cosh\left(\bar{\delta}^n\right)$, $K_{42} = \sin\left(\bar{\delta}^n\right) + \sinh\left(\bar{\delta}^n\right)$, $K_{43} = \mu$, $K_{45} = \mu$,

$K_{51} = \left(1 / \alpha_M \left(\bar{\delta}^n\right)^2\right)\left(\sin\left(\bar{\delta}^n\right) + \sinh\left(\bar{\delta}^n\right)\right)$, $K_{52} = \left(1 / \alpha_M \left(\bar{\delta}^n\right)^2\right)\left(\cos\left(\bar{\delta}^n\right) + \cosh\left(\bar{\delta}^n\right)\right)$,

$$K_{54} = \begin{bmatrix} \left(\left(\alpha_{m2} \alpha_L / \alpha_M\right) + \left(1 / \mu^2 \left(\bar{\delta}^n\right)^2\right)\right) \cos\left(\lambda \bar{\delta}^n\right) - \left(\left(\alpha_{m2} \alpha_L / \alpha_M\right) - \left(1 / \mu^2 \left(\bar{\delta}^n\right)^2\right)\right) \cosh\left(\lambda \bar{\delta}^n\right) \\ + \left(\alpha_L / \mu \bar{\delta}^n\right)\left(\sin\left(\lambda \bar{\delta}^n\right) - \sinh\left(\lambda \bar{\delta}^n\right)\right) - \left(2 / \mu^2 \left(\bar{\delta}^n\right)^2\right) \end{bmatrix},$$

$$K_{55} = \left(\left(\alpha_{m_2} \alpha_L / \alpha_M\right) - \left(1 / \mu^2 \left(\bar{\delta}^n\right)^2\right)\right) \sinh\left(\lambda \bar{\delta}^n\right) + \left(\alpha_L / \mu \bar{\delta}^n\right) \cosh\left(\lambda \bar{\delta}^n\right). \tag{4.13}$$

The eigenfrequency equation for the system is obtained for the existence of non-trivial solution for the Eq. (4.12), i.e., $det\left|K\left(\bar{\delta}^n\right)\right| = 0$; here $K\left(\bar{\delta}^n\right)$ denotes the coefficient matrix. The expressions for the constants $\left(B^n{}_2, C^n{}_1 \cdots C^n{}_3,\right)$ emerging in eigenfunctions in terms of B_1 which has assumed to have unit magnitude are obtained by some mathematical manipulations as explained in previous chapter.

4.3.2 Static analysis

For the static analysis, only the effects of steady loading conditions are considered which in this case includes the gravitational forces acting on links and masses of motors attached to them in addition to the bending load. Here, the two-link manipulator shown in Fig. 4.2 is initially considered in the vertical plane. The equation of motions and associated boundary conditions can be obtained from Eqs. (4.5)-(4.8) by eliminating the temporal terms. A similar result shall be obtained by applying minimum potential energy theorem where the temporal terms in potential energy functions are ignored.

$$\rho_1 A_1 g + E_1 I_1 w_1'''' = 0.$$

$$(4.14)\ w_1(0,t) = 0, w_1'(0,t) = 0, E_1 I_1 w_{1L}''' + E_2 I_2 w_2'''(0,t) + \int_0^{L_2} \rho_2 A_2 g dx - (m_1 + m_2) g = 0,$$

$$E_1 I_1 w_{1L}'' + m_2 g\left(L_2 \sin(\theta_2 + w_{1L}') - w_{2L}\cos(\theta_2 + w_{1L}')\right) + \int_0^{L_2} \rho_2 A_2 g \begin{pmatrix} x\sin(\theta_2 + w_{1L}') + \\ w_2 \cos(\theta_2 + w_{1L}') \end{pmatrix} dx = 0. \quad (4.15)$$

$$E_2 I_2 w_2'''' + \rho_2 A_2 \sin(\theta_2 + w_{1L}') = 0. \quad (4.16)$$

$$w_2(0,t) = 0, w_2'(0,t) = 0, E_2 I_2 w_{2L}''' - m_2 g \sin(\theta_2 + w_{1L}') = 0, E_2 I_2 w_2''(L_2, t) = 0. \quad (4.17)$$

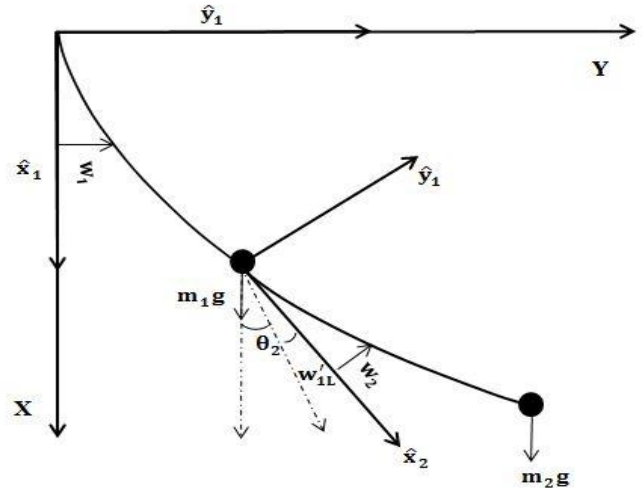

Fig. 4.2: Two-link flexible manipulator for static analysis.

However it is initially assumed that the links are being held in horizontal position before the deflection and using the boundary conditions Eq. (4.15) and Eq. (4.17), one may obtain the expressions for static condition of the first and second link as:

$$w_1(x) = (-\rho_1 A_1 g / 24 E_1 A_1) x^4 + (m_1 + 2m_2 + \rho_1 A_1 L_1 + 2\rho_2 A_2 L_2)(g / 6 E_1 I_1) x^3 -$$
$$\left((m_1 + 2m_2) L_1 + m_2 L_2 + \rho_1 A_1 L_1^2 + \rho_2 A_2 (L_1 - L_2 / 2)\right)(g / 2 E_1 I_1) x^2,$$
$$w_2(x) = (-\rho_2 A_2 g / 24 E_2 A_2) x^4 + (m_2 + \rho_2 A_2 L_2)(g / 6 E_2 I_2) x^3 - (m_2 + \rho_2 A_2 L_2 / 2)(L_2 g / 2 E_2 I_2) x^2. \quad (4.18)$$

4.3.3 Internal Resonance: 3:1

The nonlinear characteristics and stability of the two-link flexible manipulator has been studied for the case of 3:1 internal resonance. The geometric nonlinearities arising due to stretching effect and the inertial coupling in the equations of motion of both the links expressed as Eq. (4.5) and Eq. (4.7) are retained and also representative damping is included. The rotational motions of the motors and gravitational terms are neglected for the present study.
Nonlinear equations of motion for first and second link are expressed in as

$$\left(\rho_1 A_1 \ddot{w}_1 + E_1 I_1 w_1''''\right) - \frac{3E_1 A_1}{2}\left(w_1'^2 w_1''\right) + c_{d1}\dot{w}_1 = 0. \quad (4.19)$$

$$\left(\rho_2 A_2 \left(\ddot{w}_2 + x\ddot{w}_{1L}'\right) + E_2 I_2 w_2''''\right) - \frac{3E_2 A_2}{2}\left(w_2'^2 w_2''\right) + c_{d2}\dot{w}_2 = 0. \quad (4.20)$$

The nondimensional terms are: $\bar{w}_1 = w_1 / L_1$, $\bar{w}_2 = w_2 / L_2$, $\bar{x} = x / L_1$, $\tau = t\sqrt{E_1 I_1 / \rho_1 A_1 L_1^4}$, and $\bar{c}_{1,2} = c_{d1,2} L_1^2 / \sqrt{\rho_1 A_1 E_1 I_1}$. Using the nondimensional parameters, the Eqs. (4.19)-(4.20) after removing the bar for simplicity are expressed here as.

$$\ddot{w}_1 + w_1'''' - \left(3A_1 L_1^{\,2} / 2I_1\right)\left(w_1'^2 w_1''\right) + c_1 \dot{w}_1 = 0. \tag{4.21}$$

$$\left(\ddot{w}_2 + \left(\bar{x} / \alpha_L\right)\ddot{w}_1'\right) + \left(\chi / \alpha_M\right) w_2'''' - \left(3A_2 L_2^{\,2} / 2I_2\right)\left(\chi / \alpha_M\right)\left(w_1'^2 w_1'\right) + c_2 \dot{w}_2 = 0. \tag{4.22}$$

The governing equation of motion Eq. (4.21) & Eq. (4.22) are discretized by using Galerkin' principle by expressing the deflection functions as $w_1(\bar{x},\tau) = r\psi_1(\bar{x}) p_1(\tau)$, and $w_2(\bar{x},\tau) = r\psi_2(\bar{x}) p_2(\tau)$; here $\psi_1(\bar{x})$, and $\psi_2(\bar{x})$, are the eigenfunction of the first and second links, respectively given in Eqs. (4.9)-(4.10). Now ordering the terms in Eqs. (4.21)-(4.22) in terms of ε, and utilizing the orthogonal property of the mode shapes, the following nonlinear nondimensional ordinary differential equations are obtained:

$$\ddot{p}_1(\tau) + \Omega_1^{\,2} p_1(\tau) - \alpha_1 p_1^{\,3}(\tau) + 2\varepsilon^2 \xi_1 \dot{p} = 0. \tag{4.23}$$

$$\ddot{p}_2(\tau) + \alpha_2 \ddot{p}_1 + \Omega_2^{\,2} p_2(\tau) - \alpha_3 p_2^3(\tau) + 2\varepsilon^2 \xi_2 \dot{p}_2 = 0. \tag{4.24}$$

Here,

$$\Omega_1^{\,2} = \left(\int_0^1 \psi_1''''(\bar{x})\psi_1(\bar{x})\,d\bar{x} \Big/ \int_0^1 \psi_1^{\,2}(\bar{x})\,d\bar{x}\right),\ \Omega_2^{\,2} = \left(\chi / \alpha_M\right)\left(\int_0^1 \psi_2''''(\bar{x})\psi_2(\bar{x})\,d\bar{x} \Big/ \int_0^1 \psi_2^{\,2}(\bar{x})\,d\bar{x}\right),$$

$$\alpha_1 = \left(3r^2 A_1 L_1^{\,2} / I_1\right)\left(\int_0^1 \psi_1'^2(\bar{x})\psi_1''(\bar{x})\psi_1(\bar{x})\,d\bar{x} \Big/ \int_0^1 \psi_1^{\,2}(\bar{x})\,d\bar{x}\right),\ c_{d1} = 2\varepsilon^2 \xi_1,$$

$$\alpha_2 = \psi_1'(1)\left(\int_0^1 \bar{x}\psi_2(\bar{x})\,d\bar{x} \Big/ \int_0^1 \psi_2^{\,2}(\bar{x})\,d\bar{x}\right),$$

$$\alpha_3 = \left(3A_2 L_2^{\,2} r^2 / I_2\right)\left(\chi / \alpha_M\right)\left(\int_0^1 \psi_2'^2(\bar{x})\psi_2''(\bar{x})\psi_2(\bar{x})\,d\bar{x} \Big/ \int_0^1 \psi_2^{\,2}(\bar{x})\,d\bar{x}\right),\ c_{d2} = 2\varepsilon^2 \xi_2.$$

Now, method of multiple scales is exploited to obtain the analytical and closed form solution of p_1 and p_2 which have been expressed in terms of fast and slow time scales.

$$p_1 = \varepsilon p_{11}(T_0, T_1, T_2) + \varepsilon^2 p_{12}(T_0, T_1, T_2) + \varepsilon^3 p_{13}(T_0, T_1, T_2) \tag{4.25}$$

$$p_1 = \varepsilon p_{21}(T_0, T_1, T_2) + \varepsilon^2 p_{22}(T_0, T_1, T_2) + \varepsilon^3 p_{23}(T_0, T_1, T_2). \tag{4.26}$$

Using chain rule for the time derivatives and substituting Eq. (4.25) into Eq. (4.23) and after equating the coefficients of the same powers of ε, following equations are obtained:

$$O\left(\varepsilon^1\right):\ \partial^2 p_{11} / \partial T_0^{\,2} + \Omega_1^{\,2} p_{11} = 0. \tag{4.27}$$

$$O\left(\varepsilon^2\right):\ \partial^2 p_{12} / \partial T_0^{\,2} + 2\left(\partial^2 p_{11} / \partial T_0 \partial T_1\right) + \Omega_1^{\,2} p_{12} = 0. \tag{4.28}$$

$$\mathrm{O}\left(\varepsilon^3\right):\ \begin{aligned} &\partial^2 p_{13} / \partial T_0^{\,2} + 2\left(\partial^2 p_{12} / \partial T_0 \partial T_1\right) + \partial^2 p_{11} / \partial T_1^{\,2} + 2\left(\partial^2 p_{11} / \partial T_0 \partial T_2\right) + \\ &\Omega_1^{\,2} p_{13} - \alpha_1 p_{11}^{\,3} + 2\xi_1\left(\partial p_{11} / \partial T_0\right) = 0. \end{aligned} \tag{4.29}$$

Similarly for the second link the governing equations are obtained as:

$$O\left(\varepsilon^1\right):\ \partial^2 p_{21} / \partial T_0^{\,2} + \Omega_2^{\,2} p_{21} + \alpha_2\left(\partial^2 p_{11} / \partial T_0^{\,2}\right) = 0. \tag{4.30}$$

$$\mathrm{O}\left(\varepsilon^2\right):\ \partial^2 p_{22} / \partial T_0^{\,2} + 2\left(\partial^2 p_{21} / \partial T_0 \partial T_1\right) + \Omega_1^{\,2} p_{22} + \alpha_2\left(\partial^2 p_{12} / \partial T_0^2\right) + 2\alpha_2\left(\partial^2 p_{11} / \partial T_0 \partial T_1\right) = 0. \tag{4.31}$$

$$\partial^2 p_{23}/\partial T_0{}^2 + 2\left(\partial^2 p_{22}/\partial T_0 \partial T_1\right) + \partial^2 p_{21}/\partial T_1{}^2 + 2\left(\partial^2 p_{21}/\partial T_0 \partial T_2\right) + \Omega_2^2 p_{13} +$$

$$\mathrm{O}\left(\varepsilon^3\right): \alpha_2\left(\partial^2 p_{13}/\partial T_0{}^2\right) + 2\alpha_2\left(\partial^2 p_{12}/\partial T_0 \partial T_1\right) + \alpha_2\left(\partial^2 p_{11}/\partial T_1{}^2\right) + 2\alpha_2\left(\partial^2 p_{11}/\partial T_0 \partial T_2\right) - \quad (4.32)$$

$$\alpha_3 p_{21}{}^3 + 2\xi_2\left(\partial p_{21}/\partial T_0\right) = 0.$$

The general solution of Eq. (4.27) & Eq. (4.30) can be expressed as:

$$p_{11} = P\left(T_1, T_2\right)\exp\left(i\Omega_1 T_0\right) + \bar{P}\left(T_1, T_2\right)\exp\left(-i\Omega_1 T_0\right). \quad (4.33)$$

$$p_{21} = Q\left(T_1, T_2\right)\exp\left(i\Omega_2 T_0\right) + \left\{\Omega_1^2 \alpha_2 P\left(T_2\right)\Big/\left(\Omega_2^2 - \Omega_1^2\right)\right\}\exp\left(i\Omega_1 T_0\right) + cc. \quad (4.34)$$

Now, substituting Eqs. (4.33)-(4.34) into Eqs. (4.28)-(4.31) gives:

$$\partial^2 p_{12}/\partial \mathrm{T}_0{}^2 + \Omega_1{}^2 p_{12} = -2i\Omega_1\left(\partial P/\partial \mathrm{T}_1\right)\exp\left(i\Omega_1 T_0\right) + 2i\Omega_1\left(\partial \bar{P}/\partial \mathrm{T}_1\right)\exp\left(-i\Omega_1 T_0\right).$$

$$(4.35)\ \partial^2 p_{22}/\partial \mathrm{T}_0{}^2 + \Omega_2{}^2 p_{22} = -2i\Omega_2\left(\partial Q/\partial \mathrm{T}_1\right)\exp\left(i\Omega_2 T_0\right) + 2i\Omega_2\left(\partial \bar{Q}/\partial \mathrm{T}_1\right)\exp\left(-i\Omega_2 T_0\right).$$

(4.36)

The elimination of secular terms in Eqs. (4.35)-(4.36) yields the particular solution as:

$$p_{12} = 0. \quad (4.37)$$

$$p_{22} = 0. \quad (4.38)$$

Similarly, the following expression is obtained for the response of p_{13} and p_{23}:

$$\partial^2 p_{13}/\partial \mathrm{T}_0{}^2 + \Omega_1{}^2 p_{13} = -\left\{2i\Omega_1 \partial P/\partial T_2 + 3\alpha_1 P^2 \bar{P} - 2i\Omega_1 \xi_1 P\right\}\exp\left(i\Omega_1 T_0\right) + \alpha_1 P^3 \exp\left(3i\Omega_1 T_0\right) + cc \quad (4.39)$$

$$\partial^2 p_{23}/\partial \mathrm{T}_0{}^2 + \Omega_2{}^2 p_{23} = -\left\{2i\Omega_2 \partial Q/\partial T_2 - 2i\Omega_2 \xi_2 P\right\}\exp\left(i\Omega_2 T_0\right) + \left(9\alpha_1\alpha_2 P^3/8\right)\exp\left(3i\Omega_1 T_0\right) -$$

$$2i\alpha_2\Omega_1 \partial P/\partial T_2 \exp\left(i\Omega_1 T_0\right) + \alpha_3\left(\left(\Omega_1{}^2 \alpha_2 P/2\left(\Omega_2{}^2 - \Omega_1{}^2\right)\right)\exp\left(i\Omega_1 T_0\right) + Q\exp\left(i\Omega_2 T_0\right) + cc\right)^3 \quad (4.40)$$

Expression of $P\left(T_2\right)$ is written in the polar form as $P\left(T_2\right) = \left(1/2\right)a\left(T_2\right)\mathrm{e}^{\mathrm{i}\phi\left(T_2\right)}$ and substituted in Eq. (4.39). Now, eliminating the secular terms from Eq. (4.39) and separating real and imaginary parts, the following governing equations are obtained:

$$\partial a/\partial T_2 - \xi_1 a = 0,\ a\Omega_1 \partial\phi/\partial T_2 + \left(3/8\right)\alpha_1 a^3 = 0. \quad (4.41)$$

The solution of Eq. (4.41) for a and ϕ are as follows:

$$a = a_0 \exp\left(-\xi_1 T_2\right),\ \phi = -3\alpha_1 a_0^2 T_2/8\Omega_1 + \phi_0. \quad (4.42)$$

Here, a_0 and ϕ_0 are arbitrary constants that are determined by initial conditions. The particular solution of Eq. **Error! Reference source not found.** is:

$$p_{13} = -\left(\alpha_1 P^3/8\Omega_1^2\right)\exp\left(3i\Omega_1 T_0\right). \quad (4.43)$$

Substituting Eqs. (4.33), (4.37) & (4.42) into equation Eq. (4.25), and replacing the time scales by original variable τ, one may obtain the following expression for the response of first link.

$$p_1 = 0.5\varepsilon a\cos\left(\omega\tau + \phi\right) + \varepsilon^3\left(\alpha_1 a^3\cos\left(3\omega\tau + 3\phi\right)\Big/64\Omega_1^2\right). \quad (4.44)$$

Here, $\omega = \Omega_1 - \left(3/8\Omega_1\right)\varepsilon^2\alpha_1 a_0^2$.

In case of second link, it has been observed that due to the inertial coupling existing in the second link, the nondimensional frequency, Ω_2 of second link is nearly three times the nondimensional frequency Ω_1 of first link for the first mode for identical masses and link properties, which represent a condition of internal resonance. In the present case of internal resonance of 3:1 between the two links, the nearness of Ω_1 to $\left(1/3\right)\Omega_2$ can be expressed as $3\Omega_1 = \Omega_2 + \varepsilon^2\sigma$, which on substitution in Eq. (4.40), and further elimination of secular terms results in equation:

$$-2i\Omega_2\left(\partial Q/\partial T_2\right) + \alpha_3\left(3Q^2\bar{Q} + 6Qk^2 P\bar{P}\right) - 2i\Omega_2\xi_2 Q + \left(\alpha_3 k^3 P^3 - 9\alpha_1\alpha_2 P^3/8\right)\exp\left(i\sigma T_2\right) = 0 \quad (4.45)$$

Here,
$k=\left(\Omega_1{}^2\alpha_2/\left(\Omega_2{}^2-\Omega_1{}^2\right)\right)$. Expressing $Q(T_2)$ in polar form as $Q(T_2)=(1/2)b(T_2)e^{i\gamma(T_2)}$ and substituted in Eq. (4.45). Now separating real and imaginary parts from the resulting equation and transformed into an autonomous system by letting $\varphi=\sigma T_2+3\phi-\gamma$, following expressions are obtained:

$$b\Omega_2\left(\partial\varphi/\partial T_2\right)=b\Omega_2\sigma+3\alpha_3k^2a^2b/4-9\alpha_1a^2b\Omega_2/8\Omega_1+3\alpha_3b^3/8+\left(\alpha_3k^3-9\alpha_1\alpha_2/8\right)\left(a^3/8\right)\cos(\varphi)$$

$$\Omega_2\left(\partial b/\partial T_2\right)=-\Omega_2\xi_2b+\left(\alpha_3k^3-9\alpha_1\alpha_2/8\right)\left(a^3/8\right)\sin(\varphi) \qquad (4.46)$$

Eqs. (4.46) are the governing equation for modulation of the amplitude and the phase of the free oscillation term and the frequency equation for the steady-state condition can be found by eliminating the phase from the steady-state condition of Eqs. (4.46). The first order solution for the time response of second link in terms of original time variable is given by:

$$P_2=(1/2)b\cos\left(3\Omega_1\tau+3\phi+\varphi\right)+\left(\alpha_2a/16\right)\cos\left(\Omega_1\tau+\phi\right) \qquad (4.47)$$

Following a similar procedure as explained in section 3.1.3, the stability of the steady-state solutions can be determined by investigating the eigenvalues of the Jacobian matrix $[J]$ which is given by:

$$J=\begin{bmatrix} \Omega_2\xi_2 & \left(\alpha_3k^3-9\alpha_1\alpha_2/8\right)\left(a_0{}^3/8\right)\cos(\varphi_0) \\ \sigma_1/b_0+3\alpha_3k^2a_0{}^2/4b_0\Omega_2-9\alpha_1a_0{}^2/8b_0\Omega_1+ & -\left(\alpha_3k^3-9\alpha_1\alpha_2/8\right)\left(a_0{}^3/8b_0\Omega_2\right)\sin(\varphi_0) \\ 3\alpha_3b_0/8\Omega_2 & \end{bmatrix}.$$

4.3.4 Numerical results and discussion

a) *Static Analysis*

Static analysis is very important to understand the displacement profile which may further guide the designer to easily interpret the stress and strain distributions in the system before the process of its design takes place. For the deflection of the tip end, it is assumed that the payload moves vertically downwards instead of moving in a circular arc. It is valid if it is assumed to have a beam of low flexure. However, industrial manipulators may not satisfy this condition; hence, appropriate modification shall be necessary. Fig. 4.3 shows the static deflection of planar two-link manipulator. To get an idea about the variation of static defection with the material of the three different cases are considered. In first case, both the links are made of steel (E=210 GPa, ρ=7800 kg/m^3), in second case the first link is made of steel while the material of second link is aluminium (E=69 GPa, ρ=2700 kg/m^3), and in third case the first and second link are made of aluminium and steel, respectively. The beam characteristics considered are $L_1, L_2 = 0.35$ m, $b_1, b_2 = 0.03$ m, and $h_1, h_2 = 0.003$ m. It can be noticed that the static amplitude of the manipulator increases as the stiffness of the links is reduced. The manipulator experiences the maximum static deflection for the case when the first link is considered to be made of aluminum because of the combination of low Young's modulus and high loading conditions at the end of the link.

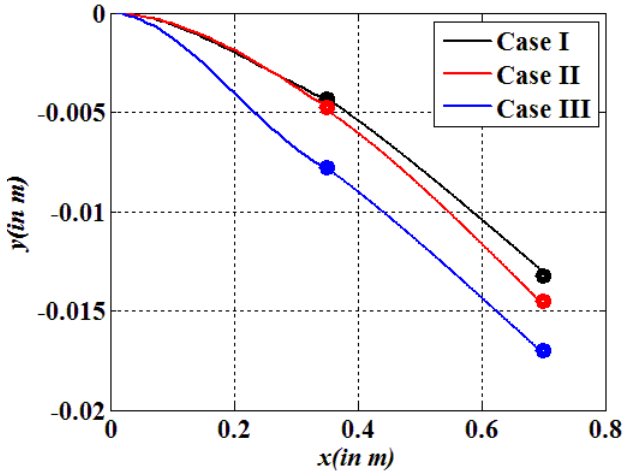

Fig. 4.3: Static deflection of two-link manipulator.

b) *Modal analysis: eigenspectrums*

In Table 4-1, for a wide range of α_{m2} (defined in Eq (4.11)), the corresponding first five eigenfrequency parameters, $\bar{\delta}$ are listed, which are the roots of the eigenfrequency equation that has been solved numerically using Newton-Raphson Method. Both the links are considered to be identical, which renders the values of α_M, α_L, and χ as unity, and also the mass parameter α_{m1} is taken as 1. From the Table 4-1, it can be observed that the $\bar{\delta}$ decreases as α_{m2} increases, which is obvious from the fact that the natural frequency of a system decreases as the inertia of the system increases. Variation of nondimensional eigenfrequency parameter with respect to system mass parameters $(\alpha_{m1},\alpha_{m2})$ is shown through Table 4-2. It can be noticed that as the system mass parameters increase, the nondimensional eigenfrequency parameter decreases.

Table 4-1: Variation of eigenfrequency parameter with tip mass parameter (α_{m2})

α_{m2}	$\bar{\delta}_1$	$\bar{\delta}_2$	$\bar{\delta}_3$	$\bar{\delta}_4$	$\bar{\delta}_5$
0	0.9346	1.7819	3.9239	4.8061	7.0686
0.1	0.9030	1.6934	3.7584	4.6858	6.8339
0.5	0.8119	1.5162	3.5476	4.5875	6.6409
1	0.7408	1.4101	3.4812	4.5560	6.5962
5	0.5420	1.1119	3.4121	4.4998	6.5555

Table 4-2: Variation of eigenfrequency parameter with system mass parameter $(\alpha_{m1},\alpha_{m2})$

α_{m1},α_{m2}	$\bar{\delta}_1$	$\bar{\delta}_2$	$\bar{\delta}_3$	$\bar{\delta}_4$	$\bar{\delta}_5$
0.1	0.9494	1.8031	3.7530	4.7450	6.8299
0.5	0.8251	1.5646	3.5457	4.6061	6.6397
1	0.7408	1.4101	3.4812	4.5560	6.5962
5	0.5302	1.0201	3.4132	4.4885	6.5561

The effect of flexural rigidity ratio $(\chi = E_2I_2 / E_1I_1)$ on the nondimensional eigenfrequency parameter is inferred from Table 4-3. The first five eigenfrequency parameters have been tabulated for a wide range of flexural rigidity ratio which shall cover all the practical values while other parameters are taken as unity. It is evident from the table that the eigenfrequencies tend to increase with increasing flexural rigidity ratio. Also, from Table 4-4 and Table

4-5 it is noticeable that the eigenfrequencies show a decreasing trend with the increase in non-dimensional beam mass density and length parameters.

Table 4-3: Variation of eigenfrequency parameter with flexural rigidity ratio (χ)

χ	$\bar{\delta}_1$	$\bar{\delta}_2$	$\bar{\delta}_3$	$\bar{\delta}_4$	$\bar{\delta}_5$
0.5	0.6891	1.3488	3.0933	4.3139	5.7904
0.75	0.7215	1.3850	3.3158	4.4540	6.2580
1	0.7408	1.4101	3.4812	4.5560	6.5962
1.5	0.7627	1.4433	3.7266	4.7023	7.0504
2	0.7747	1.4645	3.9079	4.8105	7.3136

Table 4-4: Variation of eigenfrequency parameter with beam mass density parameter (α_M)

α_M	$\bar{\delta}_1$	$\bar{\delta}_2$	$\bar{\delta}_3$	$\bar{\delta}_4$	$\bar{\delta}_5$
0.5	0.7693	1.4586	3.8799	4.8018	7.2327
0.75	0.7544	1.4332	3.6581	4.6337	6.9300
1	0.7408	1.4101	3.4812	4.5560	6.5962
1.5	0.7169	1.3693	3.2295	4.4758	6.0793
2	0.6964	1.3342	3.0575	4.4263	5.7273

Table 4-5: Variation of eigenfrequency parameter with length parameter (α_L)

α_L	$\bar{\delta}_1$	$\bar{\delta}_2$	$\bar{\delta}_3$	$\bar{\delta}_4$	$\bar{\delta}_5$
0.25	0.9944	2.6042	4.6789	7.5458	10.5097
0.75	0.9057	1.8908	4.3939	6.7740	7.9547
1	0.7408	1.4101	3.4812	4.5560	6.5962
1.5	0.6148	1.2211	2.4867	4.1111	4.8004

In further text, the effect of variation of essential system parameters over mode shapes of the system is studied. The first four mode shapes of the two-link flexible manipulator system considering α_{m1}, α_{m2}, α_L, χ, and μ as unity is shown in Fig. 4.4. The effect of variation of system mass parameters on the mode shapes is depicted in Fig. 4.5. A significant decrease in deflection of manipulator with increase in system mass parameter can be noticed for the lower mode shapes however higher mode shapes tend to clutter together along the length of manipulator.

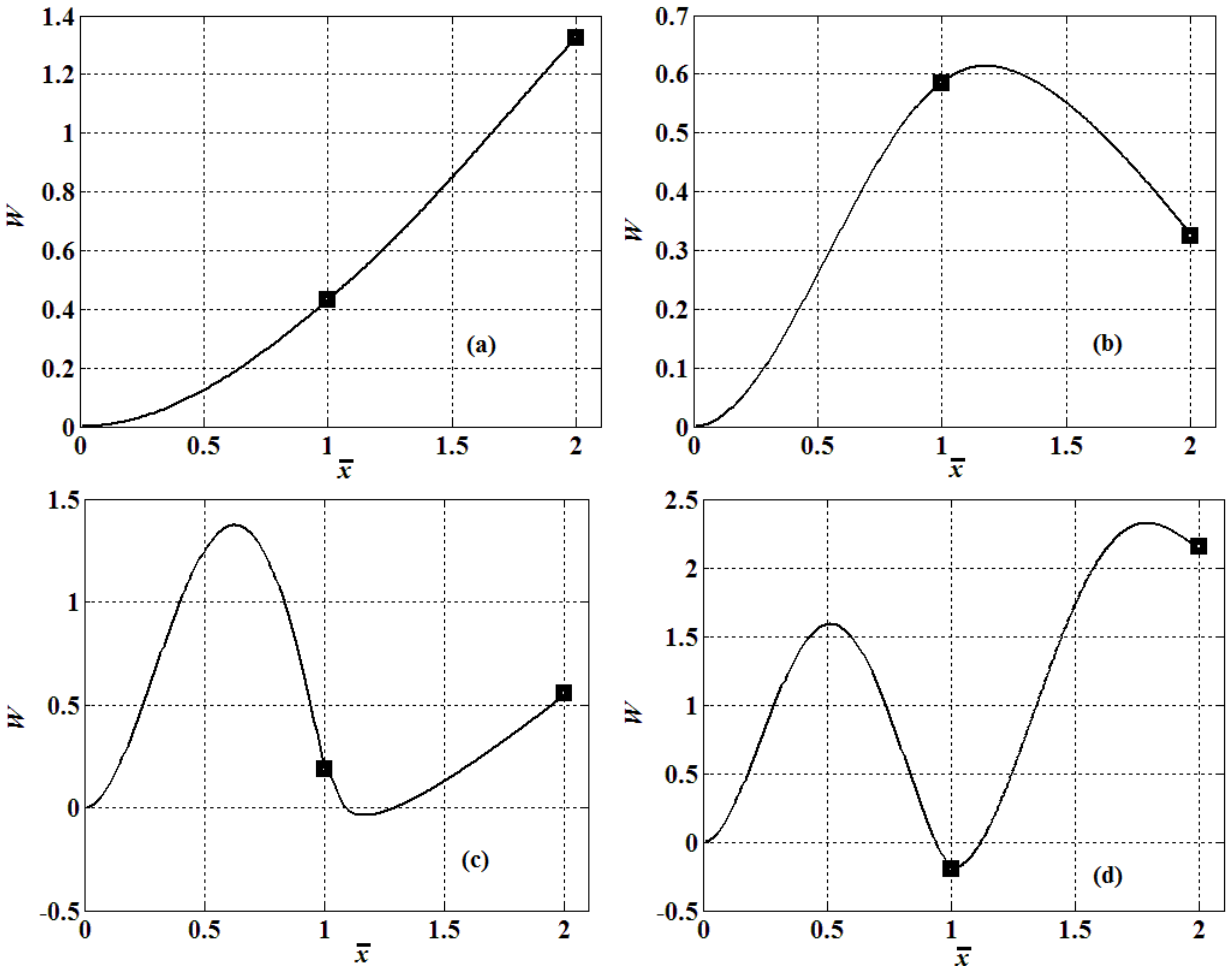

Fig. 4.4: Mode shapes of flexible two-link manipulator (a) mode 1 (b) mode 2 (c) mode 3 (d) mode 4.

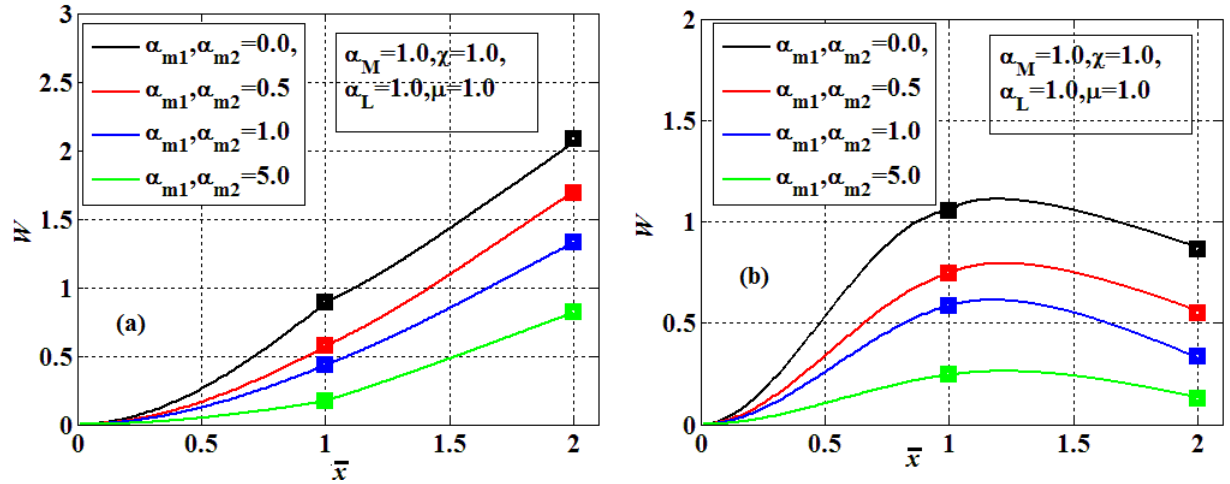

Fig. 4.5: Effect of system $(\alpha_{m1},\alpha_{m2})$ mass parameters on the mode shapes of the two-link manipulator (a) mode 1 (b) mode 2.

The flexural rigidity ratio (χ) has a noticeable effect on lower as well as higher mode shapes of the manipulator which is shown in Fig. 4.6. The mode shapes tend to spread out along the length of manipulator and the deflection of manipulator tends to decrease as the flexural rigidity ratio increases. This effect can be very much useful while designing the arms of a robot manipulator made of different materials, as the changes in the flexibility may cause the variation in the deflection pattern of manipulator.

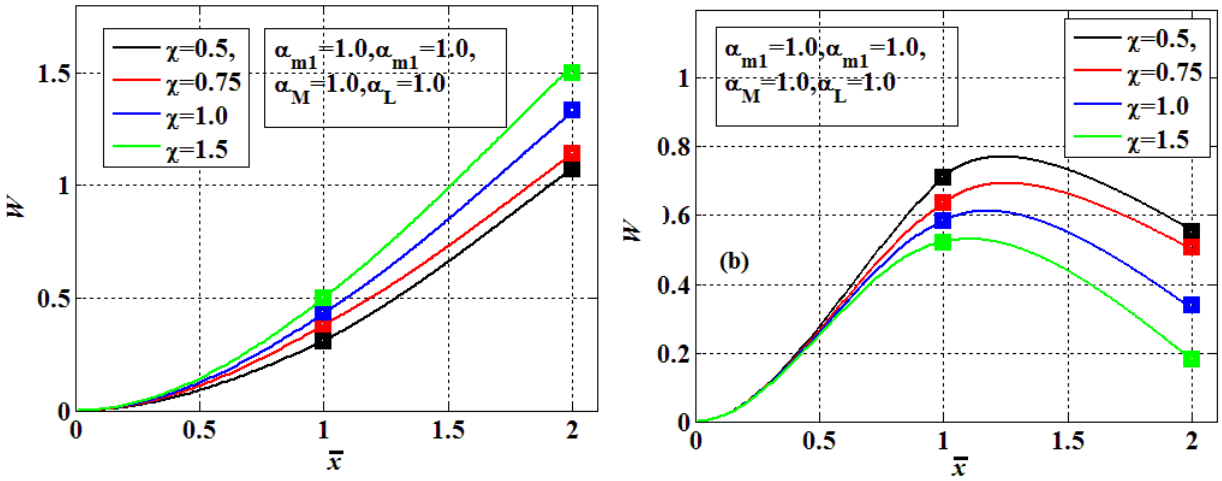

Fig. 4.6: Effect of flexural rigidity ratio (χ) on the mode shapes of the two-link manipulator (a) mode 1 (b) mode 2.

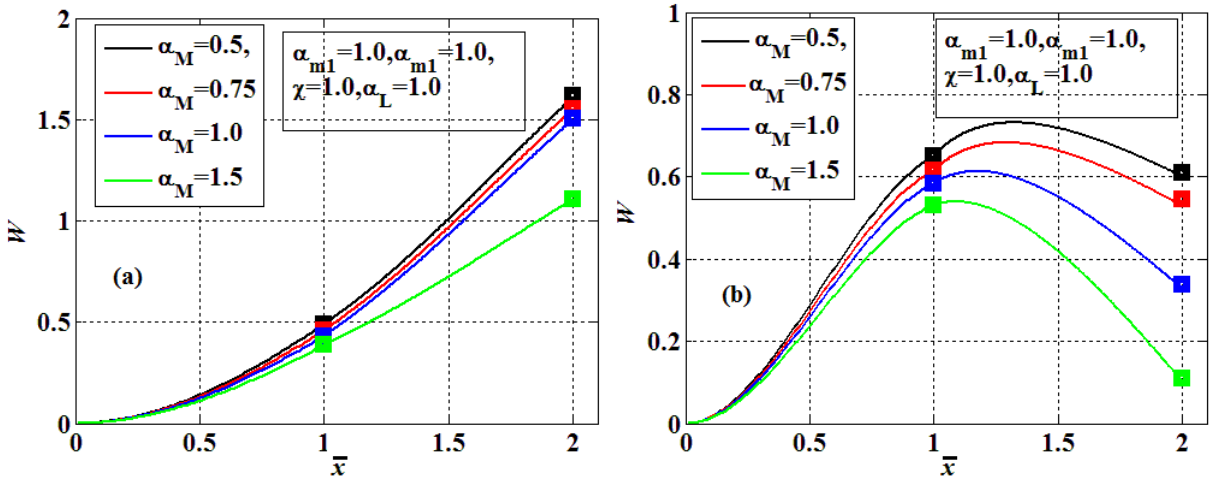

Fig. 4.7: Effect of beam mass density ratio (α_M) on the mode shapes of the two-link manipulator (a) mode 1 (b) mode 2.

The effect of variation of beam mass density parameter (α_M) on the mode shapes can be observed in Fig. 4.7. Here also, the effect of mass density is pronounced over the mode shapes for both lower and higher order of vibration. So, it can be concluded that the variation of materials in two different arms of the two-link manipulator can cause the significant changes in the amplitude of payload.

c) *Nonlinear analysis: bifurcation and stability*

Internal resonance arising due to the inertial coupling between the links of two-link flexible manipulator has been investigated in the present section. The beam characteristics considered here are same as those employed in the static analysis. The dimensionless parameter, scaling factor and nondimensional representative damping coefficient is considered as 0.1. The initial conditions for first and second link are $p_{10}=0.1$, $\dot{p}_{10}=0.1$, $p_{20}=0.0$, and $\dot{p}_{20}=0.0$. For the steady-state response the system exhibits spring softening behavior as shown Fig. 4.8 in which the bending represents the presence of geometric nonlinearity in the system. Jump up and Jump down phenomena, represented by dotted arrow, is observed at the critical points, B and E, respectively during starting and stopping of the system. This jump phenomenon observed for the existence of saddle-node bifurcation, may cause catastrophic failure of the manipulator. The solid lines represent the stable steady-state solution the while dotted line symbolizes the unstable solutions.

The effect of payload mass parameter is also shown in Fig. 4.8. It is noticed that the maximum amplitude of the steady-state response decreases when the mass parameter of the payload is increased. The demonstration of variation in beam mass density (α_M) and flexural rigidity (χ) ratio on the frequency response curve is shown in Fig. 4.9. The maximum amplitude tends to increase with the beam mass density. The increase in flexural rigidity ratio also tends to increase the amplitude of the system; however, the jump-up phenomena start at a higher frequency.

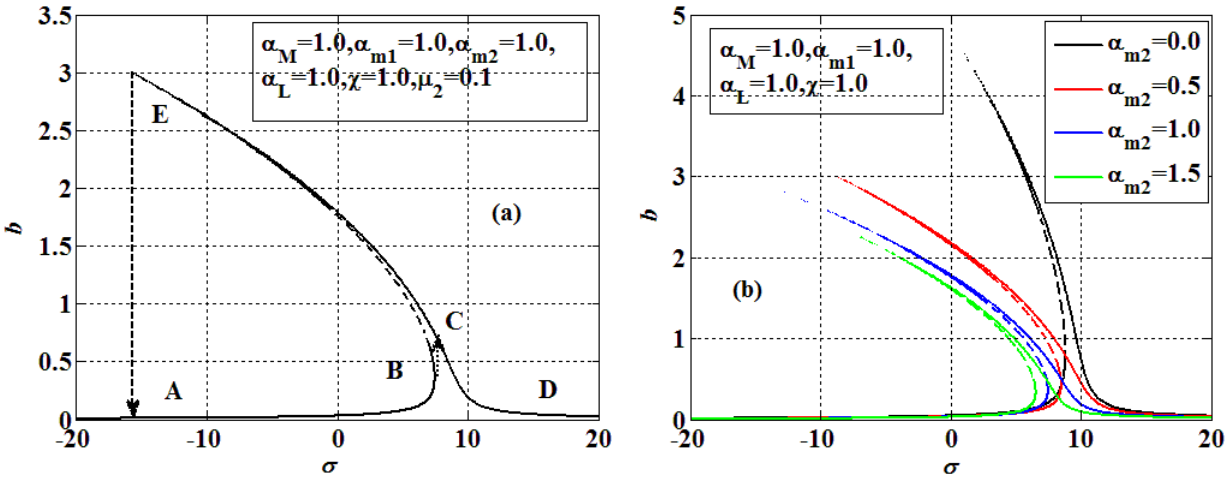

Fig. 4.8: Representative (a) frequency response curve and (b) effect of payload mass parameter (α_{m2}) for second link.

The coefficients corresponding to cubic nonlinear terms arising due to the axial stretching in both the links can be varied by their respective geometric properties as given in Eq. **Error! Reference source not found.**. The effect of nonlinearity variation associated with the first (α_1) and the second (α_3) link on the frequency characteristics is elucidated through Fig. 4.10. A sharp increase in amplitude of system response along with the shifting of response curve is observed with the increase in nonlinear coefficient associated with first link. However, the response curve witness substantial decrease in jump length with the increase in cubic nonlinear coefficient associated with second link.

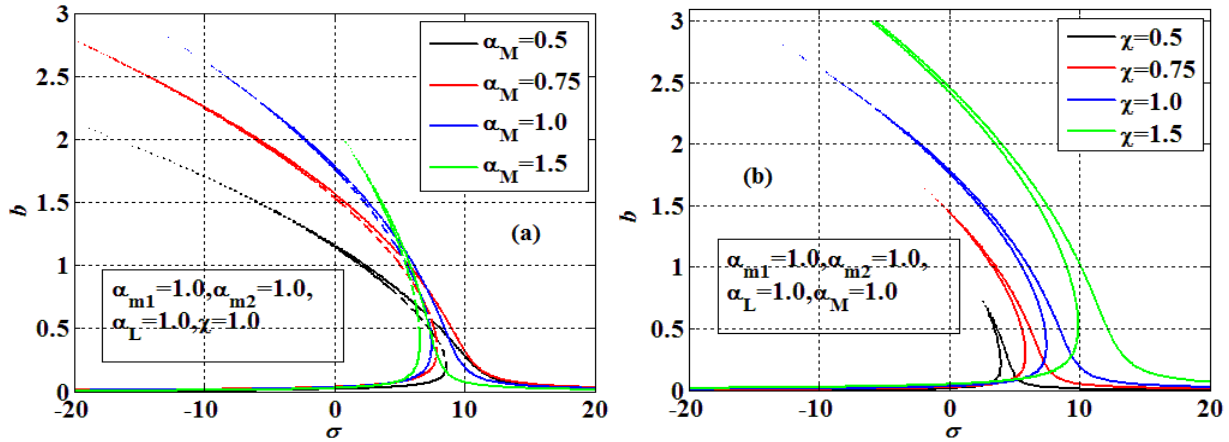

Fig. 4.9: Effect of (a) beam mass density (α_M) and (b) flexural rigidity (χ) ratio on frequency response curve of second link.

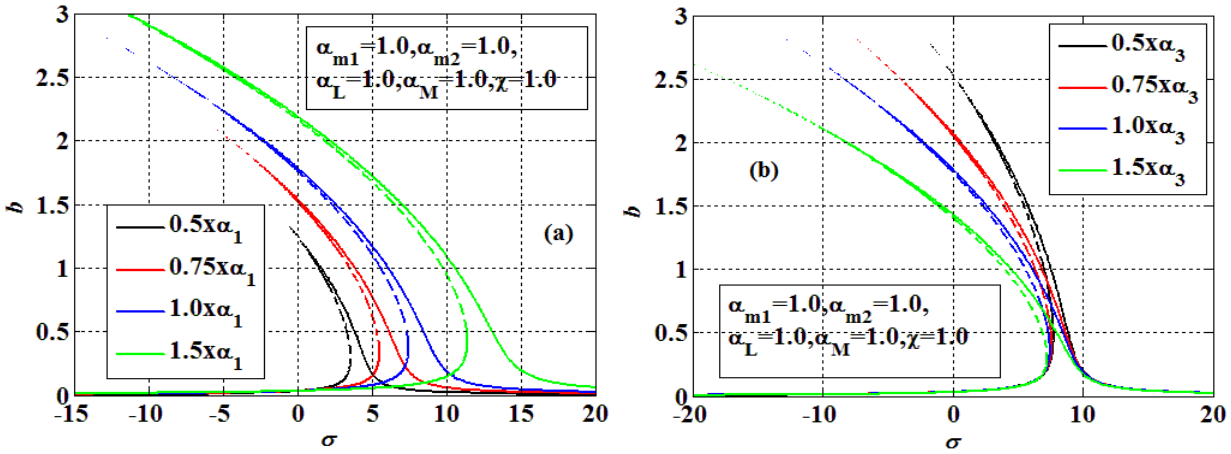

Fig. 4.10: Effect of geometric nonlinearity due to (a) axial stretching (α_1) of first and (b) second (α_3) link on frequency response curve of second link.

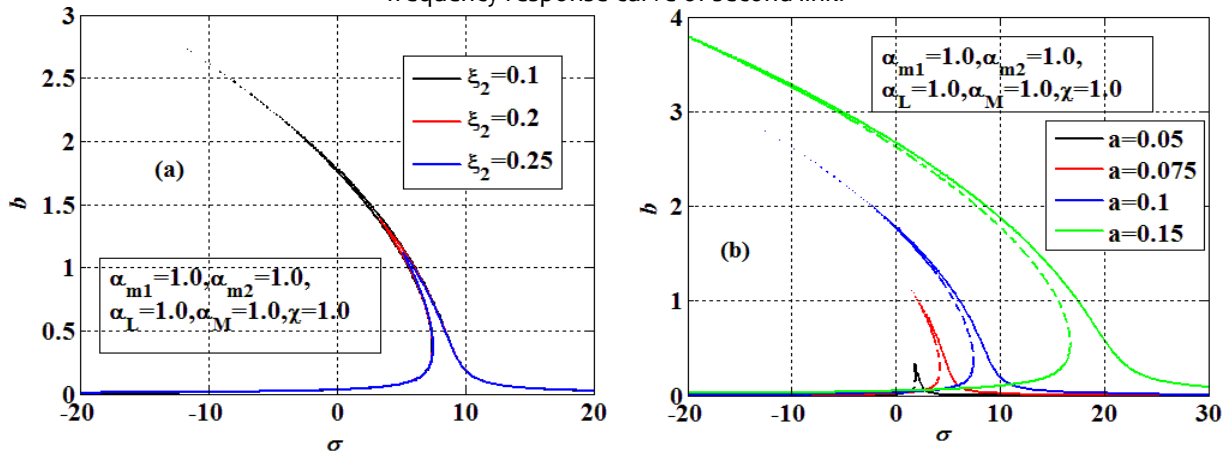

Fig. 4.11: Effect of (a) damping and (b) amplitude of first link on frequency response curve of second link.

The effect of nondimensional damping and the excitation amplitude on the frequency response curve of second link is shown in Fig. 4.11 and it can be observed that the slight increase in damping results in large reduction of peak amplitude of the system. The initial excitation given to first link has a pronounced effect on the amplitude of the second link. A large variation in amplitude of second link is observed for a slight increase in excitation. Also, the jump phenomenon starts at a higher frequency for larger excitation amplitude of first link. The modal parameters as well as the nonlinear behaviors of the flexible two-link manipulator are significantly influenced by the system parameters. The in-built internal resonance between the links may cause large vibrations in the system. Further investigations should be carried out to examine the system behavior under external excitations and joint motions.

4.4 FLEXIBLE MANIPULATOR ATTACHED WITH GENERIC PAYLOAD

Fig. 4.12 shows a schematic diagram of a deformed planar flexible two-link manipulator incorporating generic payload at the distal end. An axial constraint pulsating force $\left(F_0 + F_1 \cos(\Omega t)\right)$ having static and dynamic component is applied on the payload which models the disturbances in working environment in which the manipulator is supposed to perform.

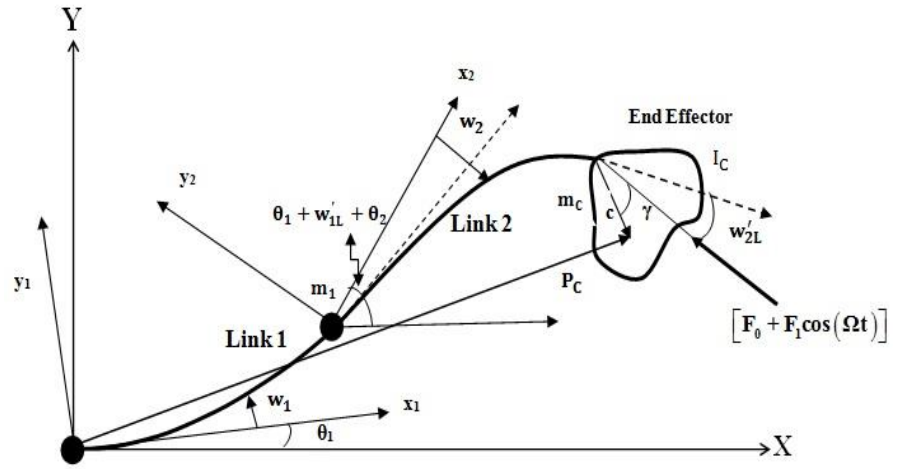

Fig. 4.12: A schematic diagram of planar two-link flexible manipulator with generic payload.

The vector equation of centre of gravity of payload is given as:

$$\vec{P}_C = \vec{P}_j + \left(L_j + u_{jL} + c\cos\left(\gamma + \sum_{i=1}^{j} w'_{jL} \right) \right) \hat{x}_j + \left(w_{jL} + c\sin\left(\gamma + \sum_{i=1}^{j} w'_{jL} \right) \right) \hat{y}_j,\ j = 2. \tag{4.48}$$

Total kinetic energy (T_{total}) and potential energy (U_{total}) of the system is given by:

$$T_{total} = (1/2)\sum_{i=1}^{2}\left(\int_0^{L_i} \rho_i \dot{\vec{q}}_i^{\,T} \dot{\vec{q}}_i dx \right) + (1/2)\left\{ m_i \vec{P}_i^{\,T} \vec{P}_i + m_C \left(\vec{P}_C^{\,T} \vec{P}_C \right) \right\} + (1/2)\left\{ I_C \left(\sum_{i=1}^{2} \dot{w}'_{iL} + \dot{\theta}_i \right)^2 \right\}. \tag{4.49}$$

$$U_{total} = (1/2)\sum_{i=1}^{2}\int_0^{L_i} E_i I_i \left(w_i'' \right)^2 dx + (1/2)\sum_{i=1}^{2}\int_0^{L_i} E_i A_i \left(u_i' + (1/2) w_i'^2 \right)^2 dx. \tag{4.50}$$

Here, the kinetic energy constitutes of energy due to translatory motion of the links, masses at the end of links and rotational energy of payload. The potential energy comprises of strain energy due to elastic bending and stretching effect of the links. The governing equations of the two-link manipulator system are obtained by using extended Hamilton's principle are expressed here as.

The governing equations of motion and boundary conditions in longitudinal and transverse directions of first link are:

$$\begin{aligned} \{w_1\}: \ & \rho_1 A_1 \left(\ddot{w}_1 + x\ddot{\theta}_1 - w_1\dot{\theta}_1^{\,2} + u_1\ddot{\theta}_1 + 2\dot{u}_1\dot{\theta}_1 \right) - E_1 A_1 \left\{ \left(u_1'' + w_1' w_1'' \right) w_1' + \left(u_1' + (1/2) w_1'^{\,2} \right) w_1'' \right\} \\ & + E_1 I_1 w_1'''' - \left\{ F_0 + F_1 \cos(\Omega t) \right\} w_1'' = 0, \end{aligned} \tag{4.51}$$

$$\{E_1 I_1 w_1\}_{(0,t)} = 0, \{E_1 I_1 w_1'\}_{(0,t)} = 0,$$

$$(m_1 + m_C)\left(\ddot{w}_{1L} + L_1\ddot{\theta}_1 \right) + \int_0^{L_2} \rho_2 A_2 \left(\ddot{w}_{1L} + L_1\ddot{\theta}_1 \right) dx - E_1 I_1 w_{1L}''' + \{E_2 I_2 w_2'''\}_{(0,t)} = 0,$$

$$\begin{aligned} & E_1 I_1 w_{1L}'' + I_C\left(\ddot{\theta}_1 + \ddot{w}'_{1L} + \ddot{\theta}_2 + \ddot{w}'_{2L} \right) + \int_0^{L_2} \rho_2 A_2 \left(x\ddot{w}_2 + x^2\ddot{w}'_{1L} + x^2\ddot{\theta}_1 + x^2\ddot{\theta}_2 \right) dx \\ & + m_C \begin{Bmatrix} c^2\ddot{w}'_{2L} - c\ddot{u}_{2L}\sin\left(\gamma + w'_{2L} \right) + c^2\ddot{\theta}_1 + c^2\ddot{\theta}_2 + c^2\ddot{w}'_{1L} + L_2\ddot{w}_{2L} + c\ddot{w}_{2L}\cos\left(\gamma + w'_{2L} \right) \\ + cL_2\ddot{w}'_{2L}\cos\left(\gamma + w'_{2L} \right) + L_2^{\,2}\ddot{\theta}_1 + L_2^{\,2}\ddot{\theta}_2 + 2cL_2\ddot{\theta}_1\cos\left(\gamma + w'_{2L} \right) + 2cL_2\ddot{\theta}_2\cos\left(\gamma + w'_{2L} \right) \\ + 2cL_2\ddot{w}'_{1L}\cos\left(\gamma + w'_{2L} \right) + 2L_2\ddot{w}'_{1L} \end{Bmatrix} = 0. \end{aligned} \tag{4.52}$$

$$\{u_1\}: \ \rho_1 A_1 \left(\ddot{u}_1 - w_1\ddot{\theta}_1 - 2\dot{w}_1\dot{\theta}_1 - x\dot{\theta}_1^{\,2} - u_1\dot{\theta}_1^{\,2} \right) - E_1 A_1 \left(u_1'' + w_1' w_1'' \right) - \left\{ F_0 + F_1 \cos(\Omega t) \right\} = 0. \tag{4.53}$$

$$\{E_1 A_1 u_1\}_{(0,t)} = 0, (m_1 + m_C)\left(\ddot{u}_{1L} \right) + E_1 A_1 u'_{1L} - \{E_2 A_2 u'\}_{2(0,t)} = 0. \tag{4.54}$$

The governing equations of motion in axial and transverse directions for second link are:

$$\begin{aligned}
&\rho_2 A_2\{\ddot{w}_2 + x\ddot{w}'_{1L} + x\ddot{\theta}_1 + x\ddot{\theta}_2 - w_2\dot{\theta}_1{}^2 - w_2\dot{w}'_{1L}{}^2 - 2\dot{\theta}_1\dot{\theta}_2 v_2 - 2\dot{\theta}_2 w_2\dot{w}'_{2L} + \\
&\{w_2\}: 2\dot{u}_2\dot{\theta}_1 + 2\dot{u}_2\dot{\theta}_2 + 2\dot{u}_2\dot{w}'_{1L} + u_2\ddot{w}'_{1L} + u_2\ddot{\theta}_1 + u_2\ddot{\theta}_2 + 2\dot{\theta}_1 w_2\dot{w}'_{2L} - w_2\dot{\theta}_2{}^2\} + E_2 I_2 w_2'''' - \\
&E_2 A_2\{(u_2'' + w_2' w_2'')w_2' + \left(u_2' + (1/2)w_2'^2\right)w_2''\} - \{F_0 + F_1\cos(\Omega t)\}w_2'' = 0.
\end{aligned} \tag{4.55}$$

$$\{E_2 I_2 w_2\}_{(0,t)} = 0, \{E_2 I_2 w_2'\}_{(0,t)} = 0,$$

$$\begin{aligned}
&E_2 I_2 w_2''(L_2,t) + I_C\left(\ddot{\theta}_1 + \ddot{w}'_{1L} + \ddot{\theta}_2 + \ddot{w}'_{2L}\right) + m_C\{c^2\ddot{\theta}_1 + c^2\ddot{w}'_{1L} + c^2\ddot{\theta}_2 + c^2\ddot{w}'_{2L} + cL_2\ddot{w}'_{1L}\cos(\gamma + w'_{2L}) + \\
&L_2\ddot{\theta}_1\cos(\gamma + w'_{2L}) + cL_2\ddot{\theta}_2\cos(\gamma + w'_{2L}) + c\ddot{w}_{2L}\cos(\gamma + w'_{2L}) - c\ddot{u}_{2L}\sin(\gamma + w'_{2L})\} = 0,
\end{aligned}$$

$$\begin{aligned}
&m_C\left\{\begin{matrix} L_2\ddot{\theta}_1 + L_2\ddot{\theta}_2 + \ddot{w}_{2L} + L_2\ddot{w}'_{1L} + c\ddot{\theta}_1\cos(\gamma + w'_{2L}) + c\ddot{\theta}_2\cos(\gamma + w'_{2L}) + \\ c\ddot{w}'_{1L}\cos(\gamma + w'_{2L}) + c\ddot{w}'_{2L}\cos(\gamma + w'_{2L}) \end{matrix}\right\} + \\
&E_2 I_2 w'''_{2L} - E_2 A_2\left\{u'_{2L} + (1/2)w'_{2L}{}^2\right\}w'_{2L} = 0.
\end{aligned} \tag{4.56}$$

$$\begin{aligned}
&\rho_2 A_2(\ddot{u}_2 - w_2\ddot{\theta}_1 - w_2\ddot{\theta}_2 - w_2\ddot{w}'_{1L} - 2\dot{w}_2\dot{\theta}_1 - 2\dot{w}_2\dot{\theta}_2 - 2\dot{w}_2\dot{w}'_{1L} - x\dot{\theta}_1{}^2 - x\dot{\theta}_2{}^2 - x\dot{w}'_{1L}{}^2 \\
&\{u_2\}: -u_2\dot{\theta}_2{}^2 - u_2\dot{w}'_{1L}{}^2 - 2x\dot{\theta}_1\dot{\theta}_2 - 2x\dot{\theta}_2\dot{w}'_{1L} - 2x\dot{\theta}_1\dot{w}'_{1L} - 2u_2\dot{\theta}_1\dot{\theta}_2 - 2u_2\dot{\theta}_2\dot{w}'_{1L} - 2u_2\dot{\theta}_1\dot{w}'_{1L} - \\
&u_2\dot{\theta}_1{}^2) - E_1 A_1\left(u_2'' + w_2' w_2''\right) - \{F_0 + F_1\cos(\Omega t)\} = 0,
\end{aligned} \tag{4.57}$$

$$m_C\left(\ddot{u}_{2L} - c\ddot{w}'_{1L}\sin(\gamma + w'_{1L}) - c\ddot{w}'_{2L}\sin(\gamma + w'_{1L}) - c\ddot{\theta}_1\sin(\gamma + w'_{1L}) - c\ddot{\theta}_2\sin(\gamma + w'_{1L})\right) + E_2 A_2 u'_{2L} = 0.$$

$$\{E_2 A_2 u_2\}_{(0,t)} = 0, \tag{4.58}$$

If the dynamics of the second link is neglected and the payload is being considered having vertical offset, the Eqs. (4.51-4.58) reduce to those obtained by [Anderson, 1978].

4.4.1 Free vibration analysis

A similar procedure as presented in section 4.3.1 is followed to obtain the eigenfunctions for n^{th} mode shapes of vibration for transverse vibration and longitudinal directions are obtained as:

$$\begin{aligned}
&W_1{}^n(x) = B^n{}_1\sin\left(\delta^n x\right) + B_2\cos\left(\delta^n x\right) + B^n{}_3\sinh\left(\delta^n x\right) + B^n{}_4\cosh\left(\delta^n x\right), \\
&W_2^n(x) = C^n{}_1\sin\left(\mu\delta^n x\right) + C^n{}_2\cos\left(\mu\delta^n x\right) + C^n{}_3\sinh\left(\mu\delta^n x\right) + C^n{}_4\cosh\left(\mu\delta^n x\right) - W_1^{n\prime}(L_1)x
\end{aligned} \tag{4.59}$$

$$\begin{aligned}
&U^n{}_1(x) = D^n{}_1\sin\left(\delta^2 L_1\kappa x\right)^n + D^n{}_2\cos\left(\delta^2 L_1\kappa x\right)^n, \\
&U^n{}_2(x) = E^n{}_1\sin\left(\delta^2\mu^2 L_1\kappa x\right)^n + E^n{}_2\cos\left(\delta^2\mu^2 L_1\kappa x\right)^n.
\end{aligned} \tag{4.60}$$

The integration constants and the eigenfrequency equation are determined by substituting the mode shapes in the boundary conditions and arranging them in matrix form similar to Eq. (4.12) whose elements are expressed here as:

$$K_{13} = \left(\alpha_{mC}\bar{\delta}^n/\chi\mu^3\right)\left(\sin\left(\lambda\bar{\delta}^n\right) + \alpha_C\mu\bar{\delta}^n\cos(\gamma)\cos\left(\lambda\bar{\delta}^n\right)\right) - \cos\left(\lambda\bar{\delta}^n\right),$$

$$\begin{aligned}
&K_{14} = \left(\alpha_{mC}\bar{\delta}^n/\chi\mu^3\right)\left(\cos\left(\lambda\bar{\delta}^n\right) - \cosh\left(\lambda\bar{\delta}^n\right) - \alpha_C\mu\bar{\delta}^n\cos(\gamma)\left(\sin\left(\lambda\bar{\delta}^n\right) + \sinh\left(\lambda\bar{\delta}^n\right)\right)\right) + \\
&\left(\sin\left(\lambda\bar{\delta}^n\right) - \sinh\left(\lambda\bar{\delta}^n\right)\right),
\end{aligned}$$

$$K_{15} = \left(\alpha_{mC}\bar{\delta}^n/\chi\mu^3\right)\left(\alpha_C\mu\bar{\delta}^n\cos(\gamma)\cosh\left(\lambda\bar{\delta}^n\right) + \sinh\left(\lambda\bar{\delta}^n\right)\right) + \cosh\left(\lambda\bar{\delta}^n\right),$$

$$K_{23}=\left(\alpha_{mC}\left(\bar{\delta}^{n}\right)^{2}/\chi\mu^{2}\right)\left(\alpha_{C}\cos(\gamma)\sin\left(\lambda\bar{\delta}^{n}\right)+\alpha_{C}^{2}\mu\bar{\delta}^{n}\cos\left(\lambda\bar{\delta}^{n}\right)\right)+\sin\left(\lambda\bar{\delta}^{n}\right)+$$

$$\left(\alpha_{I}\left(\bar{\delta}^{n}\right)^{3}/\chi\mu\right)\cos\left(\lambda\bar{\delta}^{n}\right),$$

$$K_{24}=\left(\alpha_{mC}\left(\bar{\delta}^{n}\right)^{2}/\chi\mu^{2}\right)\left\{\alpha_{C}\cos(\gamma)\left(\cos\left(\lambda\bar{\delta}^{n}\right)-\cosh\left(\lambda\bar{\delta}^{n}\right)\right)-\alpha_{C}^{2}\mu\bar{\delta}^{n}\left(\sin\left(\lambda\bar{\delta}^{n}\right)+\sinh\left(\lambda\bar{\delta}^{n}\right)\right)\right\}+$$

$$\left\{\cos\left(\lambda\bar{\delta}^{n}\right)+\cosh\left(\lambda\bar{\delta}^{n}\right)\right\}-\left(\alpha_{I}\left(\bar{\delta}^{n}\right)^{3}/\chi\mu\right)\left\{\sin\left(\lambda\bar{\delta}^{n}\right)+\sinh\left(\lambda\bar{\delta}^{n}\right)\right\},$$

$$K_{25}=\left(\alpha_{mC}\left(\bar{\delta}^{n}\right)^{2}/\chi\mu^{2}\right)\left\{\alpha_{C}\cos(\gamma)\sinh\left(\lambda\bar{\delta}^{n}\right)+\alpha_{C}^{2}\mu\bar{\delta}^{n}\cosh\left(\lambda\bar{\delta}^{n}\right)\right\}-\sinh\left(\lambda\bar{\delta}^{n}\right)+$$

$$\left(\alpha_{I}\left(\bar{\delta}^{n}\right)^{3}/\chi\mu\right)\cosh\left(\lambda\bar{\delta}^{n}\right),$$

$$K_{27}=-\left(\alpha_{mC}\alpha_{c}\left(\bar{\delta}^{n}\right)^{2}/\chi\mu\right)\sin(\gamma)\sin\left\{\left(\bar{\delta}^{n}\right)^{2}\mu^{2}\varepsilon\alpha_{L}\right\},$$

$$K_{31}=\left(\alpha_{m_{1}}+\alpha_{mC}+\alpha_{M}\alpha_{L}\right)\bar{\delta}^{n}\left\{\sin\left(\bar{\delta}^{n}\right)-\sinh\left(\bar{\delta}^{n}\right)\right\}-\left\{\cos\left(\bar{\delta}^{n}\right)+\cosh\left(\bar{\delta}^{n}\right)\right\},$$

$$K_{32}=\left(\alpha_{m_{1}}+\alpha_{mC}+\alpha_{M}\alpha_{L}\right)\bar{\delta}^{n}\left\{\cos\left(\bar{\delta}^{n}\right)-\cosh\left(\bar{\delta}^{n}\right)\right\}+\left\{\sin\left(\bar{\delta}^{n}\right)-\sinh\left(\bar{\delta}^{n}\right)\right\},$$

$$K_{33}=\chi\mu^{3},\ K_{41}=-\cos\left(\bar{\delta}^{n}\right)+\cosh\left(\bar{\delta}^{n}\right),\ K_{42}=\sin\left(\bar{\delta}^{n}\right)+\sinh\left(\bar{\delta}^{n}\right),\ K_{43}=\mu,\ K_{45}=\mu,$$

$$K_{51}=\sin\left(\bar{\delta}^{n}\right)+\sinh\left(\bar{\delta}^{n}\right),\ K_{52}=\cos\left(\delta^{n}\right)+\cosh\left(\delta^{n}\right),$$

$$K_{53}=\alpha_{mC}\left(\delta^{n}\right)^{2}\left\{\begin{matrix}\alpha_{C}\alpha_{L}\mu\delta^{n}\cos(\gamma)\cos\left(\lambda\delta^{n}\right)+\alpha_{C}{}^{2}\alpha_{L}\mu\delta^{n}\cos\left(\lambda\delta^{n}\right)+\alpha_{C}\cos(\gamma)\sin\left(\lambda\delta^{n}\right)+\\ \alpha_{L}\sin\left(\lambda\delta^{n}\right)\end{matrix}\right\}$$

$$+\alpha_{I}\left(\delta^{n}\right)^{3}\mu\cos\left(\lambda\delta^{n}\right)+\left(\alpha_{M}/\mu^{2}\right)\left\{\sin\left(\lambda\delta^{n}\right)-\lambda\delta^{n}\cos\left(\lambda\delta^{n}\right)\right\},$$

$$K_{54}=\alpha_{mC}\left(\delta^{n}\right)^{2}\left\{\begin{matrix}\alpha_{L}\left(\cos\left(\lambda\delta^{n}\right)-\cosh\left(\lambda\delta^{n}\right)\right)-\alpha_{C}\alpha_{L}\cos(\gamma)\mu\delta^{n}\left(\sin\left(\lambda\delta^{n}\right)+\sinh\left(\lambda\delta^{n}\right)\right)+\\ \alpha_{C}\cos(\gamma)\left(\cos\left(\lambda\delta^{n}\right)\cosh\left(\lambda\delta^{n}\right)\right)-\alpha_{C}{}^{2}\mu\delta^{n}\left(\sin\left(\lambda\delta^{n}\right)+\sinh\left(\lambda\delta^{n}\right)\right)\end{matrix}\right\}$$

$$+\alpha_{I}\left(\delta^{n}\right)^{3}\mu\left\{\sin\left(\lambda\delta^{n}\right)+\sinh\left(\lambda\delta^{n}\right)\right\}+\left(\alpha_{M}/\mu^{2}\right)\left\{\begin{matrix}\cos\left(\lambda\delta^{n}\right)+\lambda\delta^{n}\sin\left(\lambda\delta^{n}\right)-\lambda\delta^{n}\sinh\left(\lambda\delta^{n}\right)+\\ \cosh\left(\lambda\delta^{n}\right)-2\end{matrix}\right\},$$

$$K_{55}=\alpha_{mC}\bar{\delta}^{2}\left\{\begin{matrix}\alpha_{L}\alpha_{C}\mu\delta^{n}\cos(\gamma)\cosh\left(\lambda\delta^{n}\right)+\alpha_{C}{}^{2}\mu\delta^{n}\alpha_{L}\cosh\left(\lambda\delta^{n}\right)+\alpha_{C}\cos(\gamma)\sinh\left(\lambda\delta^{n}\right)+\\ \alpha_{L}\sinh\left(\lambda\delta^{n}\right)\end{matrix}\right\}$$

$$+\alpha_{I}\left(\delta^{n}\right)^{3}\mu\cosh\left(\lambda\delta^{n}\right)+\left(\alpha_{M}/\mu^{2}\right)\left(\beta\delta^{n}\cosh\left(\lambda\delta^{n}\right)-\sinh\left(\lambda\delta^{n}\right)\right),$$

$$K_{57}=-\left\{\alpha_{mC}\alpha_{c}\left(\bar{\delta}^{n}\right)^{2}\right\}\sin(\gamma)\sin\left\{\left(\bar{\delta}^{n}\right)^{2}\mu^{2}\kappa\right\},$$

$$K_{66}=\cos\left\{\left(\delta^{n}\right)^{2}\kappa\right\}-\left(\alpha_{mC}+\alpha_{m1}\right)\left(\delta^{n}\right)^{2}\kappa\sin\left\{\left(\delta^{n}\right)^{2}\kappa\right\},\ K_{67}=-\chi\mu^{2},$$

$$K_{73}=\alpha_{mC}\alpha_{c}\mu\left(\delta^{n}\right)^{3}\kappa\sin(\gamma)\cos\left(\lambda\delta^{n}\right),\ K_{74}=-\alpha_{mC}\alpha_{c}\mu\left(\delta^{n}\right)^{3}\kappa\sin(\gamma)\left\{\sin\left(\lambda\delta^{n}\right)+\sinh\left(\lambda\delta^{n}\right)\right\},$$

$$K_{75}=\alpha_{mC}\alpha_{c}\mu\left(\delta^{n}\right)^{3}\kappa\sin(\gamma)\cosh\left(\lambda\delta^{n}\right),\ K_{76}=\left(\delta^{n}\right)^{2}\alpha_{mC}\kappa\sin\left\{\left(\delta^{n}\right)^{2}\mu^{2}\kappa\alpha_{L}\right\}-\chi\mu^{2},\ K_{77}=-\chi\mu^{2},$$

$K_{11}, K_{12}, K_{16}, K_{17}, K_{21}, K_{22}, K_{23}, K_{26}, K_{34}, K_{36}, K_{37}, K_{44}, K_{46}, K_{47}, K_{56}, K_{61}, K_{62}, K_{63}, K_{64}, K_{65},$
$K_{71}, K_{72}=0.$

The elements are expressed in terms of nondimensional system parameters expressed in Eq. (4.11) along with the payload and other parameters given as:

$\alpha_{mC} = m_C / \rho_1 A_1 L_1, \alpha_c = c / L_1, \alpha_I = I_C / \rho_1 A_1 {L_1}^3$, and $\kappa^2 = I_1 / A_1 {L_1}^2$.

4.4.2 Nonlinear forced vibration analysis

The two-link manipulator is assumed to be acted upon by variable constraint giving rise to subharmonic resonance in both the links. The effects of the generic payload and other system parameters on the system stabilities are investigated in this section. For the sake of simplicity, the longitudinal and rotational motions of links are neglected while geometric nonlinearity arising due to axial stretching and the coupled nonlinear terms in Eq. (4.51) and Eq. (4.55), are retained with addition of structural damping in both the links.

$$\rho_1 A_1 \ddot{w}_1 + E_1 I_1 w_1'''' - \left\{ (3/2) E_1 A_1 {w_1'}^2 w_1'' - \left(F_0 + F_1 \cos(\Omega_1 t) \right) w_1'' \right\} + c_{d1} \dot{w}_1 = 0. \tag{4.61}$$

$$\rho_2 A_2 \left(\ddot{w}_2 + x \ddot{w}_{1L}' \right) + E_2 I_2 w_2'''' - \left\{ (3/2) E_2 A_2 {w_2'}^2 w_2'' + \rho_2 A_2 w_2 {\dot{w}_{1L}'}^2 - \left(F_0 + F_1 \cos(\Omega_1 t) \right) w_2'' \right\} + c_{d2} \dot{w}_2 = 0. \tag{4.62}$$

The nonlinear equations of motion of the links of manipulator expressed in Eqs. (4.61)-(4.62) are nondimensionalized using terms:

$\bar{w}_1 = w_1 / L_1$, $\bar{w}_2 = w_2 / L_2$, $\bar{x} = x / L_1, \tau = t \sqrt{E_1 I_1 / \rho_1 A_1 {L_1}^4}$, $\bar{c}_1 = c_{d1} {L_1}^2 / \sqrt{\rho_1 A_1 E_1 I_1}$, $\bar{\bar{F}}_0 = \pi^2 \bar{F}_0 / 4$, $\bar{\bar{F}}_0 = \pi^2 \bar{F}_0 / 4$, $\bar{\bar{F}}_0 = \pi^2 \bar{F}_0 / 4$, $\bar{c}_2 = c_{d2} {L_1}^2 / \alpha_M \sqrt{\rho_1 A_1 E_1 I_1}$, and $\bar{\bar{F}}_1 = F_1 {L_1}^2 / E_1 I_1$.

Here, $\bar{F}_0$ is the critical buckling load of fixed-fixed columns. After executing discretization of the resulting nondimensionalized equations using Galerkin's principle by exploiting the mode shapes obtained in previous section, the appropriately ordered equations are expressed as:

$$\ddot{p}_1(\tau) + \bar{\omega}_1^2 p_1(\tau) + 2\varepsilon\xi_1 \dot{p}_1 + \varepsilon\eta_2 p_1(\tau) \cos\left(\bar{\Omega}_1 \tau\right) - \varepsilon^2 \eta_1 {p_1}^3(\tau) = 0.$$

(4.63)

$$\ddot{p}_2(\tau) + \bar{\omega}_2^2 p_2(\tau) + 2\varepsilon\xi_2 \dot{p}_2(\tau) + \varepsilon\left(\eta_3 \ddot{p}_1 + \eta_4 p_2(\tau) \cos\left(\bar{\Omega}_1 \tau\right) \right) - \varepsilon^2 \left(\eta_5 {p_2}^3(\tau) + \eta_6 p_2 {\dot{p}_1}^2 \right) = 0.$$

(4.64)

Following a similar procedure explained in section 4.3.3, the governing equations of motion for the first link in different time scales are obtained as:

$$O\left(\varepsilon^1\right): \ \Theta_1(p_{10}) = 0, \tag{4.65}$$

$$O\left(\varepsilon^2\right): \Theta_1(p_{11}) = -2\xi_1 D_0 p_{10} - 2D_0 D_1 p_{10} - \eta_2 u_{10} \cos\left(\bar{\Omega}_1 T_0\right). \tag{4.66}$$

$$O\left(\varepsilon^3\right): \Theta_1(p_{12}) = -2\xi_1 \left(D_0 p_{11} + D_1 p_{10} \right) - 2D_0 D_2 p_{10} - 2D_0 D_1 p_{11} - D_1^2 p_{10} - \eta_2 p_{11} \cos\left(\bar{\Omega}_1 T_0\right) + \eta_1 {p_{11}}^3. \tag{4.67}$$

Similarly for second link:

$$O\left(\varepsilon^1\right): \ \Theta_2(p_{20}) = 0.$$

(4.68)

$$O\left(\varepsilon^2\right): \Theta_2(p_{21}) = -2\xi_2 D_0 p_{20} - 2D_0 D_1 p_{20} - \eta_4 p_{20} \cos\left(\bar{\Omega}_1 T_0\right) - \eta_3 D_0^2 p_{10}. \tag{4.69}$$

$$O\left(\varepsilon^3\right): \begin{array}{l} \Theta_2(p_{22}) = -2\xi_2 \left(D_0 p_{21} + D_1 p_{20} \right) - 2D_0 D_2 p_{20} - 2D_0 D_1 p_{21} - D_1^2 p_{20} - \\ \eta_3 \left(D_0^2 p_{11} + 2D_0 D_1 p_{10} \right) - \eta_4 p_{21} \cos\left(\bar{\Omega}_1 T_0\right) + \eta_5 {p_{21}}^3 + \eta_6 p_{20} \dot{p}_{10}^2. \end{array} \tag{4.70}$$

Here, Θ_i is the linear differential operator defined for any function f as: $\Theta_i = D_0^2 f + \bar{\omega}_i^2 f (i = 1,2)$. The general solution of Eqs. (4.65) & (4.68) can be expressed as: $p_{10} = G(T_1, T_2) \exp\left(i\bar{\omega}_1 T_0\right) + \bar{G}(T_1, T_2) \exp\left(-i\bar{\omega}_1 T_0\right)$.

(4.71)

$$p_{20} = H(T_1, T_2) \exp\left(i\bar{\omega}_2 T_0\right) + \bar{H}(T_1, T_2) \exp\left(-i\bar{\omega}_2 T_0\right). \tag{4.72}$$

Now, substituting Eqs. (4.71)-(4.72) into Eqs. (4.66)-(4.69) gives:

$$\Theta_1(p_{11})=-2i\bar{\omega}_1\left\{\xi_1 G+(\partial G/\partial T_1)\right\}\exp(i\bar{\omega}_1 T_0)-(\eta_2/2)\left\{G\exp i(\bar{\omega}_1+\bar{\Omega}_1)T_0+\bar{G}\exp i(\bar{\Omega}_1-\bar{\omega}_1)T_0\right\}+cc. \tag{4.73}$$

$$\Theta_2(p_{21})=-2i\bar{\omega}_2\left\{\mu_2 H+(\partial H/\partial T_1)\right\}\exp(i\bar{\omega}_2 T_0)+\eta_3\bar{\omega}_1{}^2 G\exp(i\bar{\omega}_1 T_0)-$$
$$(\eta_4/2)\left\{H\exp i(\bar{\omega}_2+\bar{\Omega}_1)T_0+\bar{H}\exp i(\bar{\Omega}_1-\bar{\omega}_2)T_0\right\}+cc, \tag{4.74}$$

The Eqs. (4.73)-(4.74) contain the secular terms which lead to unbounded solutions when the forcing frequency $(\bar{\Omega})$ becomes equal or nearly equal to twice the link's normalized frequencies $(2\bar{\omega}_{1,2})$ leading to the subharmonic resonance which in turn causes large vibrations in the system and eventually leads to catastrophic failure of the system.

4.4.3 Subharmonic resonance case in first link: $(\bar{\Omega}_1 \approx 2\bar{\omega}_1)$

For this subharmonic resonance case in first link, the nearness of $\bar{\Omega}_1$ to $\bar{\omega}_1$, is expressed by introducing the detuning parameter σ_1 as $\bar{\Omega}_1 = 2\bar{\omega}_1 + \varepsilon\sigma_1$, which on the substitution in Eq. (4.73) results in the equation involving both secular and non-secular terms. In order to obtain the bounded solution the terms corresponding to $\exp(i\bar{\omega}_1 T_0)$ have to be eliminated and a process similar as that of section 3.1.3 is followed to obtain the solution in terms of time variable τ as:

$$2i\bar{\omega}_1(\partial G/\partial\tau)+2i\bar{\omega}_1\varepsilon\mu_1 G+G\left[\varepsilon^2\eta_2^2/16\bar{\omega}_1^2-\varepsilon^2\eta_2^2/4\left\{\bar{\omega}_1^2-(\bar{\omega}_1^2+\Omega^2)\right\}-\varepsilon^2\mu_1^2\right]+$$
$$\bar{G}(\varepsilon\eta_2/2-\varepsilon^2\eta_2\sigma_1/4\bar{\omega}_1)\exp(\sigma_1 T_1)-3\eta_1\varepsilon^2 G^2\bar{G}=0. \tag{4.75}$$

Now, $G(\tau)$ is expressed in the polar form as $G(\tau)=(1/2)a_1(\tau)e^{i\beta_1(\tau)}$ which on substituting in Eq. (4.75) result in the autonomous set of governing equations of modulation amplitude and phase after separating real and imaginary parts as:

$$\bar{\omega}_1(\partial a_1/\partial\tau)+\bar{\omega}_1\varepsilon\mu_1 a_1+a_1(\varepsilon\eta_2/4-\varepsilon^2\eta_2\sigma_1/8\bar{\omega}_1)\sin(\gamma_1)=0,\ \gamma_1=\sigma_1 T_1-2\beta_1.$$
$$a_1\bar{\omega}_1(\partial\gamma_1/\partial\tau)-a_1\varepsilon\bar{\omega}_1\sigma_1+a_1\left[\varepsilon^2\eta_2^2/16\bar{\omega}_1^2-\varepsilon^2\eta_2^2/4\left\{\bar{\omega}_1^2-(\bar{\omega}_1^2+\Omega^2)\right\}-\varepsilon^2\mu_1^2\right]+$$
$$a_1(\varepsilon\eta_2/2-\varepsilon^2\eta_2\sigma_1/4\bar{\omega}_1)\cos(\gamma_1)-(3/4)\alpha_1\varepsilon^2 a_1{}^3=0, \tag{4.76}$$

The first order solution in terms of original variable τ is expressed as:

$$u_1(\tau)=a_1\cos(\Omega/2-\gamma_1/2)\tau+(\varepsilon a_1\eta_2/16\omega_1^2)\cos(3\Omega/2-\gamma_1/2)\tau+O(\varepsilon^2)$$

The elimination of γ_1 for the steady-state response $\left[(\partial a_1/\partial\tau=\partial\gamma_1/\partial\tau)=0\right]$ of Eq.**Error! Reference source not found.**, renders the frequency response equation along with the trivial solution $(a_1=0)$. To determine the stability of trivial solution, the solutions of the linearized form of Eq. (4.75) are investigated; that is:

$$\left[2i\bar{\omega}_1(\partial G/\partial\tau)+2i\bar{\omega}_1\varepsilon\mu_1 G+G\Gamma_1+\bar{G}\Gamma_2\exp(\sigma_1 T_1)\right]=0 \tag{4.77}$$

Here, $\Gamma_1=\left\{\varepsilon^2\eta_2^2/16\bar{\omega}_1^2-\varepsilon^2\eta_2^2/2\left(\bar{\omega}_1^2-(\bar{\omega}_1^2+\Omega^2)\right)-\varepsilon^2\mu_1^2\right\}$, and $\Gamma_2=(\varepsilon\eta_2/2-\varepsilon^2\eta_2\sigma_1/4\bar{\omega}_1)$.

Letting G be expressed as $G(\tau)=(G_r+iG_i)\exp(i\varepsilon\sigma_1\tau/2)$ (G_r and G_i are real), substituted in Eq. (4.77) and after separating real and imaginary terms following expressions are obtained:

$$G_r'+\varepsilon\mu_1 G_r-(\sigma_1\varepsilon/2-\Gamma_1/2\bar{\omega}_1+\Gamma_2/2\bar{\omega}_1)G_i=0,$$
$$G_i'+\varepsilon\mu_1 G_i-(\Gamma_1/2\bar{\omega}_1+\Gamma_2/2\bar{\omega}_1-\sigma_1\varepsilon/2)G_r=0. \tag{4.78}$$

Here, Eq. (4.78) admits the solution in the form of $(G_r, G_i) = (\hat{G}_r, \hat{G}_i)\exp(\varepsilon\lambda_1\tau)$, where $(\hat{G}_r, \hat{G}_i)$ are arbitrary real constants. The resulting equations form an eigenvalue problem in the form expressed as:

$$\begin{vmatrix} \lambda_1 + \mu_1 & -\Gamma_{11}/\varepsilon \\ -\Gamma_{22}/\varepsilon & \lambda_1 + \mu_1 \end{vmatrix} = 0 \text{ i.e. } \lambda_1 = \mu_1 \pm \sqrt{\Gamma_{11}\Gamma_{22}/\varepsilon^2}. \tag{4.79}$$

Consequently, a trivial solution is unstable if and only if $\Gamma_{11}\Gamma_{22} > \mu_1^2\varepsilon^2$ and otherwise it is stable. The stability of the nontrivial response of the first link of the manipulator depends on the stability of the steady-state solution for the modulation amplitude and phase. The stability of the nontrivial steady-state solutions is determined by the nature of eigenvalues of the Jacobian matrix *[J]* given here as:

$$[J] = \begin{bmatrix} \varepsilon\mu_1 + \Gamma_3\sin(\gamma_{10})/\bar{\omega}_1 & a_{10}\Gamma_3\cos(\gamma_{10})/\bar{\omega}_1 \\ 2\Gamma_3\cos(\gamma_{10})/a_{10}\bar{\omega}_1 + 2\Gamma_4/a_{10}\bar{\omega}_1 - 9\varepsilon^2\eta_1 a_{10}/\bar{\omega}_1 & -2\Gamma_3\sin(\gamma_{10})/\bar{\omega}_1 \end{bmatrix}$$

Here, $\Gamma_3 = \left(\varepsilon\eta_2/2 - \varepsilon^2\eta_2\sigma_1/4\bar{\omega}_1\right)/2$, and

$$\Gamma_4 = \left\{\varepsilon^2\eta_2^2/32\bar{\omega}_1^2 - \varepsilon^2\eta_2^2/4\left(\bar{\omega}_1^2 - \left(\bar{\omega}_1^2 + \Omega^2\right)\right) - \varepsilon^2\mu_1^2/2 - \varepsilon\bar{\omega}_1\sigma_1/2\right\}.$$

The steady-state solutions are stable only if the real part of the eigenvalues is negative otherwise unstable.

4.4.4 Subharmonic resonance case in second link: $(\bar{\Omega} \approx 2\bar{\omega}_1)$

Similarly for the second link, the nearness of forcing frequency $(\bar{\Omega}_1)$ with the normalized natural frequency $(\bar{\omega}_2)$ is expressed as $\bar{\Omega}_1 = 2\bar{\omega}_2 + \varepsilon\sigma_2$. After eliminating the secular terms from Eq. (4.70) and Eq. (4.74), the governing equations of modulation amplitude and phase is obtained as:

$$\begin{aligned} &\bar{\omega}_1(\partial a_2/\partial\tau) + \bar{\omega}_2\varepsilon\mu_2 a_2 + a_2\left(\varepsilon\eta_4/4 - \varepsilon^2\eta_4\sigma_1/8\bar{\omega}_4\right)\sin(\gamma_2) = 0, \\ &a_2\bar{\omega}_2(\partial\gamma_2/\partial\tau) - a_2\varepsilon\bar{\omega}_2\sigma_2 + a_2\left(\varepsilon\eta_4/2 - \varepsilon^2\eta_4\sigma_2/4\bar{\omega}_2\right)\cos(\gamma_2) - (3/4)\eta_5\varepsilon^2 {a_2}^3 + \\ &a_2\left[\varepsilon^2\eta_4^2/16\bar{\omega}_2^2 - \alpha_6\bar{\omega}_1^2 a_1^2\varepsilon^2/2 - \varepsilon^2\eta_4^2/4\left\{\bar{\omega}_2^2 - \left(\bar{\omega}_2^2 + \Omega^2\right)\right\} - \varepsilon^2\mu_2^2\right] = 0. \end{aligned} \tag{4.80}$$

The first order solution for the second link in terms of original variable τ is obtained as:

$$u_2(\tau) = a_2\cos(0.5\Omega - 0.5\gamma_2)\tau + \varepsilon\left(a_2\eta_4/16\omega_2^2\right)\cos(1.5\Omega - 0.5\gamma_2)\tau$$
$$+\varepsilon\left(a_1\eta_3\omega_1^2/\left(\omega_1^2 + \omega_2^2\right)\right)\cos(\omega_1 + \phi)\tau + O\left(\varepsilon^2\right).$$

The stability of the trivial and nontrivial solutions of Eq. (4.80) can be investigated by following the procedure explained in previous subsection.

4.4.5 Numerical Results and Discussion

a) *Modal analysis: eigenspectrums*

This section has been dedicated to determine the modal parameters, i.e., natural frequency and modal displacement and their quantitative and qualitative evolution under the effect of variation in payload mass (α_{mC}), inertia(α_I), offset (α_c), and the offset angle(γ) is studied. The results thus obtained for various loading and configurations of the links are presented next. The first five eigenfrequencies which are obtained as the roots of the eigenfrequency equation have been plotted for the sake of comparison. The other parameters considered for the analysis are duly indicated in the respective figures.

The variation of system eigenfrequencies with payload (α_{mC}), inertia (α_I) and offset ratio (α_c) which can be regarded, respectively as the change in payload mass, inertia and variation of centre of gravity of payload is shown in Fig. 4.13. It is observed that the eigenfrequencies decrease with the increase in payload mass $\left(\omega_n \propto \sqrt{K/M}\right)$, payload inertia and also with the combined increase of both parameters. Here, the offset ratio $(\alpha_c = c/L_1)$ defines the ratio between distance of center of gravity of payload from the point of attachment with the link and link length. The higher eigenfrequencies increases as the centre of gravity the payload is moved further, away from the point of attachment while at higher payload inertia (α_I) values, even the lower eigenfrequencies increase with increase in offset ratio (α_c). Thus, the influence of combined effect of payload inertia (α_I) and offset ratio (α_c) is significant on the fundamental mode of vibration. Hence, due diligence should be taken while controlling the manipulators with the different shapes and sizes of payloads. However, it is observed that the eigenfrequencies decrease and increase with the increase in beam mass density (α_M) and flexural rigidity ratio (χ), respectively. The beam mass density ratio and flexural rigidity ratio can be varied by manipulating the cross-sectional area of the links.

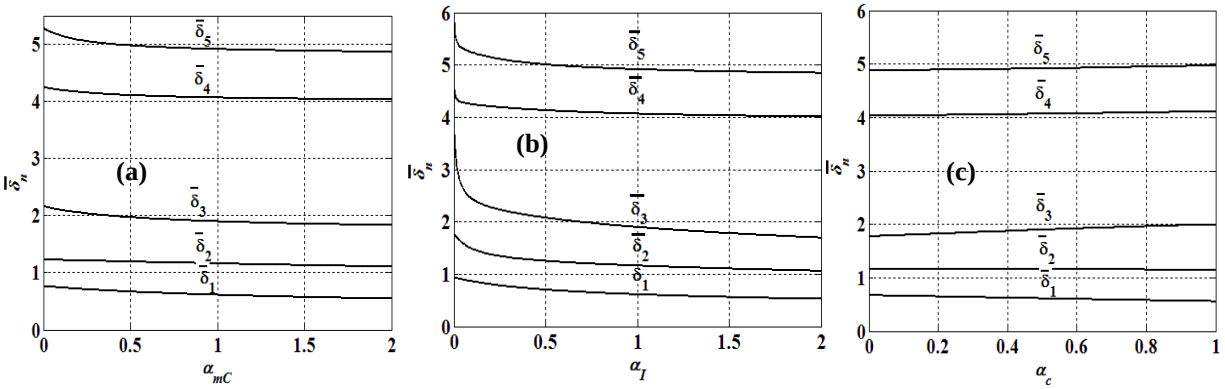

Fig. 4.13: Effect of (a) payload mass (α_{mC}), (b) inertia (α_I), and (c) offset ratio (α_c) on the eigenfrequencies of flexible two-link manipulator for (α_{m1}) =0, α_M =1.0, χ =1.0, α_L =1.0, and γ =0.

Modal displacements $W_1^n(\bar{x})$ and $W_2^n(\bar{x})$ are expressed by Eq. **Error! Reference source not found.** that represent the eigenfunctions of the first and second link, respectively for nth mode of vibration. The influences of various decision variables on the eigenspectrums are investigated in the next section. The variation of first four mode shapes of two-link manipulator when the mass of the payload lifted by manipulator represented by payload mass (α_{mC}) is shown in Fig. 4.14. Mode shape for no payload condition $(\alpha_{mC} = 0)$ has also been reported. Modal deflection along the length of manipulator for lower modes of vibration decreases as the payload mass increases. Figure also depicts the cluttering of the mode shapes in the higher modes of vibration. The mode shapes of the manipulator carrying payload vary significantly as compared with the no payload condition.

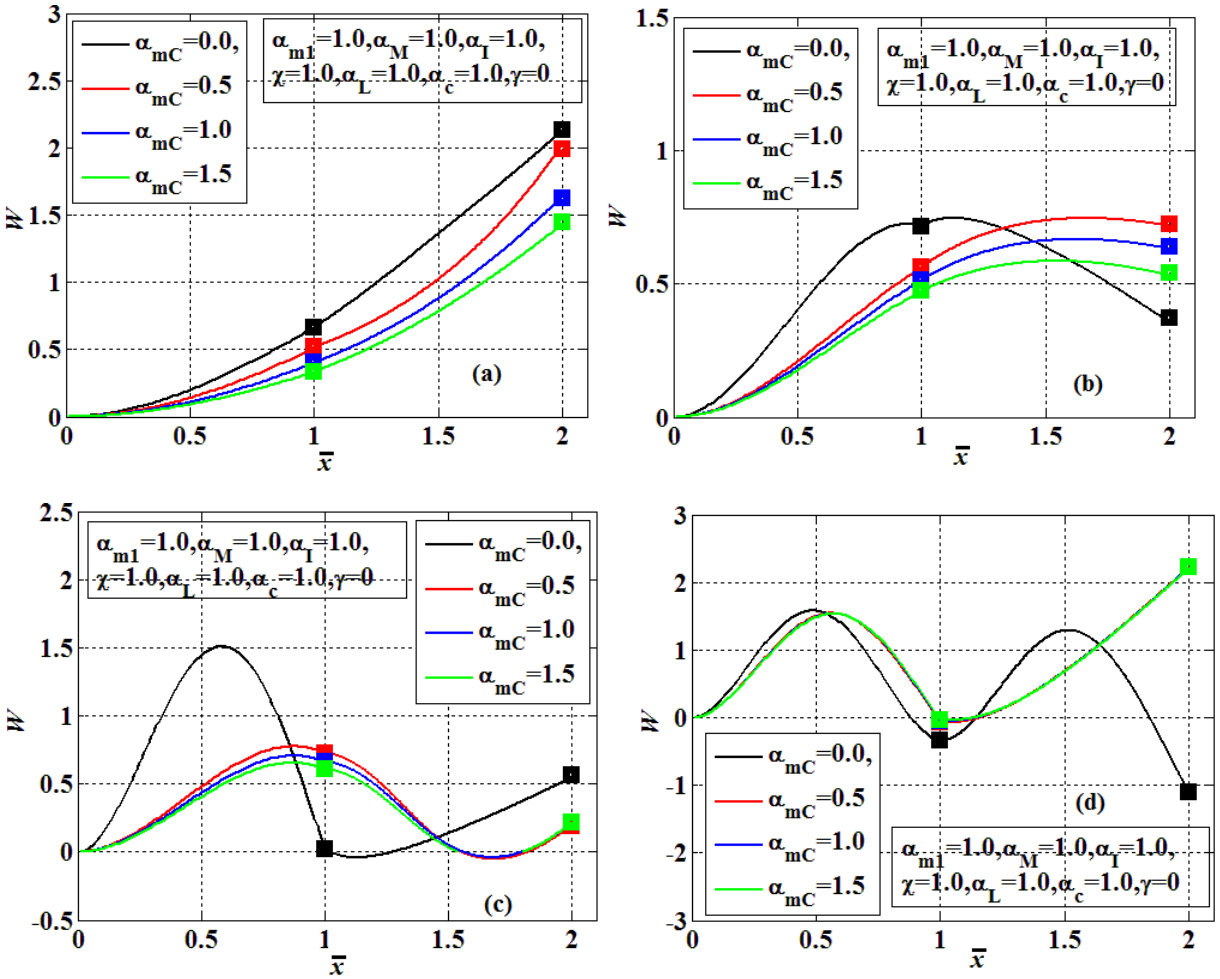

Fig. 4.14: Variation of first four mode shapes of flexible two-link manipulator with payload mass (α_{mc}) (a) mode 1 (b) mode 2 (c) mode 3 (d) mode4.

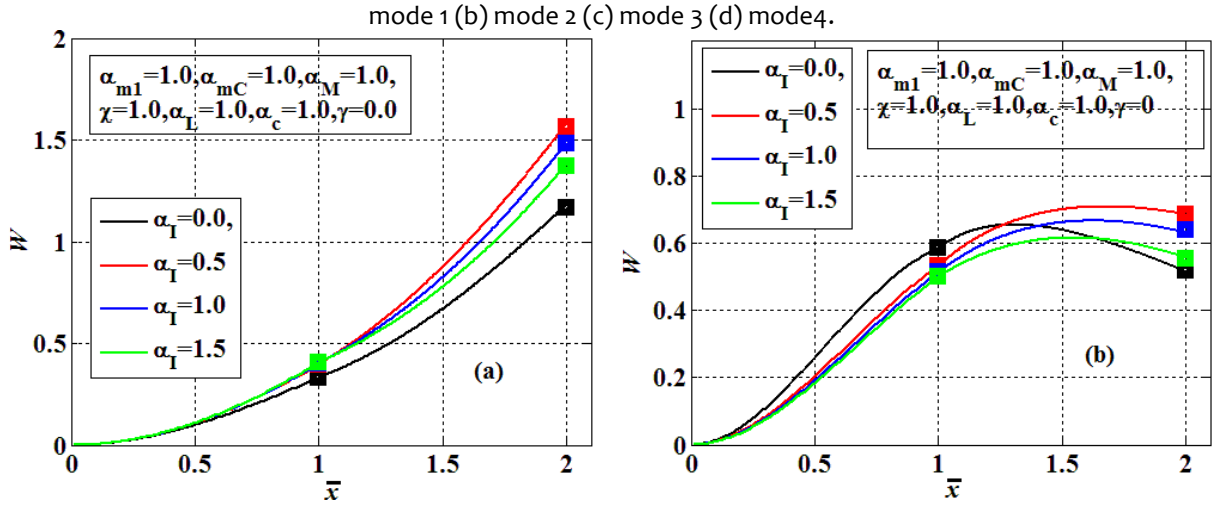

Fig. 4.15: Variation of mode shapes of flexible two-link manipulator with payload inertia parameter (α_I) (a) mode 1 (b) mode 2.

The influence of payload inertia (α_I) on the eigenspectrums is illustrated in Fig. 4.15. The modal deflection suddenly increases with the introduction of inertia $(\alpha_I \neq 0)$ in the payload and thereafter there is subsequent decrease in deflection with the increase in payload inertia. Cluttering of mode shapes can be observed in higher modes of vibration when the inertia parameter is varied.

The influence of offset ratio (α_c) on the eigenspectrums is shown in Fig. 4.16. The offset ratio is varied from 0 to 1.0, which shall be sufficient to cover all the practical values while

$\alpha_c = 0$ corresponds to the condition when the centre of gravity is coincident with the point of attachment with the second link. It is observed that the first mode deflection decreases as the offset ratio (α_c) increases. However, in higher modes of vibration as the offset ratio increases the mode shapes tend to clutter together along the length of manipulator. As the orientation of the payload (γ) is changed from axial $(\gamma = 0)$ to the perpendicular $(\gamma = 90^0)$, the modal deflection decreases while higher modes of vibration tend to clutter together as depicted in Fig. 4.17.

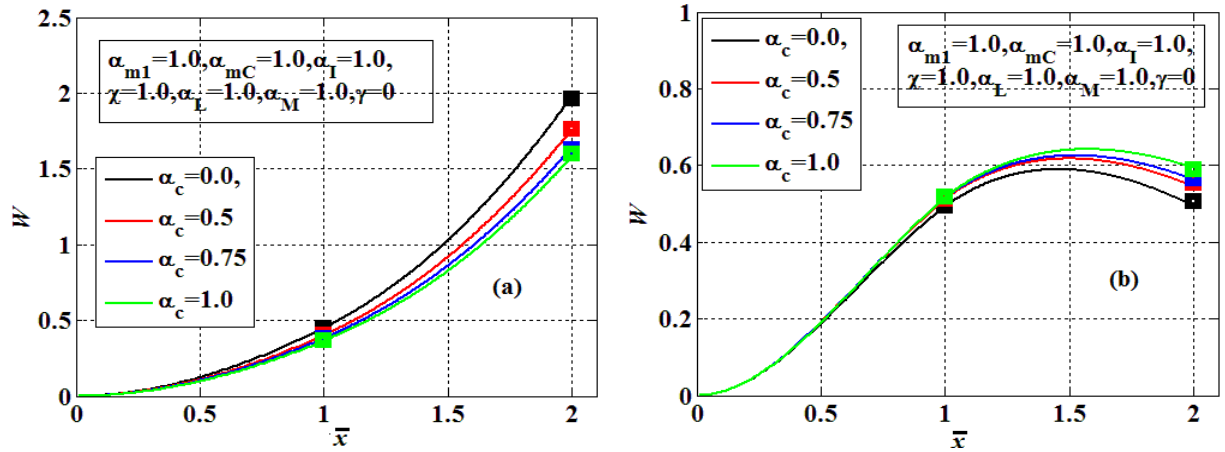

Fig. 4.16: Variation of mode shapes of flexible two-link manipulator with offset ratio (α_c) (a) mode 1 (b) mode 2.

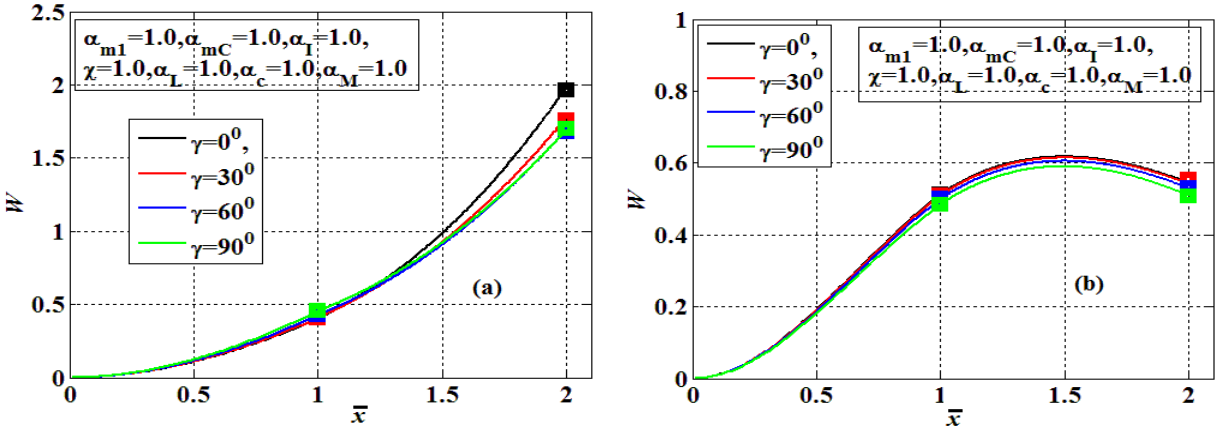

Fig. 4.17: Variation of mode shapes of flexible two-link manipulator with offset angle (γ) (a) mode 1 (b) mode 2.

The significant influence of offset payload parameters on the fundamental frequency and eigenspectrums of the manipulator shall be an essential consideration while designing the control strategies for the flexible manipulator involved in operations where the terminal link of the manipulator is involved in lifting/grabbing payloads of different shapes and sizes because the fundamental frequency of the manipulator is significantly affected by the payload parameters.

b) *Nonlinear analysis: bifurcation and stability*

The geometrical and physical characteristics considered in nonlinear analysis for both links are, width b = 0.03 m, height h = 0.003 m and length L = 0.3 m. The nondimensional damping coefficients $(\xi_{1,2})$, amplitude ratio of $\bar{F}_0$, and $\bar{F}_1$ are chosen as 0.01, 0.005 and 0.005, respectively. In all numerical simulations, bookkeeping parameter *(ε)* and scaling factor *(r)* are selected as 0.1 and 0.001, respectively; the other parameters are indicated in the figures. The frequency response equations obtained from Eqs. **Error! Reference source not found.**-**Error! Reference source not found.** for first and second link, respectively are a nonlinear algebraic equations in terms of steady-state amplitudes $a_{1,2}$, and detuning parameters $\sigma_{1,2}$. The

equations are solved numerically and the results are presented in Figs. 4.18-4.25 as the amplitudes have been plotted against the external frequency at the given values of essential system parameters. The solid lines in the figures represent stable solutions, while the dashed line depicts the unstable solutions. A representative frequency curve for the first and second link is shown in Fig. 4.18 from which it can be deduced that the amplitude of second link at a particular frequency is significantly larger than that of first link.

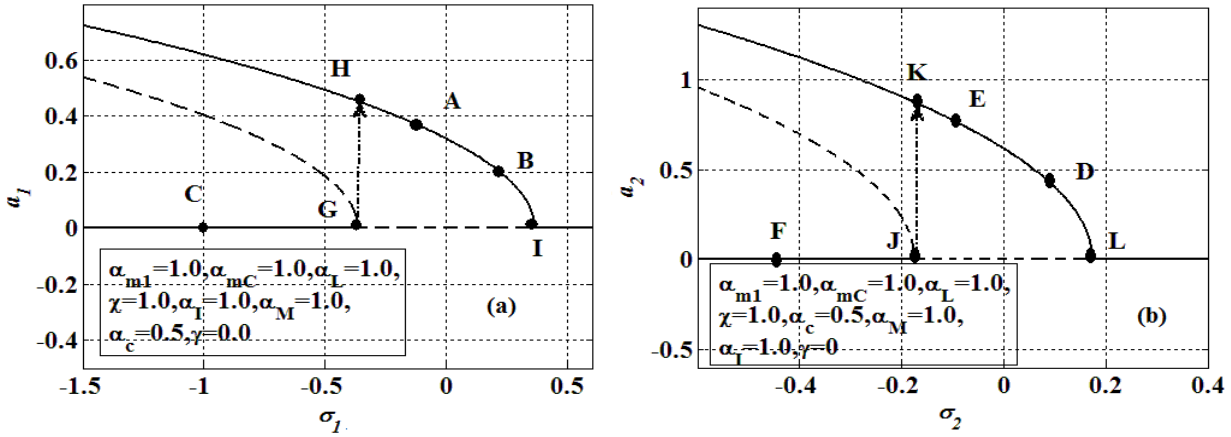

Fig. 4.18: Frequency response characteristics of (a) first and (b) second link of two-link manipulator with generic payload.

It is also noted that the frequency curves are bent towards the left for both the links, indicating softening type nonlinearities leading to multivalued amplitudes at the same forcing frequency (Ω_1). The jump phenomenon is observed at the bifurcation points G and J for first and second link respectively. In the detuning parameter region $-0.4 \leq \sigma_1 \geq 0.4$ for first link and $-0.18 \leq \sigma_2 \geq 0.18$ for second link, there are two solutions, the trivial solutions and upper branch solutions. Since the trivial solution is unstable in this region, the only possible response for the link's operation in this frequency range lies on the upper branch. On the left region of $-0.4 < \sigma_1$ for first link and $-0.18 < \sigma_2$ for second link, the system has three possible solutions, a stable trivial solution, an unstable nontrivial solution of smaller amplitude and a stable nontrivial solution of larger amplitude. In these regions the amplitudes of the link can be trivial or nontrivial depending on the initial conditions considered for performance. For large values of detuning parameters, the links vibrate at the nontrivial amplitudes for small initial conditions. However, as the detuning parameters is slowly increased to the left bifurcation point (a subcritical pitchfork bifurcation) G for first link (J for second link), the link experiences a sudden jump to the upper branch at point H for first link (K for second link). Further increase in detuning parameter leads to the decrease in amplitude till the right bifurcation point (a supercritical pitchfork bifurcation) at I for first link (L for second link) where the solution again becomes trivial. This sudden jump in the system's vibration may cause catastrophic failure which can be avoided by operating the manipulator in safe zones indicated in the frequency response curves. The equation of motion represented by Eq. **Error! Reference source not found.** is solved numerically by using fourth-order Runge-Kutta method and the results are found to be in good agreement with analytical outcomes for assorted critical points. Fig. 4.19 shows the time response, phase portrait, and FFT of first link at the critical points A, B, and C keyed to Fig. 4.18.

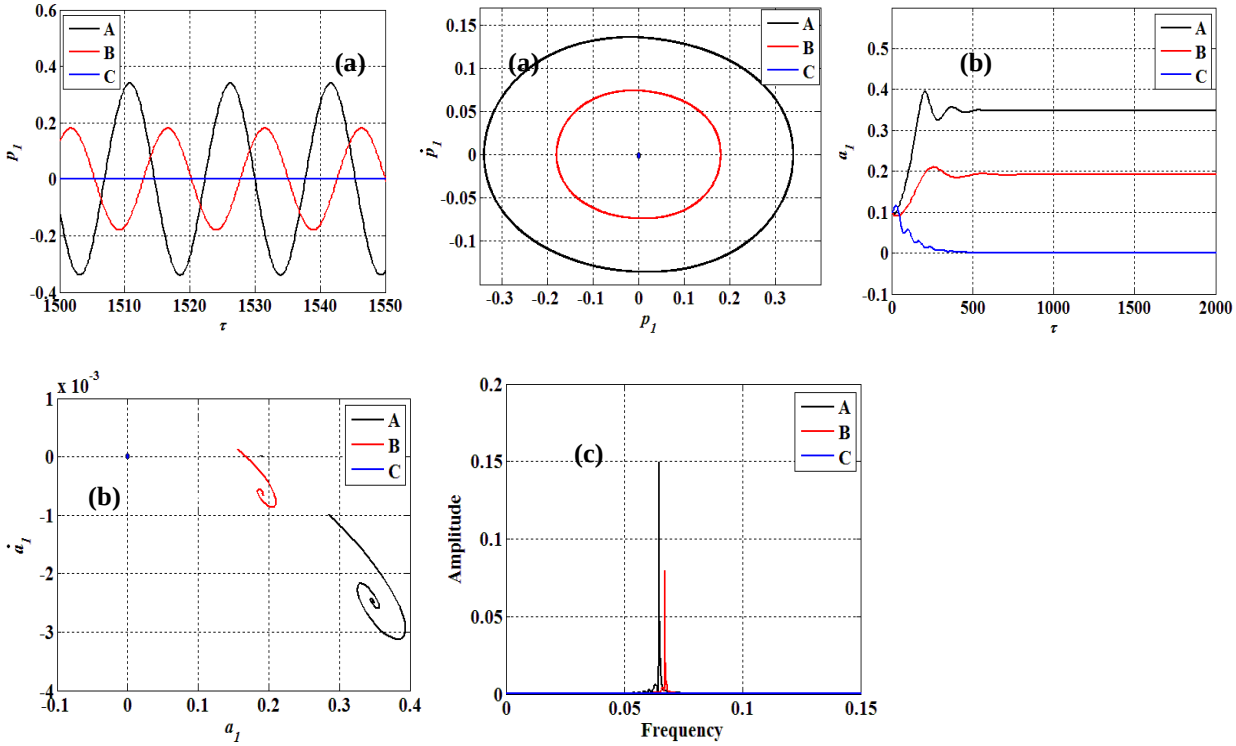

Fig. 4.19: Analytical (a) numerical (b) time history, phase portrait, and FFT (c) of first link identified in Fig. 4.18 at the point A, B, and C.

Four cases of different payload conditions and inclusion of nonlinearity have been compared in Fig. 4.20. Case I represents no payload $(\alpha_{mC}=0)$ condition and in case II the payload is considered as a point mass having no inertia $(\alpha_{mC}\neq 0,\alpha_I=0,\alpha_c=0)$. It is evident that the amplitude and the unstable region increase significantly with the inclusion of payload. Case III denotes the condition when inertia is included $(\alpha_{mC}\neq 0,\alpha_I\neq 0,\alpha_c=0)$ in the payload and Case IV represents a generic payload having mass, inertia and offset $(\alpha_{mC}\neq 0,\alpha_I\neq 0,\alpha_c\neq 0)$ as well. The unstable region again widens with the consideration of inertia and offset, however, the amplitude at a specific forcing frequency decreases with the inclusion of generic payload. It can also be noticed from the figure that the consideration of nonlinearity bends the frequency response curve exhibiting multiple solutions and jump phenomenon. Now in the further text, the effect of system parameters variation on the frequency response curved of both the links has been thoroughly studied.

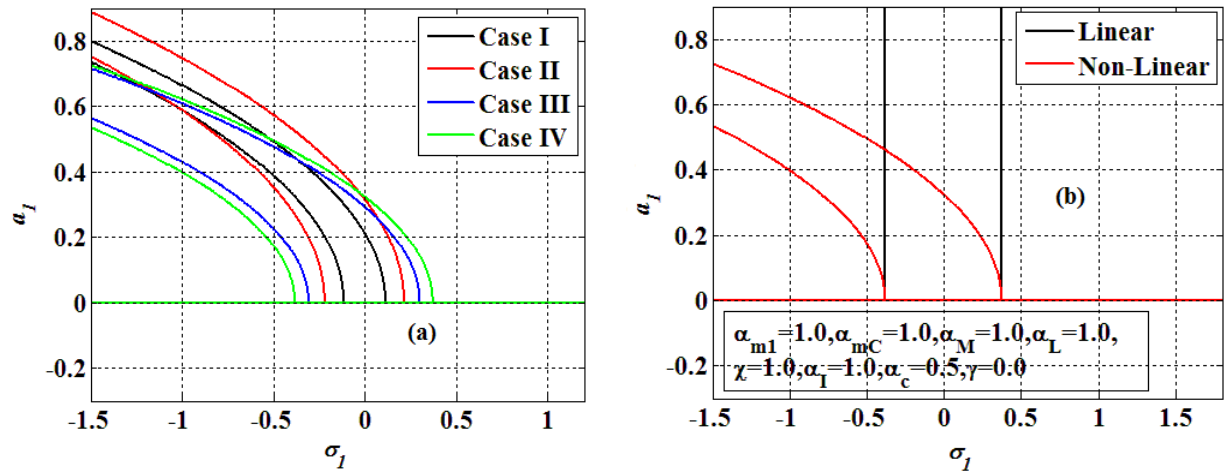

Fig. 4.20: Comparison of (a) four different payload conditions and (b) linear and nonlinear model.

The effect of payload mass (α_{mC}) on the frequency response curves of first and second link is illustrated in Fig. 4.21. The amplitude at a particular forcing frequency increases with the increase in payload mass (α_{mC}) and it is also observed that the unstable region between the critical bifurcation points increases for both the links. The variation of frequency response curve of both the links with respect to payload inertia (α_I) is shown in Fig. 4.22. It is observed that the amplitude of the links for a particular frequency decrease with the increase in payload inertia. Also, the unstable region between the bifurcation points for both the links widens as the inertia of the payload is increased. The effect of increasing the distance of the centre of gravity of the payload from the point of attachment with the link on the frequency response of links is demonstrated in Fig. 4.23. As the offset ratio (α_c) increases, the branches of the response curve for the first link converge and unstable region slightly increases, while for the second link the branches diverge resulting in increase of unstable region.

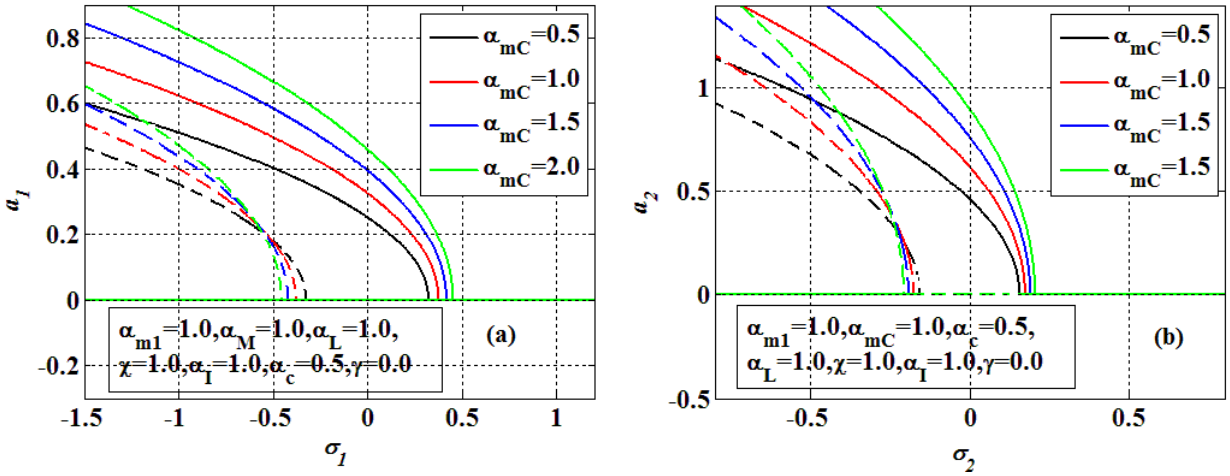

Fig. 4.21: Variation of frequency response curves of (a) first and (b) second link with payload mass (α_{mC}).

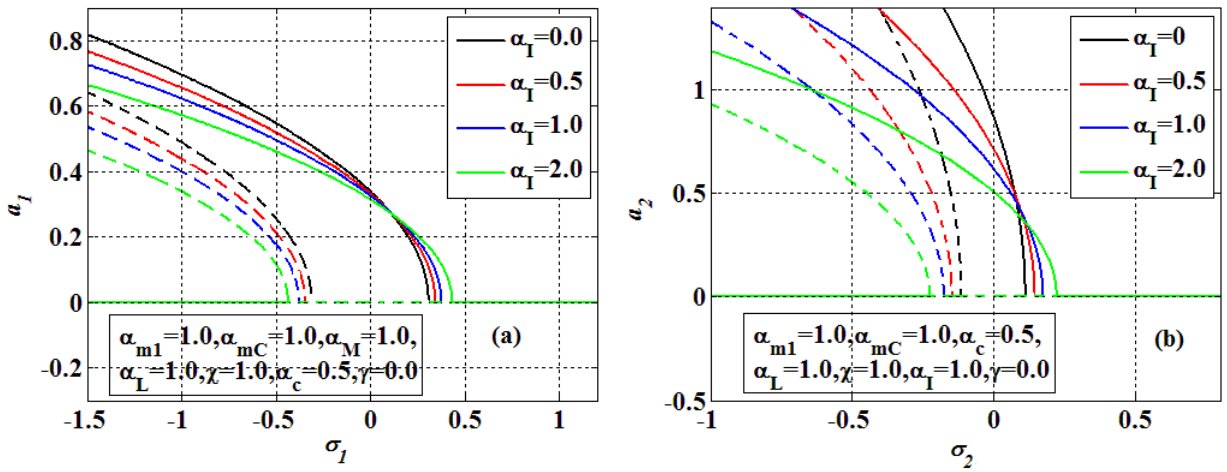

Fig. 4.22: Variation of frequency response curves of (a) first and (b) second link with payload inertia (α_I).

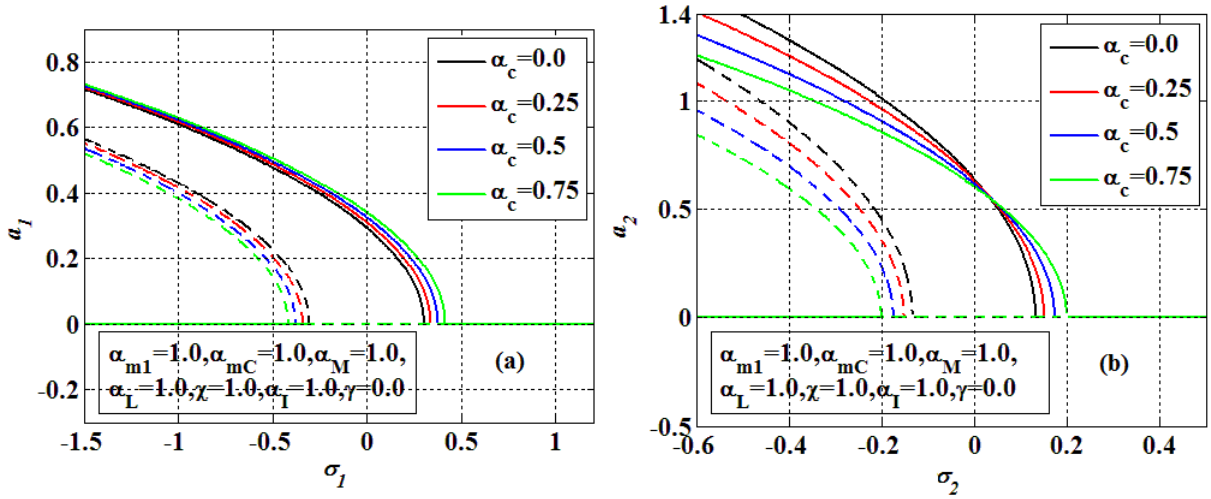

Fig. 4.23: Variation of frequency response curves of (a) first and (b) second link with payload offset (α_c).

The maximum amplitudes of both links decreases with the beam mass density (α_M) as shown in Fig. 4.24. The unstable region between two bifurcation points decrease significantly with beam density in case of second link. The effect of flexural rigidity ratio (χ) on the maximum amplitude of the link is significant in case of second link as illustrated in Fig. 4.25. The increase in flexural rigidity ratio leads to the increase in maximum amplitude with marginal effect on the region of instability.

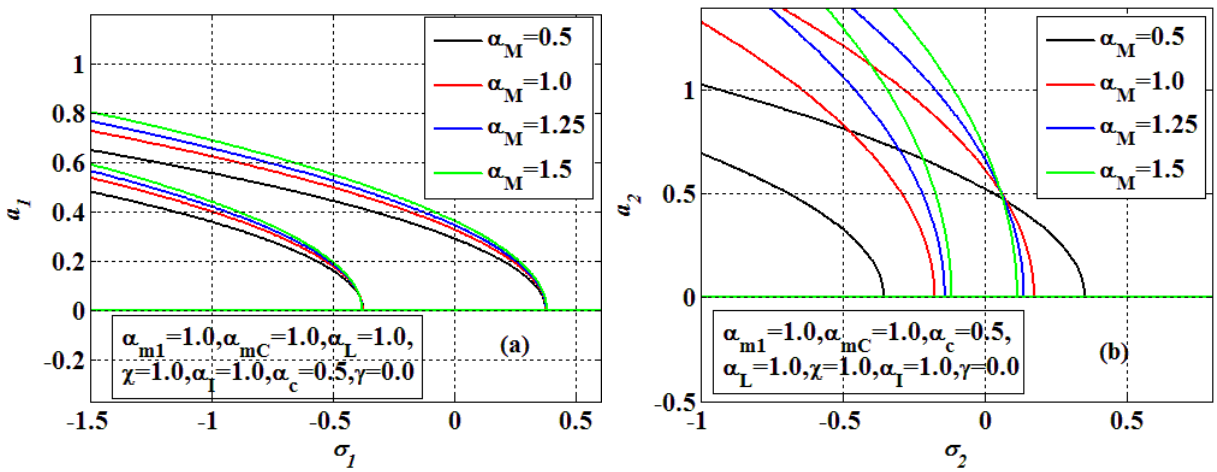

Fig. 4.24: Variation of frequency response curves of (a) first and (b) second link with beam mass density ratio (α_M).

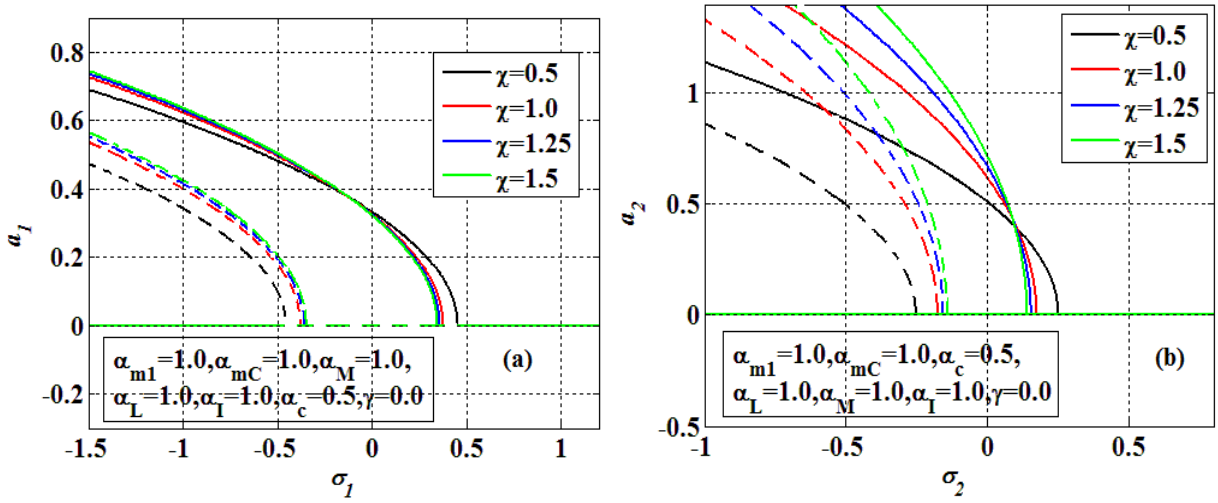

Fig. 4.25: Variation of frequency response curves of (a) first and (b) second link with flexural rigidity ratio (χ).

The fundamental eigenfrequency of the manipulator is significantly affected by the payload parameters and hence, it is very essential to take the size, shape and orientation of the payload into consideration while designing. In addition, the orientation of the externally applied constraint force may directly or parametrically excite the system depending on its orientation with respect to the centre of gravity of payload. Thus, the type of payload and its attributes may have implications on the stability of the system under external or parametric excitations. The results thus obtained shall be useful in the vibration attenuation of the flexible manipulator gripping a generic payload and working under the environment where the end-effector is subjected to pulsating force such as spraying, painting, grinding etc.

4.5 FLEXIBLE MANIPULATOR WITH HARMONIC REVOLUTE PAIRS

Consider a planar flexible two-link manipulator incorporating an extended payload being driven by two motors representing flexible joints as shown in Fig. 4.26. A brief dynamic modeling has been presented considering the planar revolute motions of the joints along with links undergoing geometric stretching. The flexible revolute joints are modeled as torsional spring-inertia elements.

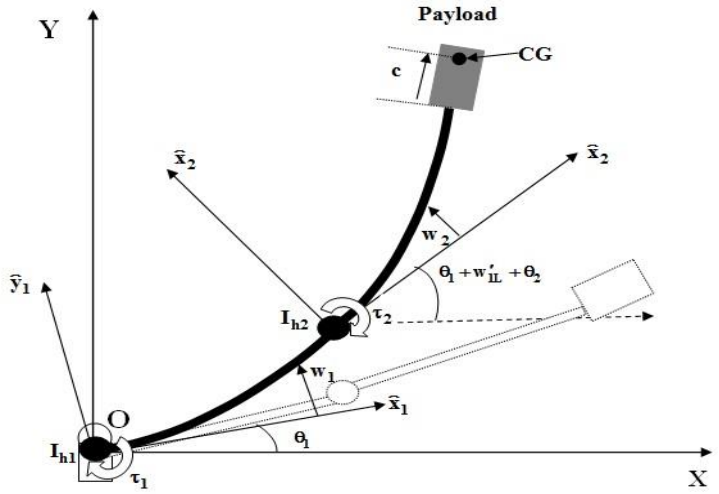

Fig. 4.26: A planar two-link flexible robotic manipulator connected with flexible revolute pair.

The position vector of general point and the position vector of centre of gravity of the extended payload are given as:

$$\vec{P}_n = \begin{bmatrix} x \\ (w_n + y) \end{bmatrix}^{(x_n, y_n)}, \quad \vec{P}_C = \vec{P}_{(n-1)L} + \begin{bmatrix} L_n + \cos(w'_{nL}) \\ u_{nL} \end{bmatrix}^{(x_n, y_n)}. \tag{4.81}$$

The expressions for the total kinetic energy (T_{Total}) and potential energy (U_{Total}) of the system are respectively given by:

$$T_{total} = (1/2)\sum_{i=1}^{2}\left(\int_0^{L_i} \rho_i \dot{\vec{q}}_i^{\,T} \dot{\vec{q}}_i dx\right) + \sum_{i=1}^{2} m_i \dot{\vec{P}}_i^{\,T} \dot{\vec{P}}_i + (1/2)\left[I_{h1}\dot{\theta}_1^{\,2} + I_{h2}\left(\dot{\theta}_1 + \dot{\theta}_2 + \dot{w}'_{1L}\right)^2\right]. \tag{4.82}$$

$$U_{total} = (1/2)\left[\sum_{i=1}^{2}\int_0^{L_i} E_i I_i \left(w_i''\right)^2 dx + \int_0^{L_i} E_i A_i \left(u_i' + (1/2)w_1'^2\right)^2 dx + \left\{k_{\theta 1}\theta_1^{\,2} + k_{\theta 2}\left(\theta_1 + \theta_2 + w'_{1L}\right)^2\right\}\right]. \tag{4.83}$$

The virtual works done by the external torques $(\tau_{1,2})$ applied at the joints and the non-conservative force due to structural damping $(c_{d1,2})$ in the links are:

$$\delta W + \delta W_{nc} = \tau_1 \delta\varphi_1 + \tau_2 \delta\varphi_2 - c_{d1}\dot{w}_1 \delta w_1 - c_{d2}\dot{w}_2 \delta w_2. \tag{4.84}$$

The kinetic energy due to revolute motion of the links, payload inertia and potential energy due the strain energy of joint stiffness is added in Eqs. (4.3)-(4.4) while the gravitational potential energy of the system is neglected. The extended Hamilton's principle $\sum_{1}^{2}\int_{t_1}^{t_2}\delta(T-U)dt=\delta W+\delta W_{nc}$, $\delta(t_1)=\delta(t_2)$ is exploited using Eqs. (4.81)-(4.84) to obtain the governing equations and boundary conditions along with the joint dynamics which are further solved to derive the eigenfrequency equation and mode shapes of the system.

Equation of motion for first link is expressed as:

$$\{w_1\}:\ \rho_1 A_1\left(\ddot{w}_1+x\ddot{\theta}_1-w_1\dot{\theta}_1^{\,2}\right)+c_{d1}\dot{w}_1+E_1I_1w_1''''-E_1A_1\left((3/2)w_1'^{\,2}w_1''\right)=0. \tag{4.85}$$

The associated boundary conditions for the first link are:

$$\{E_1I_1w_1\}_{(0,t)}=0,\{E_1I_1w_1'\}_{(0,t)}=0,$$

$$\int_0^{L_2}\rho_2A_2\left(x\ddot{w}_2+x^2\ddot{w}_{1L}'+x^2\ddot{\theta}_1+x^2\ddot{\theta}_2+2w_2\dot{w}_2\dot{\theta}_1+2w_2\dot{w}_2\dot{\theta}_2+2w_2\dot{w}_2\dot{w}_{1L}'+w_2{}^2\ddot{\theta}_1+w_2{}^2\ddot{\theta}_2+w_2{}^2\ddot{w}_{1L}'\right)dx$$

$$+E_1I_1w_{1L}''+m_C(L_2\ddot{w}_{2L}+L_2{}^2\ddot{w}_{1L}'+L_2{}^2\ddot{\theta}_2+L_2{}^2\ddot{\theta}_1+2w_{2L}\dot{w}_{2L}\dot{\theta}_1+2w_{2L}\dot{w}_{2L}\dot{\theta}_2+2w_{2L}\dot{w}_{2L}\dot{w}_{1L}'+w_{2L}^2\ddot{\theta}_1+$$

$$w_{2L}^2\ddot{\theta}_2+w_{2L}^2\ddot{w}_{1L}'+c\ddot{w}_{2L}+c^2\ddot{w}_{1L}'+c^2\ddot{\theta}_1+c^2\ddot{\theta}_2+2L_2c\ddot{\theta}_1+2L_2c\ddot{\theta}_2+L_2c\ddot{w}_{1L}'+L_2c\ddot{w}_{2L}'+c^2\ddot{w}_{2L}')+$$

$$I_{h2}\left(\ddot{\theta}_1+\ddot{\theta}_2+\ddot{w}_{1L}'\right)+I_C\left(\ddot{\theta}_1+\ddot{\theta}_2+\ddot{w}_{1L}'+\ddot{w}_{2L}'\right)+k_{\theta2}\left(\theta_1+\theta_2+w_{1L}'\right)-\{E_2I_2w_2''\}_{(x=0)}=0,$$

$$(m_1+m_C)\left(\ddot{w}_{1L}+L_1\ddot{\theta}_1-w_{1L}\dot{\theta}_1^{\,2}\right)+\int_0^{L_2}\rho_2A_2\left(\ddot{w}_{1L}+L_1\ddot{\theta}_1-w_{1L}\dot{\theta}_1^{\,2}\right)dx-E_1I_1w_{1L}'''+ \tag{4.86}$$

$$E_2I_2w_2'''(0,t)+E_1A_1\left((1/2)w_{1L}'^{\,3}\right)=0.$$

Equation of motion for second link is expressed as:

$$\{w_2\}:\ \begin{matrix}\rho_2A_2\left(\ddot{w}_2+x\ddot{w}_{1L}'+x\ddot{\theta}_1+x\ddot{\theta}_2-w_2\dot{\theta}_1^{\,2}-w_2\dot{\theta}_2^{\,2}-w_2\dot{w}_{1L}'^{\,2}-2\dot{\theta}_1\dot{\theta}_2v_2-2\dot{\theta}_2w_2\dot{w}_{2L}'+2\dot{\theta}_1w_2\dot{w}_{2L}'\right)+\\ c_{d2}\dot{w}_2+E_2I_2w_2''''-E_2A_2\left\{(3/2)w_2'^{\,2}w_2''\right\}=0.\end{matrix} \tag{4.87}$$

The associated boundary conditions for the second link are:

$$\{E_2I_2w_2\}_{(0,t)}=\{E_1I_1w_1\}_{(L_1,t)},\{E_2I_2w_2'\}_{(0,t)}=\{E_1I_1w_1'\}_{(L_1,t)},$$

$$E_2I_2w_{2L}''+m_C\begin{pmatrix}c\ddot{w}_{2L}+c^2\ddot{\theta}_1+c^2\ddot{\theta}_2+c^2\ddot{w}_{1L}'+cL_2\ddot{\theta}_1+cL_2\ddot{\theta}_2+\\ cL_2\ddot{w}_{1L}'+c^2\ddot{w}_{2L}'\end{pmatrix}+I_c\left(\ddot{\theta}_1+\ddot{\theta}_2+\ddot{w}_{1L}'+\ddot{w}_{2L}'\right)=0,$$

$$m_C\begin{pmatrix}\ddot{w}_{2L}+L_2\ddot{w}_{1L}'+L_2\ddot{\theta}_1+L_2\ddot{\theta}_2-2w_{2L}\dot{\theta}_2\dot{w}_{1L}'-w_{2L}\dot{w}_{1L}'^{\,2}-w_{2L}\dot{\theta}_1^{\,2}-w_{2L}\dot{\theta}_2^{\,2}-\\ 2w_{2L}\dot{\theta}_1\dot{\theta}_2-2w_{2L}\dot{\theta}_1\dot{w}_{1L}'\end{pmatrix} \tag{4.88}$$

$$-E_2I_2w_{2L}'''+E_2A_2\left\{(1/2)w_{2L}'^{\,3}\right\}=0.$$

The governing equation of first joint motion is expressed as:

$$
\begin{aligned}
&\int_0^{L_1}\rho_1 A_1\left(x\ddot{w}_1+x^2\ddot{\theta}_1+{w_1}^2\ddot{\theta}_1+2w_1\dot{w}_1\dot{\theta}_1\right)dx+m_1\left(L_1\ddot{w}_{1L}+{L_1}^2\ddot{\theta}_1+2w_{1L}\dot{w}_{1L}\dot{\theta}_1\right)\\
&\int_0^{L_2}\rho_2 A_2\begin{pmatrix}x^2\ddot{\theta}_1+x^2\ddot{\theta}_2+2w_{2L}\dot{w}_{2L}\dot{\theta}_1+{w_{1L}}^2\ddot{\theta}_1+{L_1}^2\ddot{\theta}_1+2w_1\dot{w}_1\dot{\theta}_1+{w_2}^2\ddot{\theta}_1+x\ddot{w}_2+\\ x^2\ddot{w}'_{1L}+L_1\ddot{w}_{1L}+{w_2}^2\ddot{w}'_{1L}+2w_2\dot{w}_2\dot{\theta}_2+{w_2}^2\ddot{\theta}_2+2w_2\dot{w}_2w'_{1L}\end{pmatrix}dx\\
\{\theta_1\}:\ &+m_2\begin{pmatrix}2w_{1L}\dot{w}_{1L}\dot{\theta}_1+{w_{1L}}^2\ddot{\theta}_1+L_1\ddot{w}_{1L}+{L_1}^2\ddot{\theta}+{w_{2L}}^2\ddot{\theta}_2+L_2\ddot{w}_{2L}+{L_2}^2\ddot{\theta}_1+{L_2}^2\ddot{\theta}_2+{L_2}^2\ddot{w}_{1L}+\\ 2w_{2L}\dot{w}_{2L}\dot{\theta}_1+2w_{2L}\dot{w}_{2L}\dot{\theta}_1+2w_{2L}\dot{w}_{2L}w'_{1L}+{w_{2L}}^2\ddot{w}'_{1L}+c\ddot{w}_{2L}+c^2\ddot{\theta}_1+c^2\ddot{\theta}_2+c^2\ddot{w}_{1L}+\\ 2cL_2\ddot{\theta}_1+2cL_2\ddot{\theta}_2+2cL_2\ddot{w}_{1L}+c^2\ddot{w}_{2L}+cL_2\ddot{w}'_{2L}\end{pmatrix}\\
&+I_{h1}\ddot{\theta}_1+I_{h2}\left(\ddot{\theta}_1+\ddot{\theta}_2+\ddot{w}'_{1L}\right)+k_{\theta 1}\theta_1+k_{\theta 2}\left(\theta_1+\theta_2+w'_{1L}\right)+I_c\left(\ddot{\theta}_1+\ddot{\theta}_2+\ddot{w}'_{1L}+\ddot{w}'_{2L}\right)=\tau_1.
\end{aligned}
\tag{4.89}
$$

The governing equation of second joint motion is expressed as:

$$
\begin{aligned}
&\int_0^{L_2}\rho_2 A_2\begin{pmatrix}x^2\ddot{\theta}_1+x^2\ddot{\theta}_2+2w_{2L}\dot{w}_{2L}\dot{\theta}_1+{w_2}^2\ddot{\theta}_1+x\ddot{w}_2+x^2\ddot{w}'_{1L}+{w_2}^2\ddot{w}'_{1L}+2w_2\dot{w}_2\dot{\theta}_2+\\ {w_2}^2\ddot{\theta}_2+2w_2\dot{w}_2w'_{1L}\end{pmatrix}dx\\
\{\theta_2\}:\ &+m_2\begin{pmatrix}{w_{2L}}^2\ddot{\theta}_2+L_2\ddot{w}_{2L}+{L_2}^2\ddot{\theta}_1+{L_2}^2\ddot{\theta}_2+{L_2}^2\ddot{w}'_{1L}+2w_{2L}\dot{w}_{2L}\dot{\theta}_1+2w_{2L}\dot{w}_{2L}\dot{\theta}_1\\ +2w_{2L}\dot{w}_{2L}w'_{1L}+{w_{2L}}^2\ddot{w}'_{1L}+c\ddot{w}_{2L}+c^2\ddot{\theta}_1+c^2\ddot{\theta}_2+c^2\ddot{w}'_{1L}+2cL_2\ddot{\theta}_1+2cL_2\ddot{\theta}_2+\\ 2cL_2\ddot{w}'_{1L}+c^2\ddot{w}'_{2L}+cL_2\ddot{w}'_{2L}\end{pmatrix}\\
&+I_{h2}\left(\ddot{\theta}_1+\ddot{\theta}_2+\ddot{w}'_{1L}\right)+k_{\theta 2}\left(\theta_1+\theta_2+w'_{1L}\right)+I_c\left(\ddot{\theta}_1+\ddot{\theta}_2+\ddot{w}'_{1L}+\ddot{w}'_{2L}\right)=\tau_2.
\end{aligned}
\tag{4.90}
$$

4.5.1 Free vibration analysis

For modal analysis, the coupled nonlinear terms from Eqs. (4.85)-(4.90) are neglected and the transverse deflections of first and second links are derived in terms of new functions in space and time as $r_1(x,t)=w_1(x,t)+x\theta_1$ and $r_2(x,t)=w_2(x,t)+x\left(\theta_1+\theta_2+w'_{1L}\right)$, which are further expressed as $r_1(x,t)=W_1^n(x)\cos(\omega_m t)$ and $r_2(x,t)=W_2^n(x)\cos(\omega_m t)$, while angular rotations are denoted as $\theta_1=\bar{\theta}_{10}\cos(\omega_m t)$, and $\theta_2=\bar{\theta}_{20}\cos(\omega_m t)$, respectively. Here, $W_1^n(\mathrm{x})$ and $W_2^n(\mathrm{x})$ are the corresponding eigenfunction for the first and second link for the n[th] mode of vibration, respectively, while $\bar{\theta}_{10}$ and $\bar{\theta}_{20}$ are the amplitudes of joint rotations and ω_m is the unknown eigenfrequency of the whole system. The mode shapes of the links are obtained by substituting above expressions in the linearized equation of motions of the links given by Eq. (4.85) & Eq. (4.87) as:

$$W_1^n(\bar{x})=G^n{}_1\left\{\cos\left(\bar{\delta}^n\bar{x}\right)-\cosh\left(\bar{\delta}^n\bar{x}\right)\right\}+G_2{}^n\sin\left(\bar{\delta}^n\bar{x}\right)+G_4{}^n\sinh\left(\bar{\delta}^n\bar{x}\right). \tag{4.91}$$

$$W_2^n(\bar{x})=H_1{}^n\cos\left(\mu\bar{\delta}^n\bar{x}\right)+H_2{}^n\sin\left(\mu\bar{\delta}^n\bar{x}\right)+H_3{}^n\cosh\left(\mu\bar{\delta}^n\bar{x}\right)+H_4{}^n\sinh\left(\mu\bar{\delta}^n\bar{x}\right). \tag{4.92}$$

A system of seven algebraic equations is obtained after substituting Eqs. (4.91)-(4.92) in the boundary conditions along with the consideration of the joint dynamics which are further arranged in the form of matrix similar to Eq. (4.12) whose elements are given as:

$K_{11}=-\cos\left(\bar{\delta}^n\right)-\cosh\left(\bar{\delta}^n\right)$, $K_{12}=-\sin\left(\bar{\delta}^n\right)$, $K_{13}=\sinh\left(\bar{\delta}^n\right)$, $K_{14}=\chi\mu^2$, $K_{16}=-\chi\mu^2$,

$K_{21}=\sin\left(\bar{\delta}^n\right)-\sinh\left(\bar{\delta}^n\right)+\left(\alpha_{m1}+\alpha_{mC}+\alpha_M\alpha_L\right)\bar{\delta}^n\left(\cos\left(\bar{\delta}^n\right)-\cosh\left(\bar{\delta}^n\right)\right)$,

$K_{22}=-\cos\left(\bar{\delta}^n\right)+\left(\alpha_{m1}+\alpha_{mC}+\alpha_M\alpha_L\right)\bar{\delta}^n\sin\left(\bar{\delta}^n\right)$,

$K_{23}=\cosh\left(\bar{\delta}^n\right)+\left(\alpha_{m1}+\alpha_{mC}+\alpha_M\alpha_L\right)\bar{\delta}^n\sinh\left(\bar{\delta}^n\right)$, $K_{25}=\chi\mu^3$, $K_{27}=-\chi\mu^3$,

$K_{34}=\chi\lambda^3\sin\left(\lambda\bar{\delta}^n\right)+\alpha_{mC}\bar{\delta}^n\left\{\cos\left(\lambda\bar{\delta}^n\right)-\bar{\delta}^n\alpha_c\mu\sin\left(\lambda\bar{\delta}^n\right)\right\}$,

$$K_{35}=-\chi\mu^3\cos\left(\lambda\bar{\delta}^n\right)+\alpha_{mC}\bar{\delta}^n\left\{\sin\left(\lambda\bar{\delta}^n\right)+\bar{\delta}^n\alpha_c\mu\cos\left(\lambda\bar{\delta}^n\right)\right\},$$

$$K_{36}=\chi\mu^3\sinh\left(\lambda\bar{\delta}^n\right)+\alpha_{mC}\bar{\delta}^n\left\{\cosh\left(\lambda\bar{\delta}^n\right)+\bar{\delta}^n\alpha_c\mu\sinh\left(\lambda\bar{\delta}^n\right)\right\},$$

$$K_{37}=\chi\mu^3\cosh\left(\lambda\bar{\delta}^n\right)+\alpha_{mC}\bar{\delta}^n\left\{\sinh\left(\lambda\bar{\delta}^n\right)+\bar{\delta}^n\alpha_c\mu\cosh\left(\lambda\bar{\delta}^n\right)\right\},$$

$$K_{44}=-\chi\mu^2\cos\left(\lambda\bar{\delta}^n\right)+\left(\alpha_{Ic}+\alpha_{mC}\alpha_c^2\right)\left(\bar{\delta}^n\right)^3\mu\sin\left(\lambda\bar{\delta}^n\right)-\alpha_{mC}\alpha_c\left(\bar{\delta}^n\right)^2\cos\left(\lambda\bar{\delta}^n\right),$$

$$K_{45}=-\chi\mu^2\sin\left(\lambda\bar{\delta}^n\right)-\left(\alpha_{Ic}+\alpha_{mC}\alpha_c^2\right)\left(\bar{\delta}^n\right)^3\mu\cos\left(\lambda\bar{\delta}^n\right)-\alpha_{mC}\alpha_c\left(\bar{\delta}^n\right)^2\sin\left(\lambda\bar{\delta}^n\right),$$

$$K_{46}=\chi\mu^2\cosh\left(\lambda\bar{\delta}^n\right)-\left(\alpha_{Ic}+\alpha_{mC}\alpha_c^2\right)\left(\bar{\delta}^n\right)^3\mu\sinh\left(\lambda\bar{\delta}^n\right)-\alpha_{mC}\alpha_c\left(\bar{\delta}^n\right)^2\cosh\left(\lambda\bar{\delta}^n\right),$$

$$K_{47}=\chi\mu^2\sinh\left(\lambda\bar{\delta}^n\right)-\left(\alpha_{Ic}+\alpha_{mC}\alpha_c^2\right)\left(\bar{\delta}^n\right)^3\mu\cosh\left(\lambda\bar{\delta}^n\right)-\alpha_{mC}\alpha_c\left(\bar{\delta}^n\right)^2\sinh\left(\lambda\bar{\delta}^n\right),$$

$$K_{51}=\alpha_{Ih2}\left(1-\Omega_{h2}^2\right)\bar{\delta}^n\left(-\sin\left(\bar{\delta}^n\right)-\sinh\left(\bar{\delta}^n\right)\right),\ K_{52}=\alpha_{Ih2}\left(1-\Omega_{h2}^2\right)\bar{\delta}^n\left(\cos\left(\bar{\delta}^n\right)-1\right),$$

$$K_{53}=\alpha_{Ih2}\left(1-\Omega_{h2}^2\right)\bar{\delta}^n\left(\cosh\left(\bar{\delta}^n\right)-1\right),$$

$$K_{54}=-\left\{\alpha_M\chi/\left(\mu\bar{\delta}^n\right)^2\right\}\left\{\cos\left(\lambda\bar{\delta}^n\right)+\mu\bar{\delta}^n\alpha_L\sin\left(\lambda\bar{\delta}^n\right)-1\right\}-\chi\alpha_{mC}\left(\alpha_L+\alpha_c\right)\cos\left(\lambda\bar{\delta}^n\right)+$$

$$\chi\bar{\delta}^n\mu\left\{\alpha_{mC}\left(\alpha_L\alpha_c+\alpha_c^2\right)+\alpha_{Ic}\right\}\sin\left(\lambda\bar{\delta}^n\right),$$

$$K_{55}=-\left\{\alpha_M\chi/\left(\mu\bar{\delta}^n\right)^2\right\}\left\{\sin\left(\lambda\bar{\delta}^n\right)-\mu\bar{\delta}^n\alpha_L\cos\left(\lambda\bar{\delta}^n\right)\right\}-\chi\alpha_{mC}\left(\alpha_L+\alpha_c\right)\sin\left(\lambda\bar{\delta}^n\right)-$$

$$\chi\bar{\delta}^n\mu\left\{\alpha_{mC}\left(\alpha_L\alpha_c+\alpha_c^2\right)+\alpha_{Ic}\right\}\cos\left(\lambda\bar{\delta}^n\right)-\alpha_{Ih2}\bar{\delta}^n\chi\mu\left(1-\Omega_{h2}^2\right),$$

$$K_{56}=-\left\{\alpha_M\chi/\left(\mu\bar{\delta}^n\right)^2\right\}\left\{\mu\bar{\delta}^n\alpha_L\sinh\left(\lambda\bar{\delta}^n\right)-\cosh\left(\lambda\bar{\delta}^n\right)+1\right\}-\chi\alpha_{mC}\left(\alpha_L+\alpha_c\right)\cosh\left(\lambda\bar{\delta}^n\right)-$$

$$\chi\bar{\delta}^n\mu\left\{\alpha_{mC}\left(\alpha_L\alpha_c+\alpha_c^2\right)+\alpha_{Ic}\right\}\sinh\left(\lambda\bar{\delta}^n\right),$$

$$K_{57}=-\left\{\alpha_M\chi/\left(\mu\bar{\delta}^n\right)^2\right\}\left\{\mu\bar{\delta}^n\alpha_L\cosh\left(\lambda\bar{\delta}^n\right)-\sinh\left(\lambda\bar{\delta}^n\right)\right\}-\chi\alpha_{mC}\left(\alpha_L+\alpha_c\right)\sinh\left(\lambda\bar{\delta}^n\right)-$$

$$\chi\bar{\delta}^n\mu\left\{\alpha_{mC}\left(\alpha_L\alpha_c+\alpha_c^2\right)+\alpha_{Ic}\right\}\cosh\left(\lambda\bar{\delta}^n\right)-\alpha_{Ih2}\bar{\delta}^n\mu\chi\left(1-\Omega_{h2}^2\right),$$

$$K_{61}=\left(1/\left(\bar{\delta}^n\right)^2\right)\left(\cos\left(\bar{\delta}^n\right)+\bar{\delta}^n\sin\left(\bar{\delta}^n\right)-\bar{\delta}^n\sinh\left(\bar{\delta}^n\right)+\cos\left(\bar{\delta}^n\right)-2\right)+$$

$$\left(\alpha_{m1}+\alpha_{mC}+\alpha_L\alpha_M\right)\left(\cos\left(\bar{\delta}^n\right)-\cosh\left(\bar{\delta}^n\right)\right),$$

$$K_{62}=\left(1/\left(\bar{\delta}^n\right)^2\right)\left(\sin\left(\bar{\delta}^n\right)-\bar{\delta}^n\cos\left(\bar{\delta}^n\right)\right)+\left(\alpha_{m1}+\alpha_{mC}+\alpha_L\alpha_M\right)\sin\left(\bar{\delta}^n\right)+\alpha_{Ih1}\bar{\delta}^n\left(1-\Omega_{h1}^2\right),$$

$$K_{63}=\left(1/\left(\bar{\delta}^n\right)^2\right)\left(\bar{\delta}^n\cosh\left(\bar{\delta}^n\right)-\sinh\left(\bar{\delta}^n\right)\right)+\left(\alpha_{m1}+\alpha_{mC}+\alpha_L\alpha_M\right)\sinh\left(\bar{\delta}^n\right)+\alpha_{Ih1}\bar{\delta}^n\left(1-\Omega_{h1}^2\right),$$

$$K_{71}=\cos\left(\bar{\delta}^n\right)-\cosh\left(\bar{\delta}^n\right),\ K_{72}=\sin\left(\bar{\delta}^n\right)-\bar{\delta}^n,\ K_{73}=\sinh\left(\bar{\delta}^n\right)-\bar{\delta}^n,$$

$$K_{74}=-\chi, K_{76}=-\chi,\ \ K_{15}, K_{17}, K_{24}, K_{26}, K_{31}, K_{32}, K_{33}, K_{41}, K_{42}, K_{43}, K_{64}, K_{65}, K_{66}, K_{75}, K_{77}=0. \quad (4.93)$$

In addition to the parameters defined in Eq. (4.11), the elements of the matrix are expressed in terms of:

$$\alpha_{mC}=m_C/\rho_1A_1L_1, \alpha_c=c/L_1, \alpha_{Ic}=I_c/\rho_1A_1L_1^3, \alpha_{Ih1}=I_{h1}/\rho_1A_1L_1^3, \alpha_{Ih2}=I_{h2}/\rho_1A_1L_1^3,$$

$$\Omega_{h1}=\left(\left(k_{\theta1}/J_1\right)/\omega_m^2\right), \text{ and } \Omega_{h2}=\left(\left(k_{\theta2}/J_2\right)/\omega_m^2\right). \quad (4.94)$$

The eigenfrequency equation shall be obtained for the condition of nontrivial solution of the obtained system of equation and the constants of integration can be evaluated as explained in section 4.4.1.

4.5.2 Nonlinear forced vibration analysis

The responses of two-link flexible manipulator have been studied for both the links of manipulator considering harmonic revolute motion being imparted to the flexible joints given by expressions as $\theta_1 = \theta_{10}\cos(\omega_1\tau)$ and $\theta_2 = \theta_{20}\cos(\omega_1\tau)$. The geometric nonlinearities due to axial stretching and the coupled nonlinear terms in Eqs. (4.85) & (4.87) have been retained and are expressed here as:

$$\rho_1 A_1\left(\ddot{w}_1 + x\ddot{\theta}_1\right) + E_1 I_1 w_1'''' - \left\{(3/2)E_1 A_1 w_1'^2 w_1'' - \rho_1 A_1 w_1 \dot{\theta}_1^2\right\} + c_{d1}\dot{w}_1 = 0 \tag{4.95}$$

$$\begin{aligned}&\rho_2 A_2\left(\ddot{w}_2 + x\ddot{w}_{1L}' + x\ddot{\theta}_1 + x\ddot{\theta}_2\right) + E_2 I_2 w_2'''' - \left\{(3/2)E_2 A_2 w_2'^2 w_2''\right\} + c_{d2}\dot{w}_2 + \\ &\rho_2 A_2\left(w_2\dot{\theta}_1^2 + w_2\dot{\theta}_2^2 + w_2\dot{w}_{1L}'^2 + 2\dot{\theta}_1\dot{\theta}_2 v_2 + 2\dot{\theta}_2 w_2\dot{w}_{2L}' + 2\dot{\theta}_1 w_2\dot{w}_{2L}'\right) = 0.\end{aligned} \tag{4.96}$$

The nondimensionalized governing equations are obtained by using the parameters defined in section 4.4.2 with further discretization by Galerkin's method using the mode shapes given in Eqs. (4.91) & (4.92) and after appropriate ordering of the involved terms expressed here as:

$$\ddot{p}_1(\tau) + \lambda_1^2 p_1(\tau) + 2\varepsilon\xi_1\dot{p}_1 - \varepsilon\alpha_4\omega_1^2\cos(\omega_1\tau) - \varepsilon^2\left[\alpha_5\omega_1^2\left\{1-\cos(2\omega_1\tau)\right\}p_1(\tau) + \alpha_1 p_1^3(\tau)\right] = 0. \tag{4.97}$$

$$\begin{aligned}&\ddot{p}_2(\tau) + \lambda_2^2 p_2(\tau) + 2\varepsilon\xi_2\dot{p}_2 + \varepsilon\left\{\alpha_2\ddot{p}_1 - \alpha_{12}\omega_2^2\cos(\omega_2\tau) - \alpha_{13}\omega_1^2\cos(\omega_1\tau)\right\} + \\ &\varepsilon^2\{\alpha_9\omega_2\dot{p}_1 p_2\sin(\omega_2\tau) + \alpha_{10}\omega_1\dot{p}_1 p_2\sin(\omega_1\tau) - \alpha_3 p_2^3(\tau) - \alpha_6\omega_2^2 p_2\sin^2(\omega_2\tau)\} + \\ &\varepsilon^2\{-\alpha_7\omega_1^2 p_2\sin^2(\omega_1\tau) - \alpha_8 p_2\dot{p}_1^2 - \alpha_{11}\omega_1\omega_2 p_2\sin(\omega_1\tau)\sin(\omega_2\tau)\} = 0.\end{aligned} \tag{4.98}$$

The steady-state solutions of the nonlinear Eqs. (4.97) & (4.98) are obtained by using second order method of multiple scales in a similar approach as explained in previous section. The governing equations for the first link are obtained after equating the coefficients of the same powers of ε as:

$$O(\varepsilon^1):\ \partial^2 p_{11}/\partial T_0^2 + \lambda_1^2 p_{11} = 0. \tag{4.99}$$

$$O(\varepsilon^2):\ \partial^2 p_{11}/\partial T_1^2 + \lambda_1^2 p_{12} + 2\xi_1(\partial p_{10}/\partial T_0) + 2\left(\partial^2 p_{10}/\partial T_0\partial T_1\right) - \alpha_4\omega_1^2\cos(\omega_1 T_0) = 0. \tag{4.100}$$

$$\begin{aligned}O(\varepsilon^3):\ &\partial^2 p_{12}/\partial T_2^2 + \lambda_1^2 p_{22} + 2\xi_1(\partial p_{11}/\partial T_0 + \partial p_{10}/\partial T_1) + 2\left(\partial^2 p_{10}/\partial T_0\partial T_2\right) \\ &+2\left(\partial^2 p_{11}/\partial T_0\partial T_1\right) + \partial^2 p_{10}/\partial T_1^2 - \alpha_5\omega_1^2\left\{1-\cos(2\omega_1 T_0)\right\}p_{10} - \alpha_1 p_{11}^3 = 0.\end{aligned} \tag{4.101}$$

In a similar manner the equations for second link are obtained as:

$$O(\varepsilon^1):\ \partial^2 p_{21}/\partial T_0^2 + \lambda_2^2 p_{21} = 0 \tag{4.102}$$

$$\begin{aligned}O(\varepsilon^2):\ &\partial^2 p_{21}/\partial T_1^2 + \lambda_2^2 p_{12} + 2\xi_2(\partial p_{20}/\partial T_0) + 2\left(\partial^2 p_{20}/\partial T_0\partial T_1\right) + \alpha_2\left(\partial^2 p_{10}/\partial T_0^2\right) - \\ &\alpha_{12}\omega_2^2\cos(\omega_2 T_0) - \alpha_{13}\omega_2^2\cos(\omega_2 T_0) = 0.\end{aligned} \tag{4.103}$$

$$\begin{aligned}O(\varepsilon^3):\ &\partial^2 p_{22}/\partial T_2^2 + \lambda_2^2 p_{22} + 2\xi_2(\partial p_{21}/\partial T_0 + \partial p_{20}/\partial T_1) + 2\left(\partial^2 p_{20}/\partial T_0\partial T_2\right) + \\ &2\left(\partial^2 p_{21}/\partial T_0\partial T_1\right) + \partial^2 p_{20}/\partial T_1^2 + \alpha_2\left(\partial^2 p_{11}/\partial T_0^2 + 2\partial^2 p_{10}/\partial T_0\partial T_1\right) - \\ &\alpha_6\omega_2^2 p_{20}\sin^2(\omega_2 T_0) - \alpha_7\omega_1^2 p_{20}\sin^2(\omega_1 T_0) - \alpha_{11}\omega_1\omega_2 p_{20}\sin(\omega_1 T_0)\sin(\omega_2 T_0) \\ &-\alpha_8\dot{p}_{10}^2 p_{20} + \alpha_9\omega_2 p_{20}\dot{p}_{10}\sin(\omega_2 T_0) + \alpha_{10}\omega_1 p_{20}\dot{p}_{10}\sin(\omega_1 T_0) - \alpha_3 p_{20}^3 = 0.\end{aligned} \tag{4.104}$$

The general solution of Eq. (4.99) & (4.102) can be expressed as:

$$p_{10} = P(T_1, T_2)\exp(i\lambda_1 T_0) + \bar{P}(T_1, T_2)\exp(-i\lambda_1 T_0). \tag{4.105}$$

$$p_{20} = Q(T_1, T_2)\exp(i\lambda_2 T_0) + \bar{Q}(T_1, T_2)\exp(i\lambda_2 T_0). \tag{4.106}$$

Substituting Eqs. (4.105)-(4.106) in Eqs. (4.100)-(4.103) gives:

$$\partial^2 \mathrm{p}_{12}/\partial \mathrm{T}_0^2 + \lambda_1^2 \mathrm{p}_{12} = -2\mathrm{i}\lambda_1\left(\xi_1 \mathrm{P} + (\partial \mathrm{P}/\partial \mathrm{T}_1)\right)\exp(i\lambda_1 T_0) + \left(\alpha_4\omega_1^2/2\right)\exp(i\omega_1 T_0) + cc. \tag{4.107}$$

$$\partial^2 p_{21}/\partial T_1^{\,2} + \lambda_2^{\,2} p_{12} = -2i\lambda_2\xi_2 Q\exp(i\lambda_2 T_0) - 2i\lambda_2(\partial Q/\partial T_1)\exp(i\lambda_2 T_0) + \alpha_2\lambda_1^{\,2} P\exp(i\lambda_1 T_0) + (\alpha_{12}\omega_2^{\,2}/2)\exp(i\omega_2 T_0) + (\alpha_{13}\omega_2^{\,2}/2)\exp(i\omega_2 T_0) + cc = 0. \quad (4.108)$$

Here, one may observe that any solution of Eq. (4.107)-(4.108) will contain secular or small divisor terms if the frequencies of joint rotations $(\omega_{1,2})$ become equal or nearly equal to link's normalized frequencies $(\lambda_{1,2})$. These secular or small divisor terms should be removed in order to have bounded solutions of Eqs. (4.100)-(4.103).

4.5.3 Primary resonance case in first and second link: ($\omega_1 \approx \lambda_1$ and $\omega_2 \approx \lambda_2$)

The nearness of ω_1 to λ_1 and ω_2 to λ_2 for simple resonance condition are, respectively expressed as $\lambda_1 + \varepsilon\sigma_1$, and $\lambda_2 + \varepsilon\sigma_2$. The Eqs. (4.107)-(4.101) and Eqs. (4.103)-(4.104) are solved simultaneously for the elimination of secular terms and subsequently, the resulting equations are expressed in terms of original time variable τ similar to the procedure in section 3.1.3.

$$-2i\lambda_1(\partial P/\partial\tau) - 2i\lambda_1\varepsilon\xi_1 P + \{\alpha_4\varepsilon\omega_1^{\,2}/2 - \alpha_4\varepsilon^2\omega_1^{\,2}\sigma_1/4\lambda_1 + (i\alpha_4\varepsilon^2\omega_1^{\,2}\xi_1/4\lambda_1)\}\exp(\sigma_1 T_1) - (\alpha_5\varepsilon^2\omega_1^{\,2}/4)\bar{P}\exp(2\sigma_1 T_1) + 3\alpha_1\varepsilon^2 P^2\bar{P} + (\alpha_5\varepsilon^2\omega_1^{\,2}/2)\bar{P} + \varepsilon^2\xi_1^{\,2} P = 0. \quad (4.109)$$

$$-2i\lambda_2(\partial Q/\partial\tau) + \{(\alpha_{12}\varepsilon\omega_2^{\,2}/2) - (\alpha_{12}\varepsilon^2\omega_2^{\,2}\sigma_2/4\lambda_2) + (i\alpha_{12}\varepsilon^2\omega_2^{\,2}\xi_2/4\lambda_2)\}\exp(\sigma_2 T_1) - (\alpha_5\varepsilon^2\omega_1^{\,2}/4)\bar{Q}\exp(2\sigma_2 T_1) + 3\alpha_3\varepsilon^2 Q^2\bar{Q} + \varepsilon^2\xi_2^{\,2} Q - 2i\lambda_2\varepsilon\xi_2 Q + \{(\alpha_6\varepsilon^2\omega_2^{\,2}/2) + (\alpha_7\varepsilon^2\omega_1^{\,2}/2) + 2\alpha_8\varepsilon^2\lambda_1^{\,2} P\bar{P}\}Q = 0. \quad (4.110)$$

Expressions of $P(\tau)$ and $Q(\tau)$ are written in the polar form as $P(\tau) = (1/2)a_1(\tau)e^{i\beta_1(\tau)}$ and $Q(\tau) = (1/2)a_2(\tau)e^{i\beta_2(\tau)}$. Now, substituting these expressions into Eq. (4.109)-(4.110) and separating real and imaginary parts, the following differential equations are obtained by letting $\beta_1 = \sigma_1 T_1 - \varphi_1$ and $\beta_2 = \sigma_2 T_1 - \varphi_2$ as:

$$-\lambda_1(\partial a_1/\partial\tau) - \lambda_1\varepsilon\xi_1 a_1 + \{\alpha_4\varepsilon\omega_1^{\,2}/2 - \alpha_4\varepsilon^2\omega_1^{\,2}\sigma_1/4\lambda_1\}\sin(\varphi_1) - (\alpha_5\varepsilon^2\omega_1^{\,2}/8)a_1\sin(2\varphi_1) + (\alpha_4\varepsilon^2\omega_1^{\,2}\xi_1/4\lambda_1)\cos(\varphi_1) = 0,$$

$$a_1\varepsilon\lambda_1\sigma_1 - a_1\lambda_1(\partial\varphi_1/\partial\tau) + \{\alpha_4\varepsilon\omega_1^{\,2}/2 - \alpha_4\varepsilon^2\omega_1^{\,2}\sigma_1/4\lambda_1\}\cos(\varphi_1) - (\alpha_5\varepsilon^2\omega_1^{\,2}/8)a_1\cos(2\varphi_1) - (\alpha_4\varepsilon^2\omega_1^{\,2}\xi_1/4\lambda_1)\sin(\varphi_1) + \{\varepsilon^2\xi_1/2 + \alpha_5\varepsilon^2\omega_1^{\,2}/4\}a_1 + (3/8)\alpha_1\varepsilon^2 a_1^{\,3} = 0. \quad (4.111)$$

$$-\lambda_2(\partial a_2/\partial\tau) - \lambda_2\varepsilon\xi_2 a_2 + \{\alpha_{12}\varepsilon\omega_2^{\,2}/2 - \alpha_{12}\varepsilon^2\omega_2^{\,2}\sigma_2/4\lambda_2\}\sin(\varphi_2) - (\alpha_6\varepsilon^2\omega_2^{\,2}/8)a_2\sin(2\varphi_2) + (\alpha_{12}\varepsilon^2\omega_2^{\,2}\xi_2/4\lambda_2)\cos(\varphi_2) = 0,$$

$$a_2\varepsilon\lambda_2\sigma_2 - a_2\lambda_2(\partial\varphi_2/\partial\tau) + \{\alpha_{12}\varepsilon\omega_2^{\,2}/2 - \alpha_{12}\varepsilon^2\omega_2^{\,2}\sigma_2/4\lambda_2\}\cos(\varphi_2) - (\alpha_6\varepsilon^2\omega_2^{\,2}/8)a_2\cos(2\varphi_2) - (\alpha_{12}\varepsilon^2\omega_2^{\,2}\xi_2/4\lambda_1)\sin(\varphi_2) + \alpha_8\varepsilon^2\lambda_1^{\,2}a_1^{\,2}a_2/4 + \{\varepsilon^2\xi_2/2 + \alpha_7\varepsilon^2\omega_1^{\,2}/4 + \alpha_6\varepsilon^2\omega_2^{\,2}/4\}a_2 + (3/8)\alpha_3\varepsilon^2 a_2^{\,3} = 0. \quad (4.112)$$

The second order approximate solutions of first and second link in terms of original time variable τ, can be expressed as:

$$p_1 = (1/2)a_1\cos(\omega_1\tau - \varphi_1) + O(\varepsilon),$$

$$p_2 = 0.5a_2\cos(\omega_2\tau-\varphi_2)+\varepsilon\left\{\alpha_2\lambda_1{}^2a_1/2\left(\lambda_2{}^2-\lambda_1{}^2\right)\right\}\cos(\omega_1\tau-\varphi_2)+\left\{\alpha_{13}\omega_1{}^2/2\left(\lambda_2{}^2-\omega_1{}^2\right)\right\}\cos(\omega_1\tau)$$
$$+O\left(\varepsilon^2\right).$$

For the steady-state conditions of Eqs. (4.111)-(4.112), the elimination of the phase (φ_n) from the resultant equation renders a frequency response equation in terms of a_n (amplitudes) and σ_n (frequencies for both the links). Stability of the steady-state solutions is determined by following a similar procedure explained in previous section by investigating the eigenvalues of the Jacobian matrices $\left[J_{1,2}\right]$ for the first and second link respectively given below:

$$J_1=\begin{bmatrix} & \left\{\left(\alpha_4\varepsilon\omega_1{}^2/2\lambda_1\right)-\left(\alpha_4\varepsilon^2\omega_1{}^2\sigma_1/4\lambda_1{}^2\right)\right\}\cos(\varphi_{10}) \\ -\varepsilon\xi_1-\left(\alpha_5\varepsilon^2\omega_1{}^2/8\lambda_1\right)\sin(2\varphi_{10}) & -2a_{10}\left(\alpha_5\varepsilon^2\omega_1{}^2/8\lambda_1\right)\cos(2\varphi_{10}) \\ & -\left(\alpha_4\varepsilon^2\omega_1{}^2\mu_1/4\lambda_1{}^2\right)\sin(\varphi_{10}) \\ & -\left\{\begin{matrix}\left(\alpha_4\varepsilon\omega_1{}^2/2a_{10}\lambda_1\right)- \\ \left(\alpha_4\varepsilon^2\omega_1{}^2\sigma_1/4\lambda_1{}^2a_{10}\right)\end{matrix}\right\}\sin(\varphi_{10})+ \\ \varepsilon\sigma_1/a_{10}+9\varepsilon^2\alpha_1a_{10}{}^2/8+ & \\ \left(\varepsilon^2\mu_1/2a_{10}\lambda_1\right)+\left(\alpha_5\varepsilon^2\omega_1{}^2/4a_{10}\lambda_1\right)+ & \left(\alpha_5\varepsilon^2\omega_1{}^2/4a_{10}\lambda_1\right)\sin(2\varphi_{10})- \\ \left(\alpha_5\varepsilon^2\omega_1{}^2/8a_{10}\lambda_1\right)\cos(2\varphi_{10}) & \left(\alpha_4\varepsilon^2\omega_1{}^2\mu_1/4a_{10}\lambda_1{}^2\right)\cos(\varphi_{10}) \end{bmatrix}$$

$$J_2=\begin{bmatrix} & \left\{\begin{matrix}\left(\alpha_{12}\varepsilon\omega_2{}^2/2\lambda_2\right)- \\ \left(\alpha_{12}\varepsilon^2\omega_2{}^2\sigma_2/4\lambda_2{}^2\right)\end{matrix}\right\}\cos(\varphi_{20}) \\ -\varepsilon\xi_2-\left(\alpha_6\varepsilon^2\omega_2{}^2/8\lambda_2\right)\sin(2\varphi_{20}) & -2a_{20}\left(\alpha_6\varepsilon^2\omega_2{}^2/8\lambda_2\right)\cos(2\varphi_{20}) \\ & -\left(\alpha_{12}\varepsilon^2\omega_2{}^2\mu_2/4\lambda_2{}^2\right)\sin(\varphi_{20}) \\ & -\left\{\begin{matrix}\left(\alpha_{12}\varepsilon\omega_2{}^2/2a_0\lambda_2\right)- \\ \left(\alpha_{12}\varepsilon^2\omega_2{}^2\sigma_2/4a_0\lambda_2{}^2\right)\end{matrix}\right\}\sin(\varphi_{20})+ \\ \varepsilon\sigma_2/a_{20}+9\varepsilon^2\alpha_3a_{20}{}^2/8+ & \\ \left\{\begin{matrix}\left(\varepsilon^2\mu_2/2a_0\lambda_2\right)+\left(\alpha_7\varepsilon^2\omega_1{}^2/4a_0\lambda_2\right)+ \\ \left(\alpha_6\varepsilon^2\omega_2{}^2/4a_0\lambda_2\right)\end{matrix}\right\} & \left(\alpha_6\varepsilon^2\omega_2{}^2/4a_0\lambda_2\right)\sin(2\varphi_{20})- \\ +\left(\alpha_6\varepsilon^2\omega_2{}^2/8a_0\lambda_2\right)\cos(2\varphi_{20}) & \left(\alpha_{12}\varepsilon^2\omega_2{}^2\mu_2/4a_0\lambda_1{}^2\right)\cos(\varphi_{20}) \end{bmatrix} \quad (4.113)$$

Stability of the steady-state solutions of links are now decided by the nature of eigenvalues of matrices of Eq. (4.113). If all the eigenvalues have negative or zero real parts, the steady-state solutions are stable.

4.5.4 Dynamic Characterization

In this section the dynamic characterization of a two-link manipulator in conjunction with the assumed mode method discretization is accomplished. A simulation of computationally efficient closed form equations of motion of the manipulator is realized to demonstrate the influence of important system parameters on the system responses specifically on the angular tip positions, modal displacements and tip accelerations. Now, the assumed mode method is used to express the deflection $(w_{1,2})$ of a point located at a distance *x* along the links of the manipulator as:

$$w_1(x,t)=\psi_1(x)q_1(t),\ \ w_2(x,t)=\psi_2(x)q_2(t). \tag{4.114}$$

Here, $q_1(t)$ and $q_2(t)$ are the modal displacements of first and second link respectively; $\varphi_1(x)$ and $\varphi_2(x)$ are the eigenfunction of first and second link for first mode of vibration respectively given in Eqs. (4.91)-(4.92). By substituting the Eq. (4.114) in Eqs. (4.85), (4.87), (4.89), & (4.90), the dynamic model of the two-link manipulator with extended payload can be expressed in matrix form as:

$$M(q_{1,2})\begin{bmatrix} q_{1tt} \\ q_{2tt} \\ \theta_{1tt} \\ \theta_{2tt} \end{bmatrix} + \eta(q_{1,2t},\theta_{1,2t})\begin{bmatrix} q_{1t} \\ q_{2t} \\ \theta_{1t} \\ \theta_{2t} \end{bmatrix} + \begin{bmatrix} \zeta_1(q_1,\theta_{1t}) \\ \zeta_2(q_{1,2},\theta_{1,2t}) \\ 0 \\ 0 \end{bmatrix} = \begin{bmatrix} 0 \\ 0 \\ \tau_1 \\ \tau_2 \end{bmatrix}. \tag{4.115}$$

Here, $M(q_{1,2})$ is the mass matrix, $\eta(q_{1,2t},\theta_{1,2t})$ is the Coriolis component matrix, $\left[\zeta(q_{1,2},\theta_{1,2t})\right]$ is the stiffness matrix while last matrix column in Eq. (4.115) represents the force matrix containing the torque exerted at the joints of the manipulator.

4.5.5 Inverse PD control

Now, the open input loop torques are calculated those are capable of replicating the given trajectories for both the joints $(\theta_{1d},\theta_{2d})$ of the manipulator system given in Eq. (4.115). Firstly for the required given trajectories, the resultant modal deflections (q_{1d},q_{2d}) are calculated by numerically integrating the governing equations of flexible manipulator dynamics from of Eq. (4.115) for zero initial conditions. Now, the required input torques (τ_{1d},τ_{2d}) of the system are obtained for the rigid body motion of the manipulator from the inverse dynamic model of Eq. (4.115) by using the desired trajectory $(\theta_{1d},\theta_{2d})$ and computed modal deflections (q_{1d},q_{2d}). In order to add robustness to the system, a linear feedback proportional-derivative (PD) controller on the joint trajectory error is used and expressed as:

$$\tau_{input}=\tau_d(q_d,\dot{q}_d,\dot{\varphi}_d,\ddot{\varphi}_d)+(1/D)\left[K_p(\varphi_d-\varphi)+K_d(\dot{\varphi}_d-\dot{\varphi})\right]. \tag{4.1}$$

Here, K_p and K_d are the proportional and derivative gains respectively and can be selected suitably so that the poles of the linearized system of Eq. (4.115) are in left half of s plane. When hubs are driven by the torques (τ_{input}) given in Eq. (4.116), the desired trajectories of the joints are obtained.

4.5.6 Numerical Results and Discussion

a) *Modal analysis: eigenspectrums*

The better understanding of eigenfrequencies of the two-link flexible manipulator with revolute pairs is essential in order to prevent the system from vibrating at undesirable amplitudes when it is subjected to a forcing frequency that is nearly equal to one of the system natural frequencies. The variation of system parameters can be viewed as the variation of operating conditions i.e., link properties, joint properties, etc. For example, variation in payload mass, beam mass density parameter, and flexural rigidity ratio, respectively, correspond to the variation in the weight of the payload being lifted by the manipulator, the use a manipulator having different link masses, and the changes in flexibility of both the links of manipulator. In a similar manner, variation of other parameters can be interpreted. Calculation of modal parameters is an essential and basic requirement prior to the analysis of the system dynamics. These variables are determined by numerically evaluating the determinant of coefficient matrix in Eq. **Error! Reference source not found.** for the nondimensional system parameters.

The influence of essential system parameters on eigenfrequencies is presented here while constant variables are indicated in the respective subsection of Table 4-6. Here the point mass and extended payloads are respectively denoted by α_{m2} and α_{mC}. Variation of eigenfrequencies with system masses $(\alpha_{m1}, \alpha_{m2})$ and beam mass density (α_M) is shown in Table along with Fig. 4.27. It is evident that the eigenfrequency decreases $\left(\omega_n \propto \sqrt{K/M}\right)$ with increase in mass either at the terminals of the links by increasing payload and joint mass $(\alpha_{m1}, \alpha_{m2})$ or when the mass density of second link is increased with respect to the first link (α_M).

Table 4-6: Variation of eigenfrequencies $(\bar{\delta}_i)$ of two-link manipulator with system parameters.

The variation of eigenfrequencies $(\bar{\delta}_i)$ with system mass payload parameter α_{m1}, α_{m2} having $\alpha_L = 1.0$, $\alpha_M = 1.0$, $\chi = 1.0$, $\alpha_{Ih1} = 1.0$, $\alpha_{Ih2} = 1.0$, $\Omega_{h1} = 1.0$, $\Omega_{h2} = 1.0$.				
α_{m1}, α_{m2}				
	0.0	0.5	1.0	5
$\bar{\delta}_1$	0.9979	0.9182	0.8868	0.8350
$\bar{\delta}_2$	2.3303	2.0551	1.9815	1.8807
$\bar{\delta}_3$	4.0535	3.7929	3.7451	3.6917
$\bar{\delta}_4$	5.0496	4.6829	4.6198	4.5345
$\bar{\delta}_5$	7.0933	6.7347	6.6935	6.6511
The variation of eigenfrequencies $(\bar{\delta}_i)$ with beam mass density parameter (α_M) having $\alpha_{m1} = 1.0$, $\alpha_{m2} = 1.0$, $\alpha_L = 1.0$, $\chi = 1.0$, $\alpha_{Ih1} = 1.0$, $\alpha_{Ih2} = 1.0$ $\Omega_{h1} = 1.0$, $\Omega_{h2} = 1.0$.				
α_M				
	0.5	0.75	1.0	1.5
$\bar{\delta}_1$	0.9089	0.8972	0.8868	0.8692
$\bar{\delta}_2$	2.0943	2.0320	1.9815	1.9033
$\bar{\delta}_3$	3.9898	3.8560	3.7451	3.5760
$\bar{\delta}_4$	4.9310	4.7271	4.6198	4.5043
$\bar{\delta}_5$	7.2284	6.9688	6.6935	6.2490
The variation of eigenfrequencies $(\bar{\delta}_i)$ with flexural rigidity ratio (χ) having $\alpha_{m1} = 1.0$, $\alpha_{m2} = 1.0$, $\alpha_L = 1.0$, $\alpha_M = 1.0$, $\alpha_{Ih1} = 1.0$, $\alpha_{Ih2} = 1.0$, $\Omega_{h1} = 1.0$, $\Omega_{h2} = 1.0$.				
χ				

	0.5	1.0	1.25	1.5
$\bar{\delta}_1$	0.7561	0.8868	0.9314	0.9683
$\bar{\delta}_2$	1.7690	1.9815	2.0460	2.0970
$\bar{\delta}_3$	3.4050	3.7451	3.8430	3.9100
$\bar{\delta}_4$	4.4360	4.6198	4.6960	4.8040
$\bar{\delta}_5$	5.9120	6.6935	6.9200	7.3130

The variation of eigenfrequencies $\left(\bar{\delta}_i\right)$ with joint inertia ratios $\left(\alpha_{Ih1}, \alpha_{Ih2}\right)$ having $\alpha_{m1}=1.0,\ \alpha_{m2}=1.0,\ \alpha_L=1.0,\ \alpha_M=1.0,\ \chi=1.0,\ \Omega_{h1}=1.0,\ \Omega_{h2}=1.0.$

$\alpha_{Ih1}, \alpha_{Ih2}$

	0.5	0.75	1.0	1.5
$\bar{\delta}_1$	0.9974	0.9291	0.8868	0.8358
$\bar{\delta}_2$	2.1229	2.0416	1.9815	1.8961
$\bar{\delta}_3$	3.8754	3.7964	3.7451	3.6832
$\bar{\delta}_4$	4.6491	4.6300	4.6198	4.6092
$\bar{\delta}_5$	6.7463	6.7132	6.6935	6.6711

The variation of eigenfrequencies $\left(\bar{\delta}_i\right)$ with joint frequency parameters $\left(\Omega_{h1}, \Omega_{h2}\right)$ having $\alpha_{m1}=1.0,\ \alpha_{m2}=1.0,\ \alpha_L=1.0,\ \alpha_M=1.0,\ \chi=1.0,\ \alpha_{Ih1}=1.0,\ \alpha_{Ih2}=1.0.$

Ω_{h1}, Ω_{h2}

	0	0.5	1.0	1.25	1.5
$\bar{\delta}_1$	0.8496	0.8868	0.59158	2.9405	3.2898
$\bar{\delta}_2$	1.9207	1.9815	1.4638	4.5386	4.5655
$\bar{\delta}_3$	3.6998	3.7451	3.5000	6.4463	6.5519
$\bar{\delta}_4$	4.6119	4.6198	4.9816	7.5819	7.6331
$\bar{\delta}_5$	6.6770	6.6935	6.5455	9.5954	9.6784

Comparison of four different cases of flexible two-link manipulator

	[Ata et al., 2012]	Case (I)	Case (II)	Case (III)
$\bar{\delta}_1$	1.8751	1.2479	0.74081	0.8868

$\bar{\delta}_2$	4.6940	1.8751	1.4101	1.9815
$\bar{\delta}_3$	7.8547	4.0311	3.4812	3.7451
$\bar{\delta}_4$	10.9955	4.6940	4.5560	4.6198
$\bar{\delta}_5$	14.1371	7.1341	6.5962	6.6935

From Fig. 4.27, it can be noticed that the beam mass density parameter has a significant effect on the higher eigenfrequencies as compared to lower natural frequencies. It is also evident from the Table 4-6 and the Fig. 4.28 that the eigenfrequencies increase with increase in flexural rigidity ratio (χ), i.e., either by reducing the flexibility of first link or by increasing the flexibility of the second link. The eigenfrequencies decrease with joint inertias $(\alpha_{Ih1}, \alpha_{Ih2})$, since effective inertia of the manipulator gets increased with increase in joint inertias.

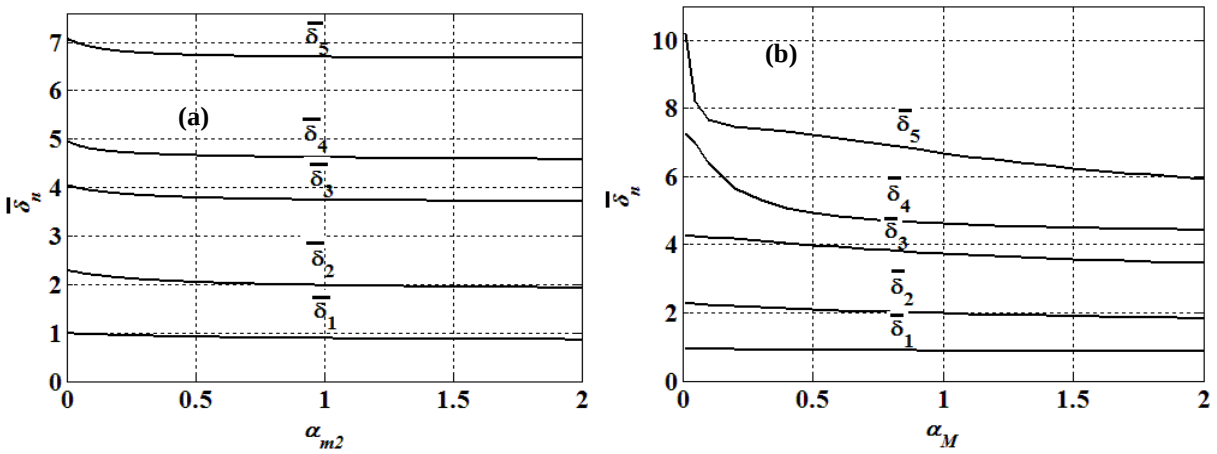

Fig. 4.27: Variation of eigenfrequencies of two-link manipulator having revolute pair with (a) payload mass parameter (α_{m2}) and (b) beam mass density parameter (α_M) for χ =1.0, α_{Ih1} =1.0, α_{Ih2} =1.0, and $\Omega_{h1,2}$ =0.5.

The variation of frequency parameters of the joints can be represented as the variation of joint stiffness while keeping other variables constant. The eigenfrequencies tend to increase with the joint frequency for $(\Omega_1, \Omega_2) \leq 1$. The unit magnitude represents the condition when system frequency becomes equal to the natural frequency of joint. Hence, Eqs. **Error! Reference source not found.-Error! Reference source not found.** representing the joints motion becomes invalid and the joints could be considered as a point mass. However, for (Ω_1, Ω_2)>1, the eigenfrequencies again increase with increase in joint frequency parameters. These conclusions can also be verified from Fig. 4.28, where it is noticed that at unit magnitudes of joint frequency parameters the eigenfrequencies observe a sudden jump nearly to higher eigenfrequency.

At the end of the table, four cases have been compared. The first column represents the eigenfrequencies evaluated by [Ata et al., 2012] for the third case when first link is considered in fixed-fixed and second link is considered fixed-free condition. The same eigenvalues can be obtained from the present model if the beam and mass inertia along with the hub-joint dynamics from the boundary conditions are neglected. The case (II) represents the conditions when the beam inertias are included in the boundary conditions resulting in the origination of another eigenfrequency around those obtained in [Ata et al., 2012]. In case (III), the beam dynamics along with the joint and payload masses have been considered and hence again the eigenfrequencies decrease further. The final case represents the present model with inclusion of hub

dynamics and payload and it is visible that the eigenfrequencies slightly increase as compared to the previous case due to the addition of joint stiffness in the boundary conditions.

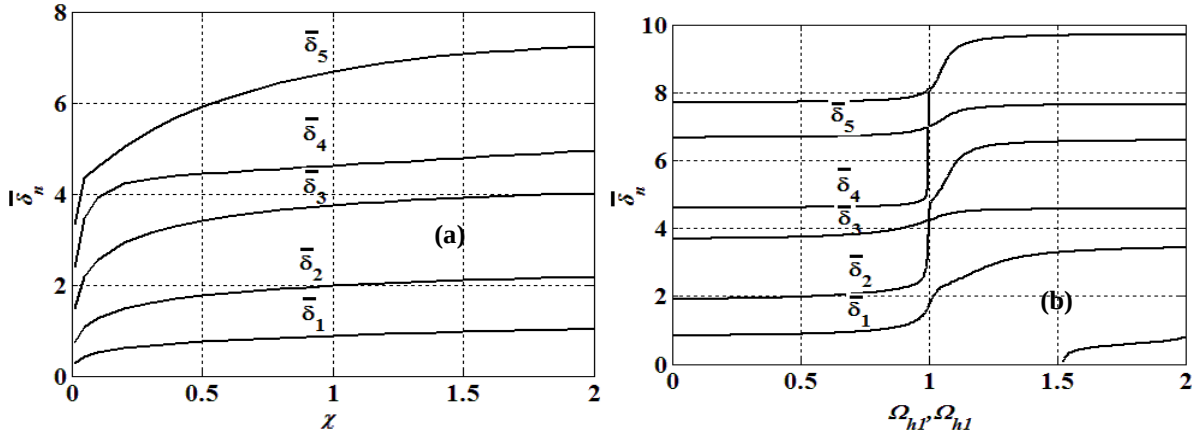

Fig. 4.28: Variation of eigenfrequencies of two-link manipulator having revolute pair with (a) flexural rigidity ratio (χ) and (b) joint frequency parameters $(\Omega_{h1,2})$ for α_{m1} =1.0, α_{m2} =1.0, α_{Ih1} =1.0, α_{Ih2} =1.0, and α_M =1.0.

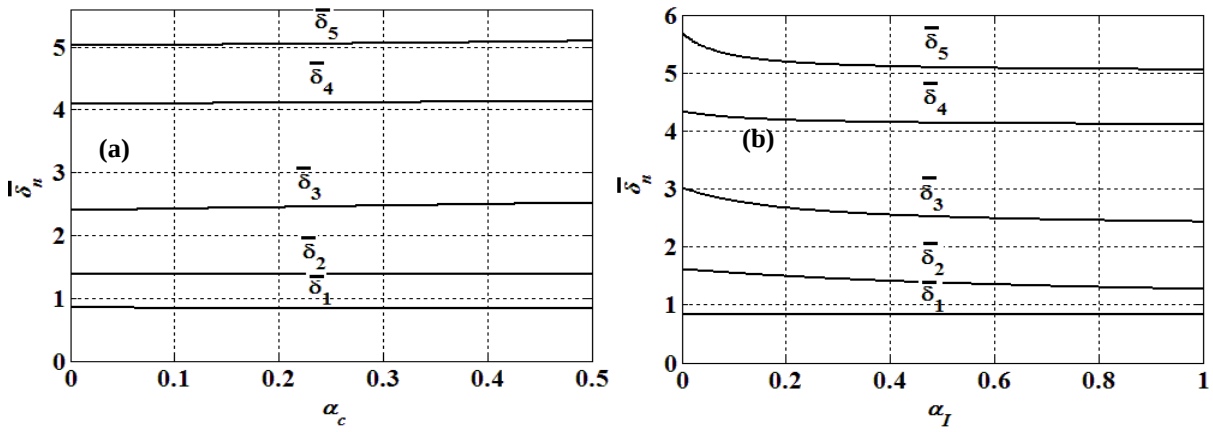

Fig. 4.29: Variation of eigenfrequencies of two-link manipulator having revolute pair with (a) axial offset length (α_c) and (b) payload inertia (α_{Ic}) for α_{mC} =1.0, α_{m1} =1.0, χ =1.0, α_M =1.0, α_{Ih1} =1.0, α_{Ih2} =1.0, Ω_{h1}, Ω_{h2} =0.

The system eigenfrequencies decrease with the addition of inertia to the system while lifting a payload with larger inertia (α_{Ic}) which is visible in Fig. 4.29. In case of offset ratio (α_c), it is observed that the eigenfrequencies tend to decrease as the centre of gravity of the payload is moved farther away from the point of attachment with the link if the payload inertia (α_{Ic}) is considered as zero. However, while the lower eigenfrequencies decrease, higher eigenfrequencies seems to be increased with payload offset (α_c) as soon as the payload with inertia (α_{Ic}) is considered in the analysis. Hence, it demonstrates the peculiar influence of the combination of payload on the system eigenfrequencies. Hence, in order to achieve precise positioning of a payload whose centre of gravity differs from the terminal point of link, the fundamental mode should be controlled appropriately.

Fig. 4.30 depicts plots to compare the first two eigenspectrums for point mass payload with an extended payload condition. It is evident that the eigenfrequencies for the case point payload are larger than the manipulator having an extended payload due to the presence of inertia as well as the offset in the centre of gravity of payload. It has been observed that the influence of extended payload is much significant on the higher modes of vibration which is evident from the comparative eigenspectrums illustrated in the figure.

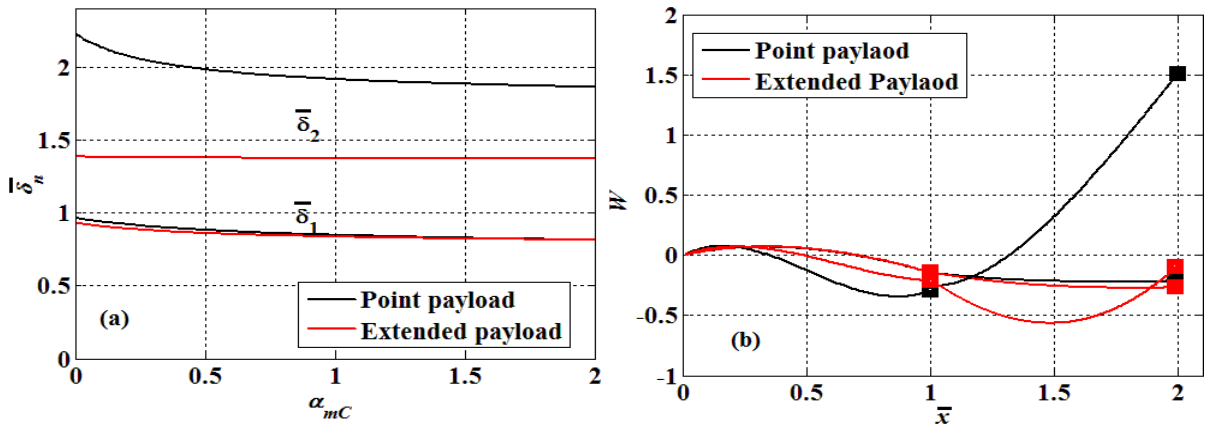

Fig. 4.30: Comparison of (a) eigenfrequencies and (b) mode shapes of two-link flexible manipulator with point and extended payload for $\alpha_{m1}=1.0 \quad \alpha_{m2},\alpha_{mC}=1.0,\ \alpha_{Ih1,2}=1.0,\ \alpha_{Ic}=1.0,\ \alpha_{c}=0.5,\ \alpha_{M}=1.0,\ \chi=1.0,\ \Omega_{h1,2}=0.$

An understanding of variation of vibration spectrums with varying system parameters shall enable efficient ways of controlling the vibration and subsequently stabilizing the overall system through vibration damping and energy dissipation of such robot systems when various boundary feedback schemes are being employed. Hence, the analysis is further extended to examine the effect of system parameters on the evaluation of the corresponding eigenspectrums of two-link flexible manipulator with revolute pairs. The influence of system mass $(\alpha_{m1},\alpha_{m2})$, i.e., either by varying payload mass or joint mass, on the mode shapes is illustrated in Fig. 4.31. The modal deflection tends to decrease with increase in system mass parameters as compared to the condition of when the masses at terminal points of links are considered as zero. The node shifting towards the payload end is also noticed with the increase in payload mass. The effect is significant in case of lower modes of vibration and mode shapes likely to spread out along the length of manipulator.

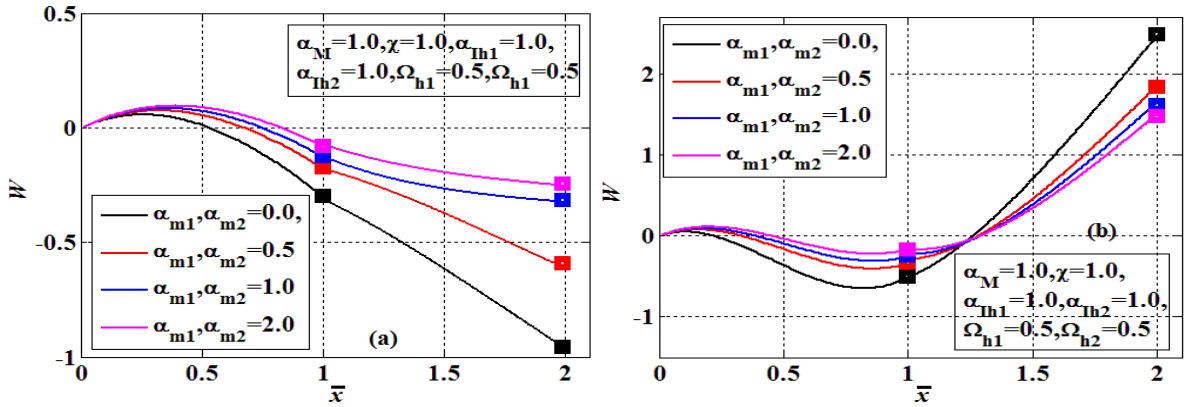

Fig. 4.31: Variation of mode shapes of two-link manipulator having revolute pair with varying payload mass parameter $(\alpha_{m1},\alpha_{m2})$ (a) mode 1 (b) mode 2 .

The variation of modes of vibration when the mass density of second link is increased or interpreted as decrease in first link beam mass density is demonstrated in Fig. 4.32. The influence of beam mass-density (α_M) is prominent in case of lower modes of vibration while the higher mode shapes tend to clutter together. However, from Fig. 4.33, it is evident that, as the flexibility of the second link is increased with respect to the first link, manipulator deflection decreases and its effect is significant for higher mode of vibration. The large manipulator deflection exists for small values of joint inertia $(\alpha_{Ih1},\alpha_{Ih2})$ which is demonstrated in Fig. 4.34. For larger values of joint inertia the mode shapes tend to adhere together.

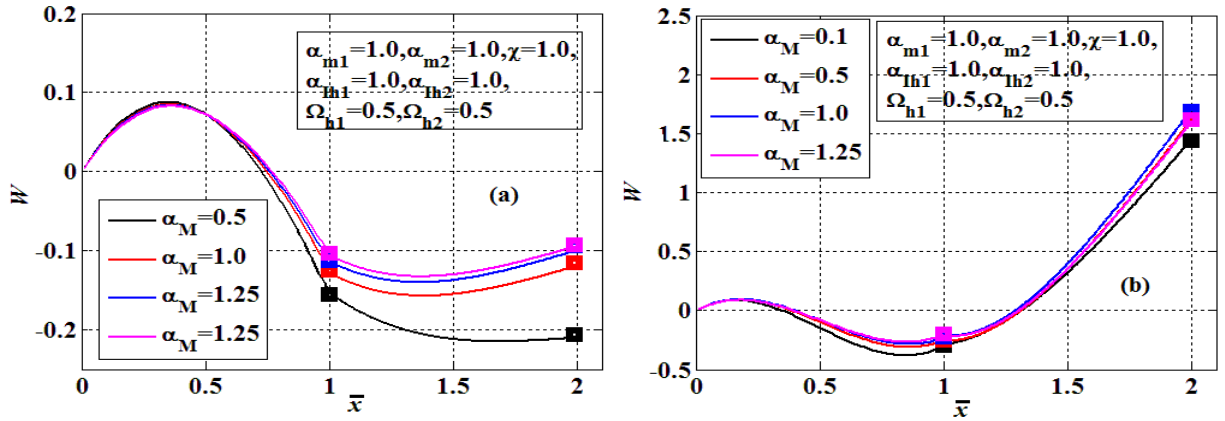

Fig. 4.32: Variation of mode shapes of two-link manipulator having revolute pair with varying beam density parameter (α_M) (a) mode 1 (b) mode 2 .

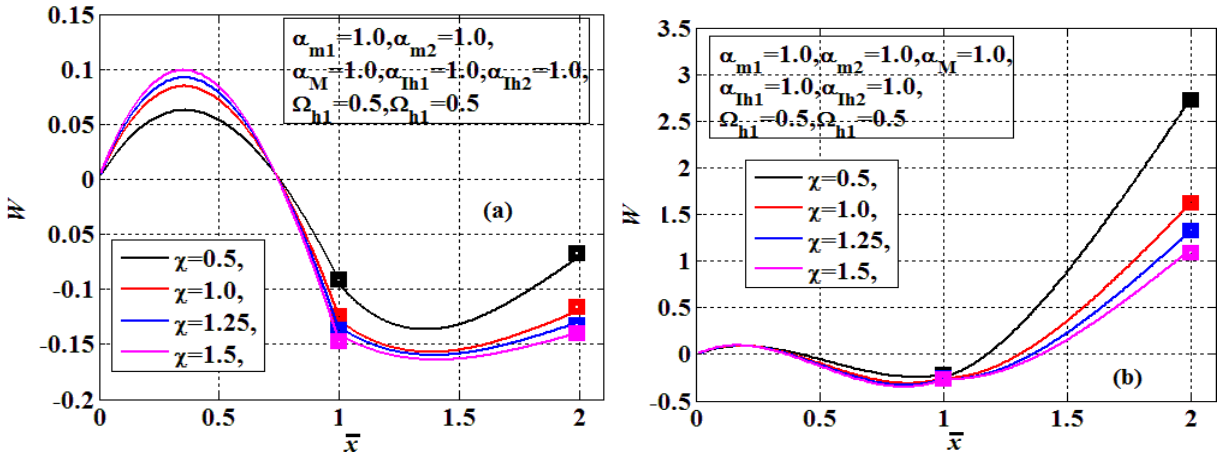

Fig. 4.33: Variation of mode shapes of two-link manipulator having revolute pair with varying flexural rigidity ratio (χ) (a) mode 1 (b) mode 2 .

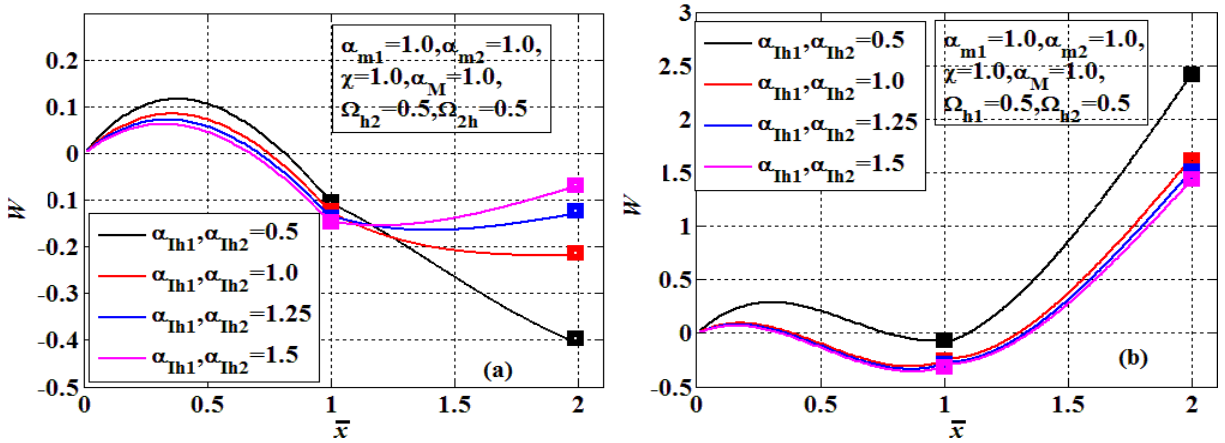

Fig. 4.34: Variation of mode shapes of two-link manipulator having revolute pair with varying joint inertia parameters $(\alpha_{Ih1},\alpha_{Ih2})$ (a) mode 1 (b) mode 2 .

Variation of frequency parameters $(\Omega_{h1,2})$ is shown in Fig. 4.35 and it is observed that the system tends to change its behavior as the frequency parameter reaches to the unit magnitude. The manipulator starts vibrating at higher modes of vibration for $\Omega_{h1,2}$>1, which is also apparent from the Table 4-6, where the eigenfrequencies observe a sudden jump at unit magnitude of frequency parameters. It is apparent from the Fig. 4.36 and Fig. 4.37 that the offset length (α_c) and inertia of the payload (α_I) considerably affects both the lower as well as higher modes of vibration for rigid joint condition and the deflection of manipulator decreases with both the payload parameters.

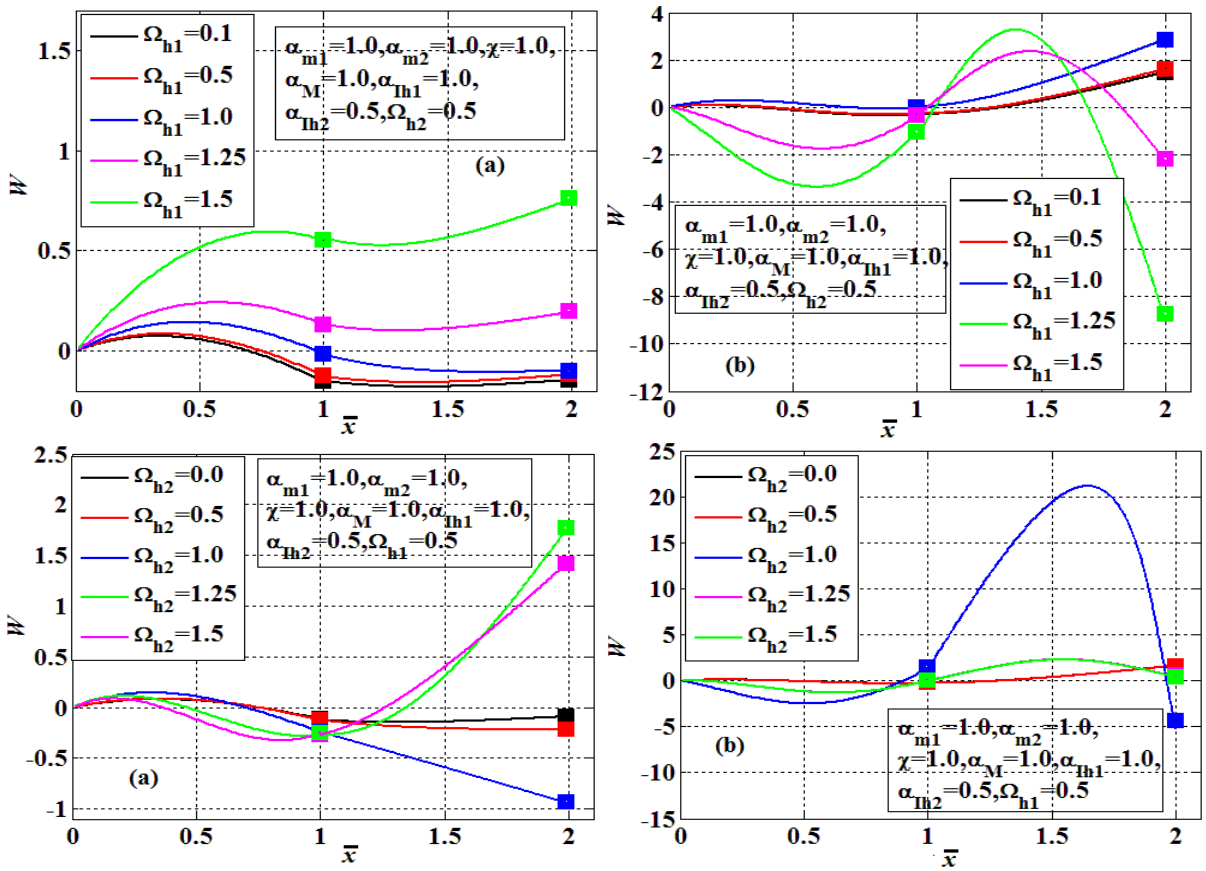

Fig. 4.35: Variation of mode shapes of two-link manipulator having revolute pair with varying joint frequency parameters $(\Omega_{h1},\Omega_{h2})$ (a) mode 1 (b) mode 2 .

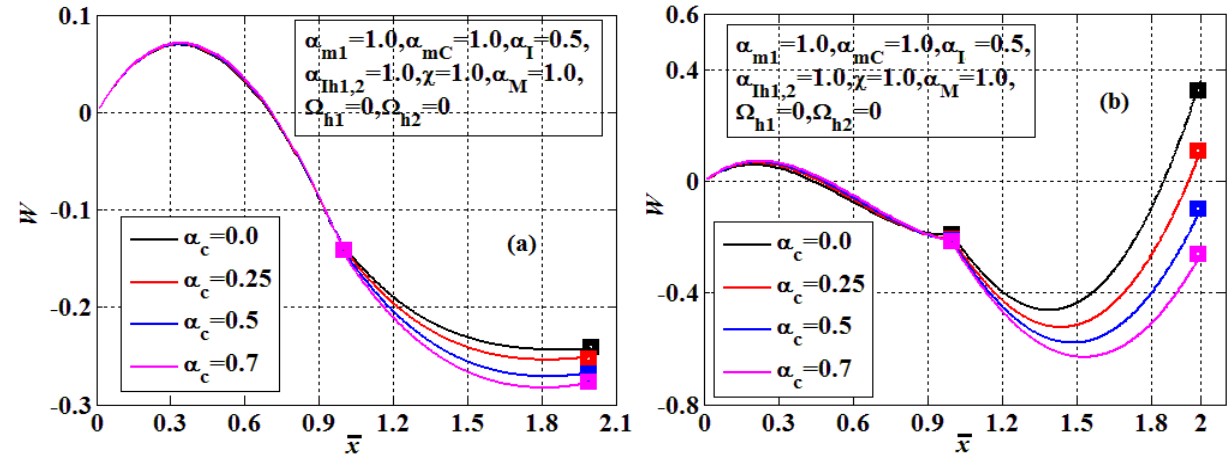

Fig. 4.36: Variation of mode shapes of two-link manipulator having revolute pair with axial offset ratio (α_c) (a) mode 1 (b) mode 2 .

These obtained modal parameters depict the inherent dynamic characteristic of a system in the form of eigenfrequencies and mode shapes. Parametric study of this modal analysis also indicates the way of improving and optimizing the dynamic characteristics of two-link manipulator. Identification of eigenfrequencies and corresponding mode shapes renders the information about the deflection shape of vibration to the design engineer when one of the natural frequencies matches with the external frequency called as resonance.

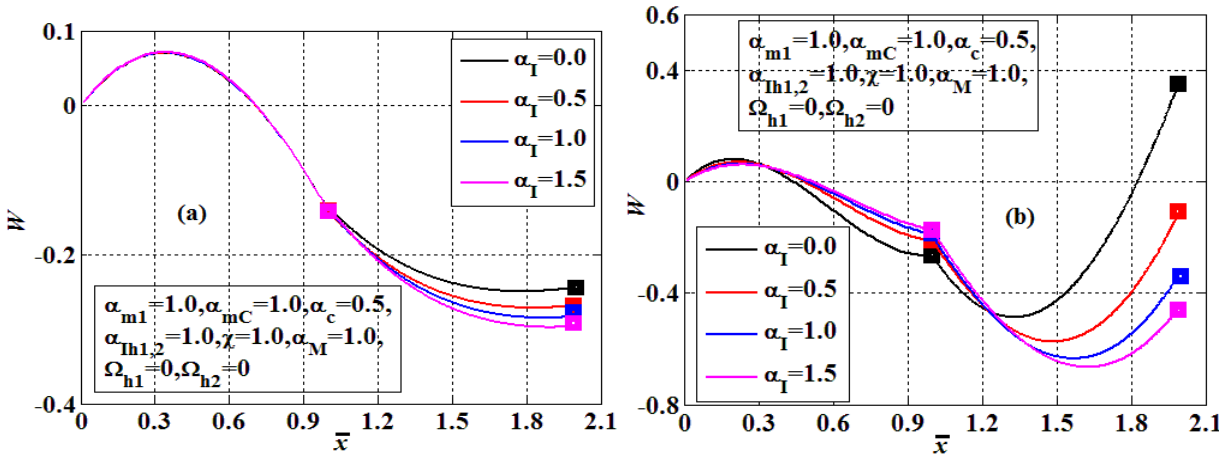

Fig. 4.37: Variation of mode shapes of two-link manipulator having revolute pair with axial offset ratio (α_l) (a) mode 1 (b) mode 2 .

b) *Nonlinear analysis: bifurcation and stability*

The earlier works lacked in the nonlinear behavior of the two-link manipulator and the major focus has been laid over the control and trajectory tracking of the manipulator. In an attempt to provide an insight and better understanding of performance of a two-link manipulator, here, further investigation of its dynamic performances to discern the level of performance safety and avoidance of undesirable behavior due to the instabilities because of the uncertain motor speed, mechanical properties and dynamic modeling is accomplished. The catastrophic failure of the two-link manipulators of various configurations can be avoided by the sufficient knowledge of the system behaviors operating at a certain speed. The different configurations of the manipulator can be achieved by varying the system parameters such as weight of payload being lifted, changing the masses of links, varying the flexibility of links, adjusting the flexibility of the joints etc. The geometrical properties of the links are the same as those considered in section 4.4.5 and the other parameters have been indicated in the figures.

It has been observed that when both links have the same properties, a 1:1 internal resonance exist between the links which iscan be avoided by considering length-ratio (α_L) equal to 1.1. The nondimensional damping coefficients $(\xi_{1,2})$ and amplitude ratios $(\theta_{10,20})$ are chosen as 0.01 and 0.0005, respectively. In all numerical simulations, book-keeping parameter (ε) and scaling factor (r) are selected as 0.1 and 0.001, respectively. In all figures, the solid line represents stable solutions and the dashed line denotes unstable solutions. The steady-state responses of both links are given by Eqs. (4.111) and (4.112) and shown in Fig 4.38-Fig. 4.45 which represent the change in amplitude of manipulator deflection $(a_{1,2})$ against the respective motor speed parameter $(\sigma_{1,2})$. The frequency response curves for the autonomous systems representing the vibration amplitudes for both the links are continuous curves exhibiting multi-valued solutions and associated phenomena due to the existence of saddle-node bifurcations manifested with the presence of nonlinearities within the system. The effect of nonlinearities on the frequency response curves is shown in Fig. 4.38 and it can be concluded that the nonlinearities induce spring softening behavior with the bending of curve resulting in the multivalued solutions at a particular frequency in both the cases. In Fig. 4.39, time response, phase portrait and FFT for three critical points A, B, and C as identified in Fig. 4.38 are compared numerically and analytically. They are found to be in good agreement.

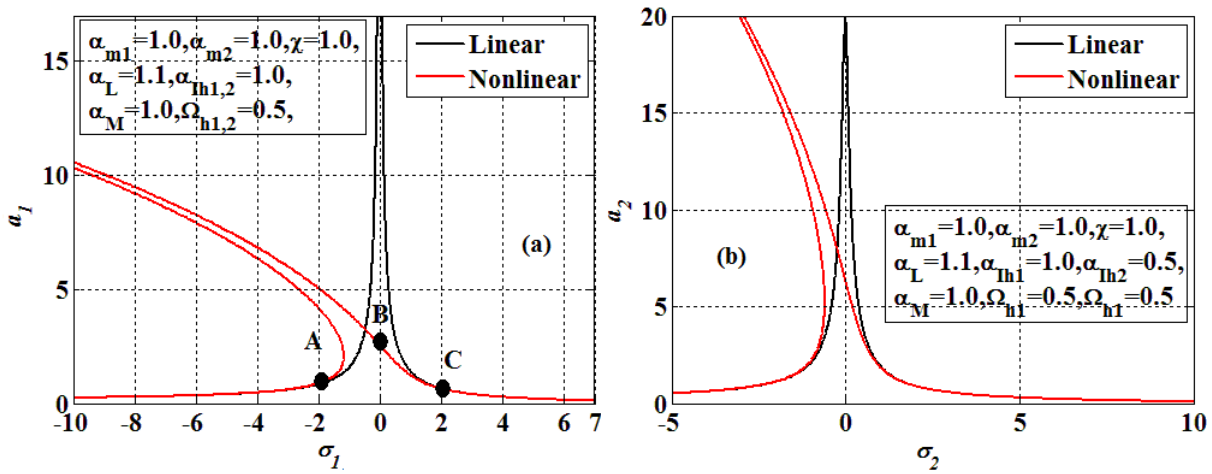

Fig. 4.38: Effect of nonlinearities on frequency response curve of (a) first and (b) second link.

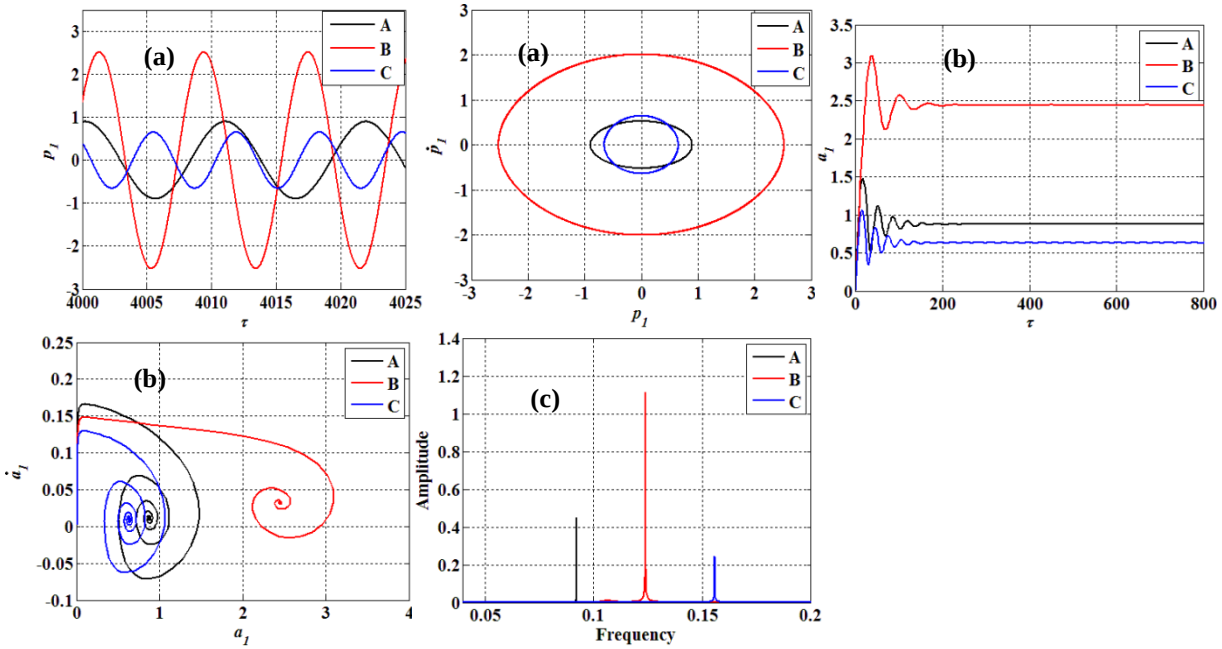

Fig. 4.39: (a) Numerical and (b) analytical time history and phase portrait, (c) FFT at critical points A, B, and C identified in Fig. 4.38.

The influence of the mass of payload (α_{m2}) lifted by the second link of the manipulator on the frequency response curves of the links are illustrated in Fig. 4.40. The first link exhibits spring softening behavior and the amplitude of responses gets increased for $0 \le \alpha_{m2} \le 1$. With a further increase in payload mass (α_{m2}) from 1 to 2, the system shows hardening effect and the maximum amplitude of the first link starts decreasing. However, the behavior of second link remains invariant with payload mass and experiences only softening effect. The amplitude of second link, first increases for $0.5 \le \alpha_{m2} < 1$ and thereafter, the amplitude starts decreasing for the rest of the values. Hence, it is noted that varying the payload mass shows the effective trend of nonlinearity, i.e., hardening/softening behavior and the undesirable vibrations due to the sudden variation of the amplitude can be avoided by operating the manipulator at safe speeds for the particular payload being handled.

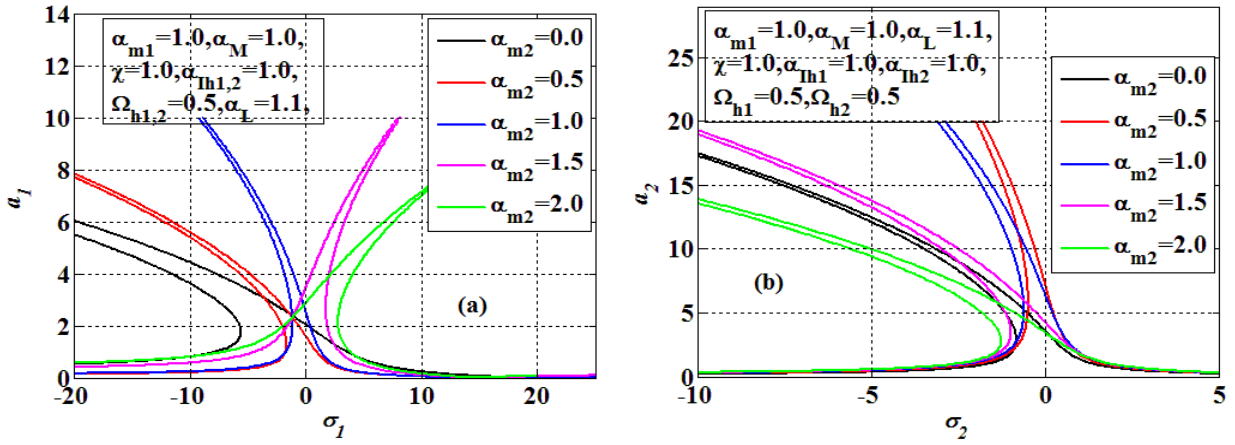

Fig. 4.40: Effect of variation of payload mass parameter (α_{m2}) on frequency response curve of (a) first and (b) second link.

The demonstration of variation of mass of the beams represented by beam mass density (α_M) on the frequency response curves for both the links is shown in Fig. 4.41. The first link of manipulator exhibits spring-softening behavior when the ratio of beam mass density of second to first link is kept between 0.5 and 1, i.e., $0.5 \le \alpha_M < 1$, and then spring-hardening behavior for $\alpha_M \ge 1$. For smaller values of α_M, the amplitude increases while for larger values of α_M, the amplitude decreases. However, the second link only experiences the spring softening behavior and maximum vibration amplitude decreases when the beam mass density of second link is increased with respect to first link. Thus, with an appropriate selection of design parameters, the trend of nonlinearity may be maintained either to softening or hardening that may further guide the control strategies and subsequent catastrophic failure due to sudden change in vibration amplitudes can be attenuated with the appropriate selection of operating limit of variable.

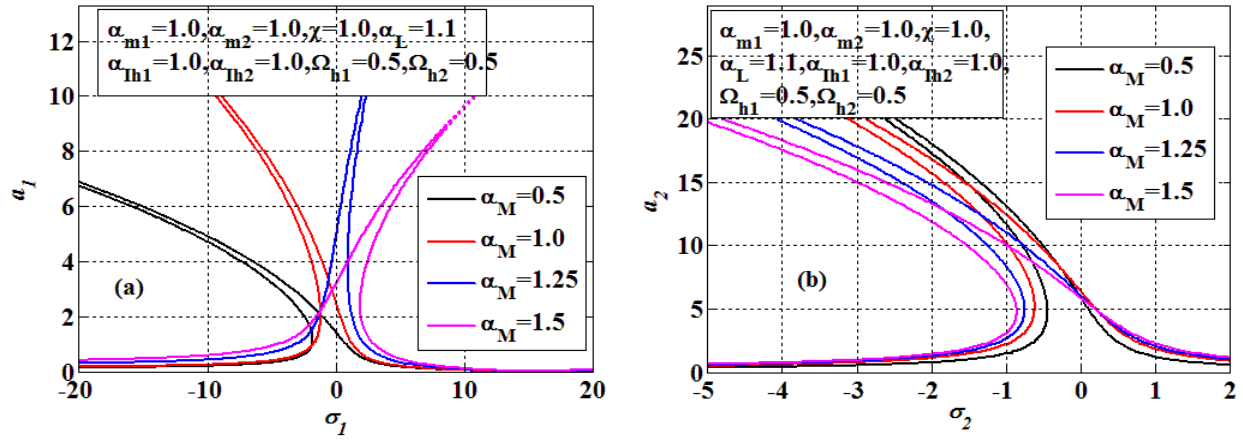

Fig. 4.41: Effect of variation of beam density parameter (α_M) on frequency response curve of (a) first and (b) second link.

The influence of increasing the flexibility of second link or decreasing the flexibility of first link, i.e., flexural rigidity ratio (χ) on the steady-state response amplitudes for both the links is shown in Fig. 4.42. The effect of flexural rigidity ratio has a negligible effect on the amplitude of first link. However, the steady-state amplitude of the second link increases with the increase in flexural rigidity ratio. The effect of joint inertias $(\alpha_{Ih1}, \alpha_{Ih2})$ on frequency response curves of the first and second link is shown in Fig. 4.43. The first link observes the alteration changes in fundamental behaviour from spring softening behavior to hardening behavior for $\alpha_{Ih1}, \alpha_{Ih2} = 1.0$. However, the second link exhibits similar spring softening behavior and the amplitude increases as the joint inertia increases.

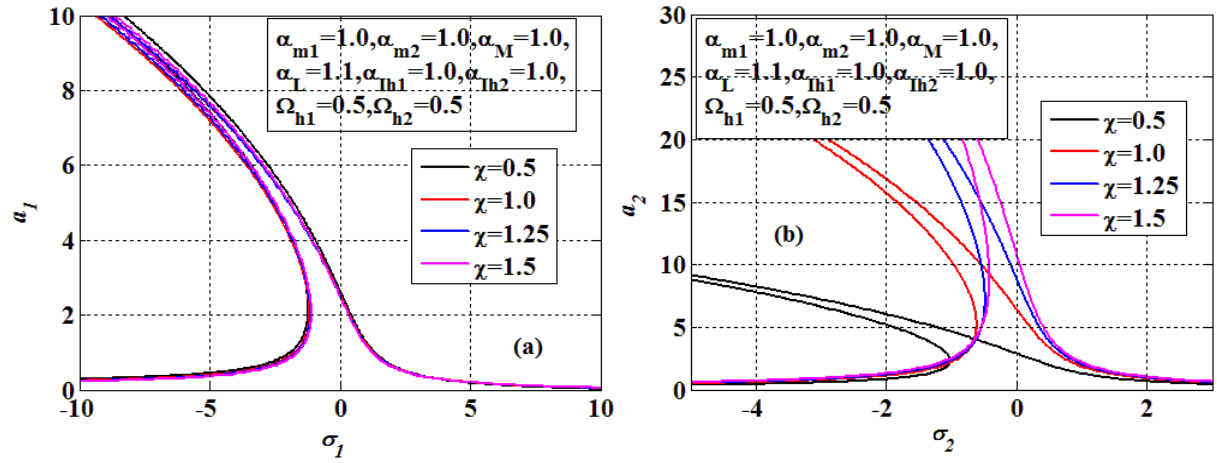

Fig. 4.42: Effect of variation of flexural rigidity ratio (χ) on frequency response curve of (a) first and (b) second link.

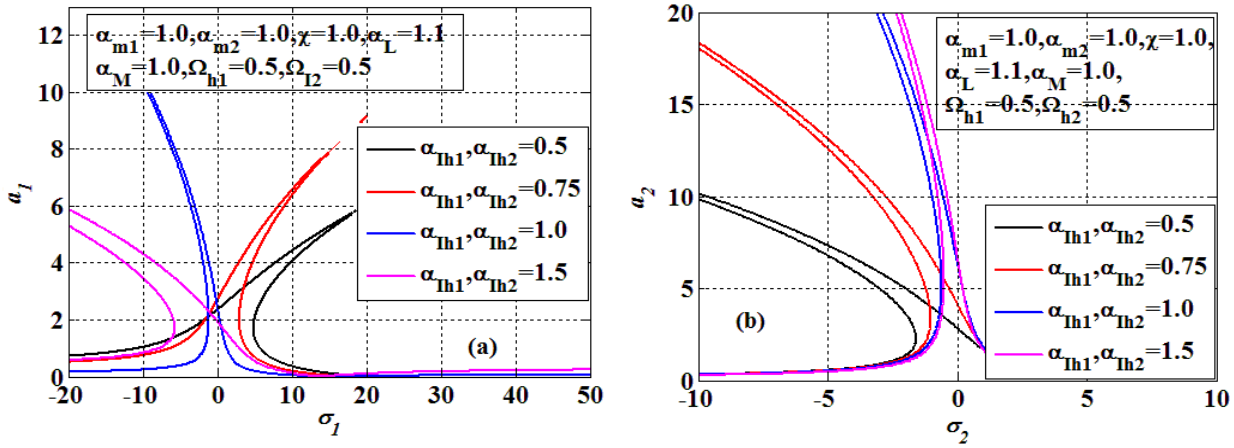

Fig. 4.43: Effect of variation of joint inertia parameters $(\alpha_{Ih1},\alpha_{Ih2})$ on frequency response curve of (a) first and (b) second link.

The joint parameter represents $(\Omega_{h1,2})$ the stiffness of the joints, if all other parameters are kept constant. The influence of frequency parameters $(\Omega_{h1,2})$ on the steady-state response of both the links of manipulator is illustrated through Fig. 4.44. For first frequency parameter Ω_{h1}, the first link alternates its behavior from spring softening to spring hardening while stiffness of first joint has a negligible effect on the behavior of the frequency response curve for second link. However, both links observe behavior alteration with the increase in stiffness of second joint (Ω_{h2}). A substantial decrease in amplitude of both the links is observed with the addition of small viscous damping as indicated in Fig. 4.45.

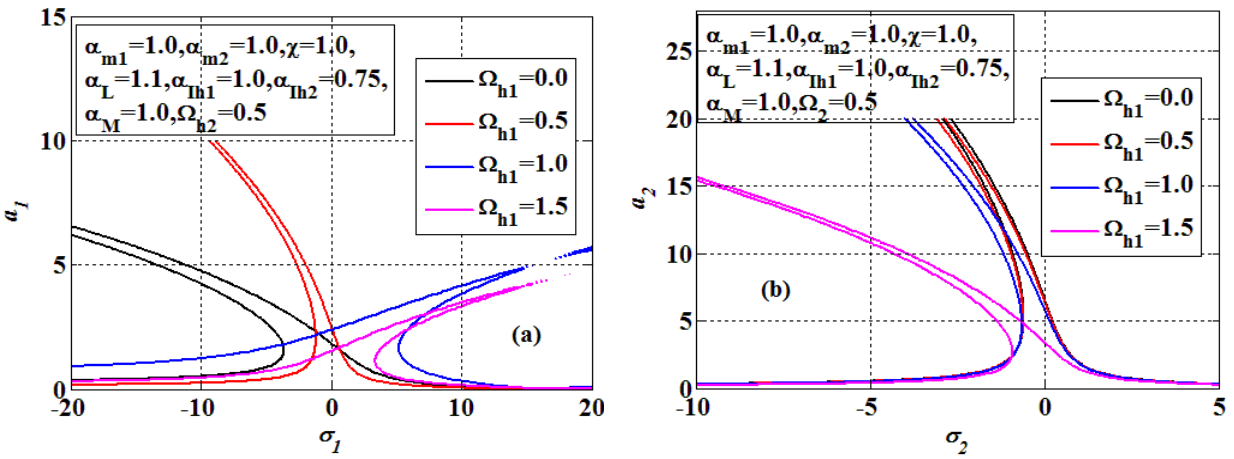

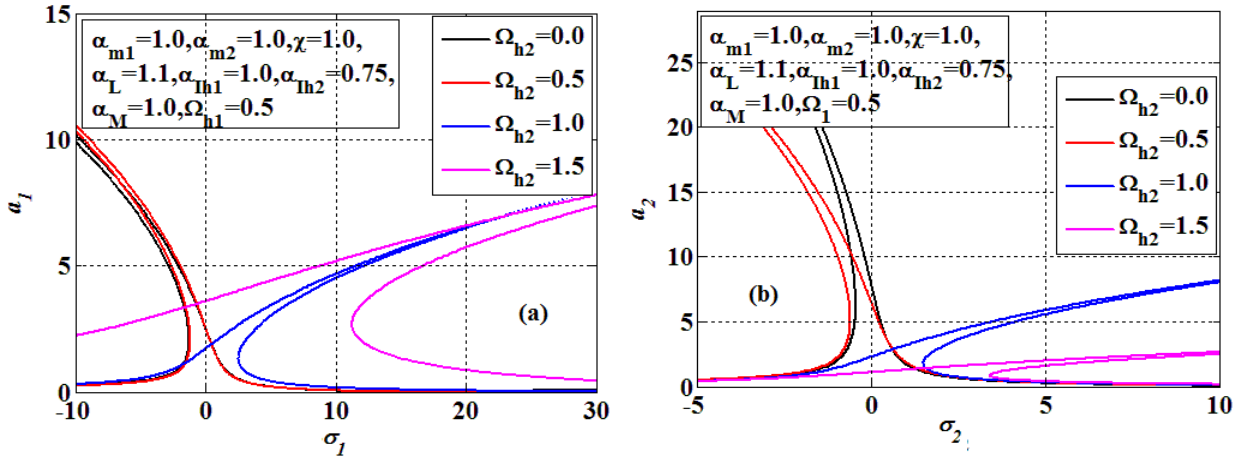

Fig. 4.44: Effect of variation of second frequency parameter $\left(\Omega_{h1,2}\right)$ on frequency response curve of (a) first and (b) second link.

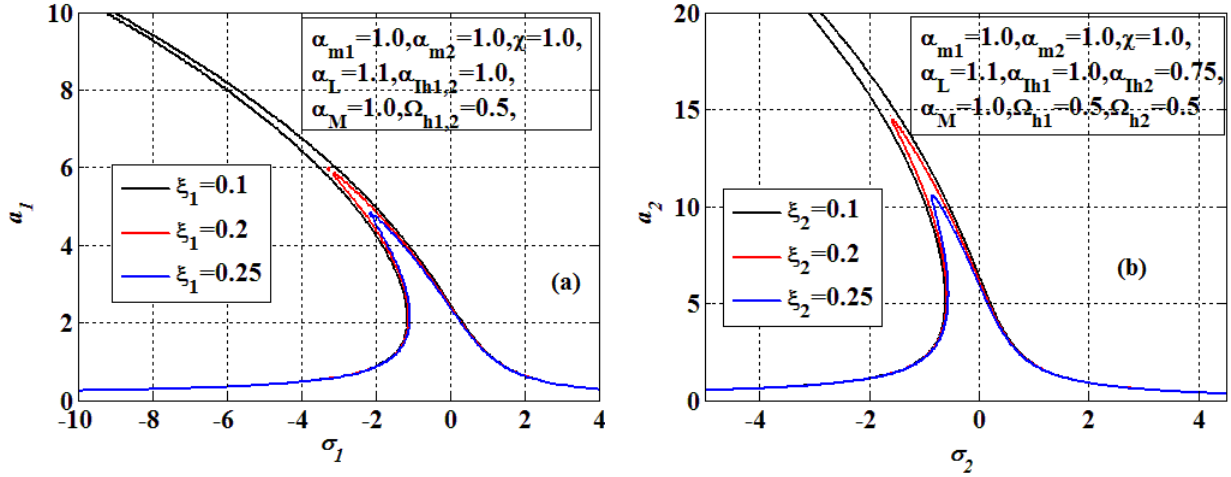

Fig. 4.45: Effect of damping parameters $\left(\xi_{1,2}\right)$ on frequency response curve of (a) first and (b) second link.

The obtained results can be successfully used to attenuate/suppress the vibrations of two-link manipulator system. They find applications in nuclear power plants, medical, and space industry. The large deflection model of the two-link manipulator result in additional non-linear terms in the equations of motion can be analyzed based on the mode shapes obtained in present analysis. Also, the configuration of the manipulator can be modified by changing beam geometry or varying the location of payload along the length of the link for more complex manipulators. Hence, a similar methodology can be adopted to investigate their dynamics. Further, the analysis can be extended to the conditions when two-link manipulator can be subjected to different forcing conditions representing the forced environment in which the manipulator is supposed to work such as axially constraint surface contact force, varying magnetic field etc. The present results also provide a framework for linear and nonlinear design of multi-link manipulators.

c) *System performance: tip Responses*

The modern flexible robot manipulators demonstrate superiority over rigid robots due to their low weight, less power consumption, small actuators, higher payload to manipulator weight ratio along with larger maneuverability and transportability. However, flexibilities in the links and joints, their control to achieve and maintain accurate positioning and trajectory tracking poses a major challenge. The dynamics of the flexible manipulator are significantly more complex by virtue of the flexible nature of the system. The simulation of the developed model subjected to specified input command is essential to form the basis for design and development of suitable control strategies for the systems. Hence, here a step towards the comprehension of

system responses in time domain for the parametric variation of manipulator attributes has been taken. The relevant characteristics of the links assumed in the simulation are as follows:

Here to conduct this analysis, the assumed geometrical and physical characteristics for both the links are width $b_{1,2} = 0.05$ m, thickness $h_{1,2} = 0.0055$ m, material density $\rho_{1,2} = 7800 \text{ kg/m}^3$, material Young's modulus $E_{1,2} = 210$ GPa, lumped mass of joint at the end of the first link $m_1 = 0.1$ Kg, extended payload mass $m_C = o.1$ Kg, inertia of joints $I_{h1,2} = 0.02 \text{ kgm}^2$, inertia of payload $I_c = 0.008 \text{ kgm}^2$, offset length $c = 0.1$ m, and lengths of links $L_{1,2} = 0.5$ m. The parameter varied to examine its effect on the time responses has been mentioned in figure itself, while other parameters remain constant as detailed earlier. The closed form dynamic model expressed in Eq. (4.115) is simulated by smooth sinusoidal input torque of duty cycle of 0.5 sec duty cycle and amplitude of 0.3 Nm at first joint as shown in Fig. 4.46 and a similar torque profile of 0.6 Nm amplitude is applied at second joint. The influence of the parametric variation on the angular tip positions, modal displacements and tip accelerations of the links have been presented graphically.

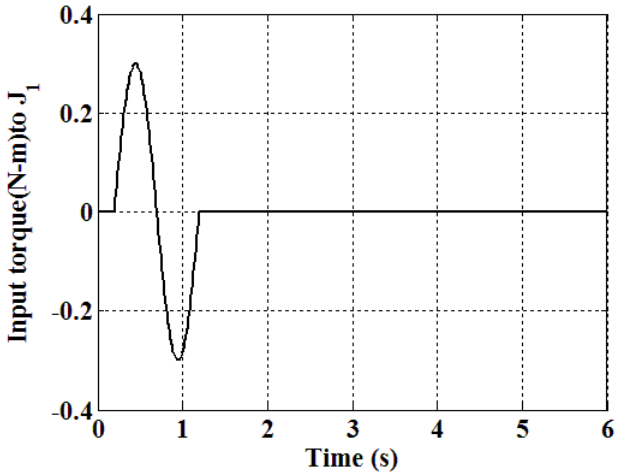

Fig. 4.46: Input torque profile to the joints.

The rise time and settling time are very essential parameters of robotic systems for their satisfactory performance in various industrial applications. The rise time indicates the time required by the manipulator to reach desired position as soon as the input torque is imparted to the joint. As the manipulator reaches its perquisite set points, the residual vibrations are noticed which delays the tip to reach its steady-state. The settling time is characteristic of a response which indicates the time required by the end-effector of the manipulator to reach the steady-state condition. Both parameters are significant for a robotic system since it is indispensable for manipulator to reach its required position and attain the steady-state condition in minimum time which in turn increases the productivity rate and precession. The payload mass (m_C) has a substantial influence on the angular tip positions, modal displacements and angular accelerations of the links which clearly evident in Fig. 4.47. While the angular tip positions and settling time decreases with the increase in payload mass (m_C), the rise time increases as the manipulator lifts a heavier payload. For the first link the tip vibrates at -0.095 rad, -0.12 rad, and -0.18 rad and for second link the tip vibrates at 0.83 rad, 0.5 rad, and 0.37 rad for 0.0 kg, 0.2 kg, and 0.4 kg payload mass respectively. The tip accelerations also decrease with the increase in payload mass owing to the fact inertia is added to the system.

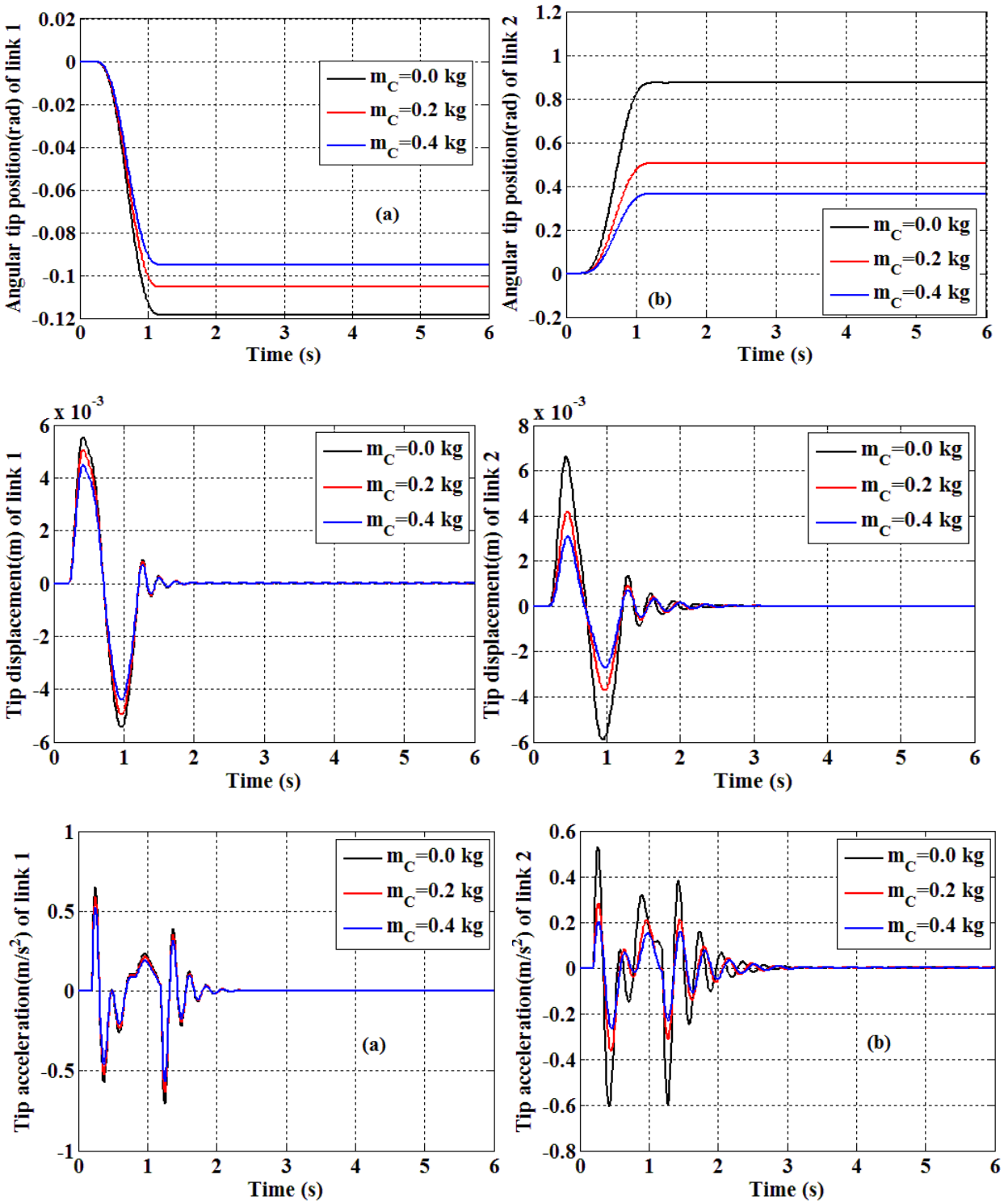

Fig. 4.47: Effect of variation of payload mass (m_c) on the angular positions, tip displacements and tip accelerations of (a) first link (b) second link.

The other payload parameters, i.e., payload inertia (I_c) and offset length (c) have a negligible effect on the characteristics of the first link which is evident from Fig. 4.48-Fig. 4.49. However, the angular position of the second link decreases as the payload inertia (I_c) is increased or the centre of gravity of payload (*c*) is moved farther away from the terminal point of the link. It is noticed that, there is a negligible influence of payload parameters on the rise time of the second link response. However, as the manipulator lifts the payload of larger inertia (I_c) and offset (c), the second link takes smaller time to reach its steady-state.

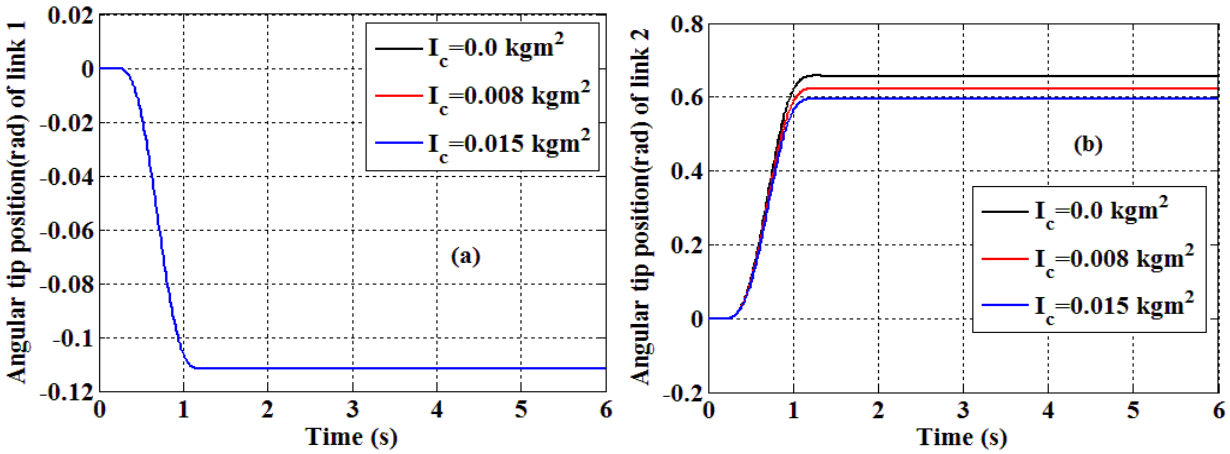

Fig. 4.48: Effect of variation of payload inertia (I_c) on the angular positions of (a) first and (b) second link.

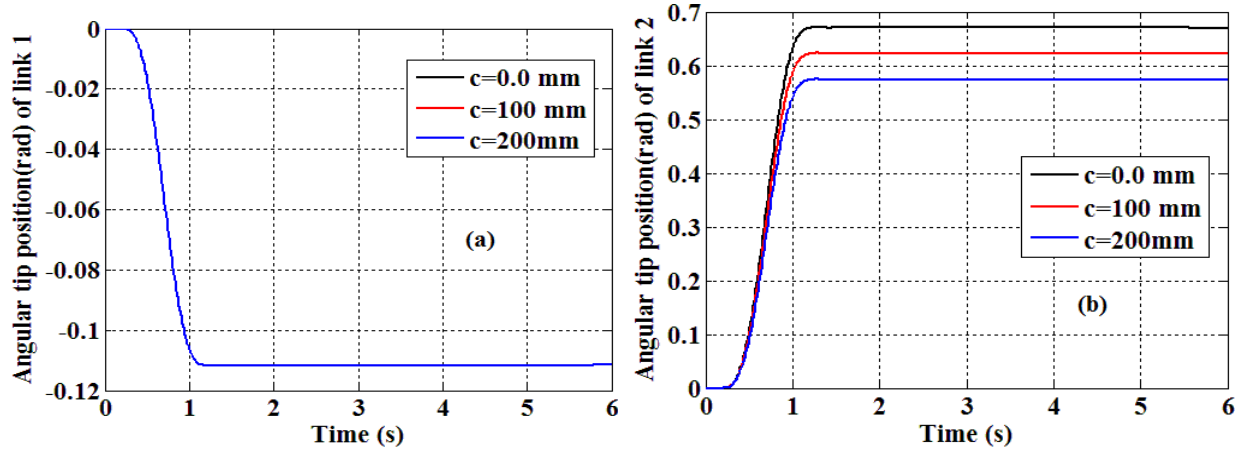

Fig. 4.49: Effect of variation of offset length (c) on the angular positions of (a) first and (b) second link.

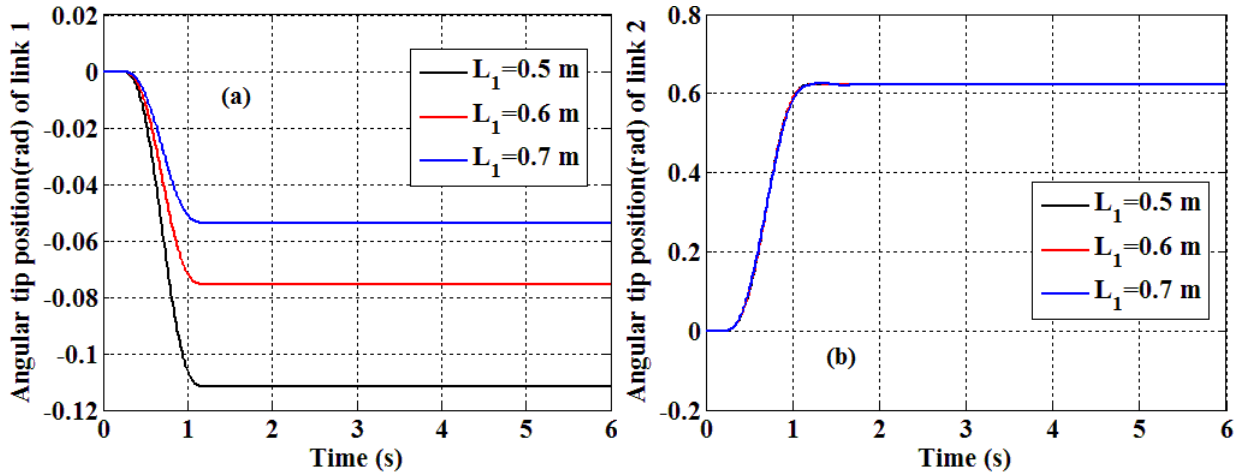

Fig. 4.50: Effect of variation of length of first link (L_1) on the angular positions of (a) first and (b) second link.

The influence of the length of the links $(L_{1,2})$ on the angular tip response of manipulator is inferred from Fig. 4.50-Fig. 4.51. It is evident that the angular tip position and the settling time of the first link response decreases with the use of a manipulator with the longer links while, a negligible effect is seen on the angular tip position of the second link by increasing the length of first link (L_1). However, the settling time of the second link (L_2) response increases. With the increase in length of the second link (L_2) from 0.5m to 0.7m, the position inaccuracy of the first and second link increases by 18 % and 51%, respectively. Thus, to reach desired set point, a longer manipulator requires a larger torque input.

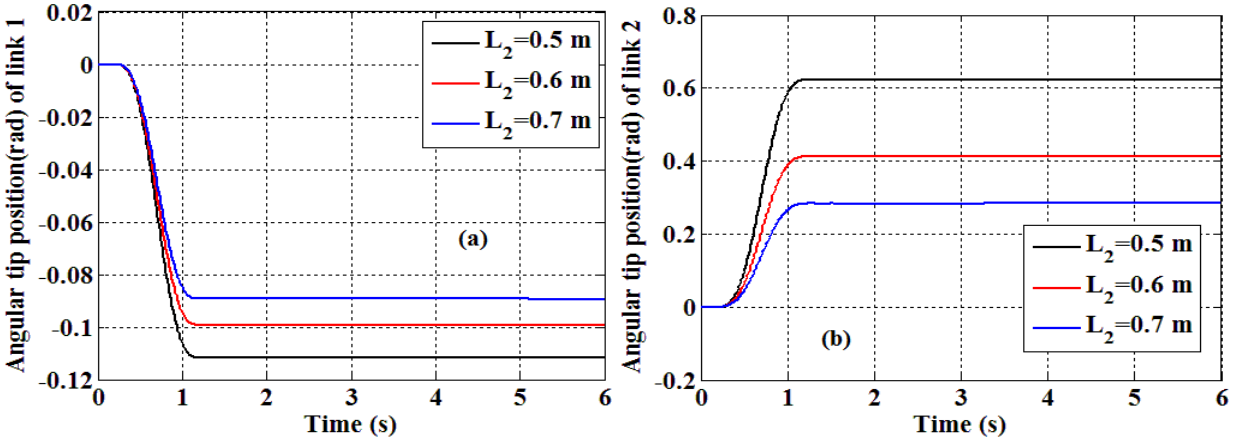

Fig. 4.51: Effect of variation of length of second link (L_2) on the angular positions of (a) first and (b) second link

The second joint mass (m_1) has a negligible influence on the time response of the second link and the settling time of the first link which is shown in Fig. 4.52. However, the amplitude of first link response decreases with increase in mass of the second joint (m_1). The tip accelerations experience large fluctuations as compared to other parameters when the joint inertias $(I_{h1,2})$ are increased and their amplitude increases with increase in joint inertias which is also observed in Fig. 4.53. Also, as the joint inertias $(I_{h1,2})$ are increased, the angular positions of both links decrease and it is also noticeable that the settling time of the first and second link responses decrease and increase, respectively.

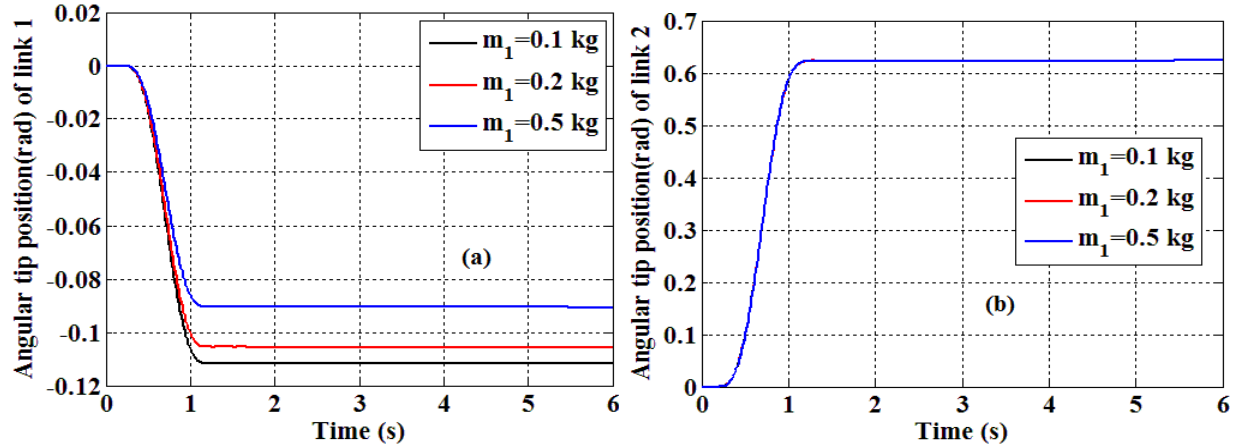

Fig. 4.52: Effect of joint mass (m_1) on the angular positions of (a) first and (b) second link.

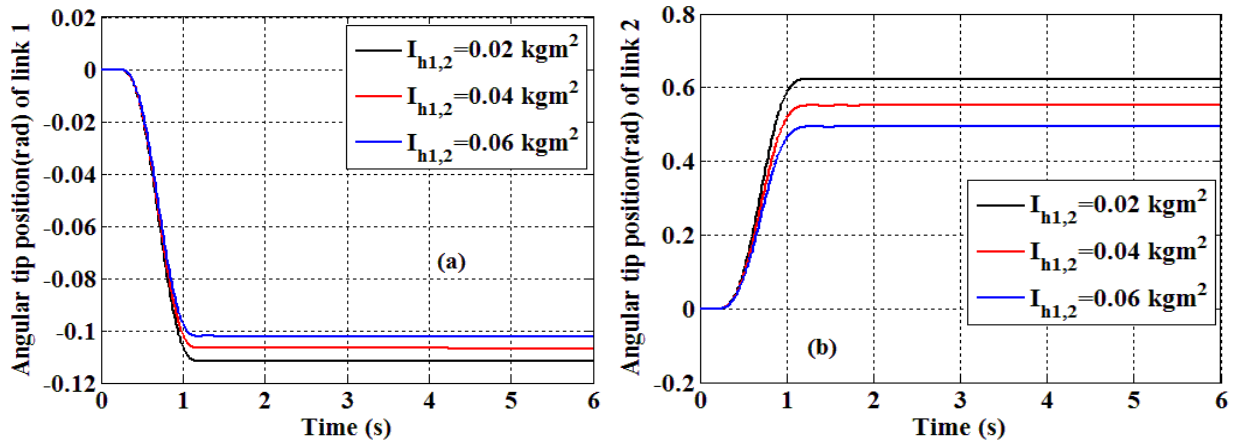

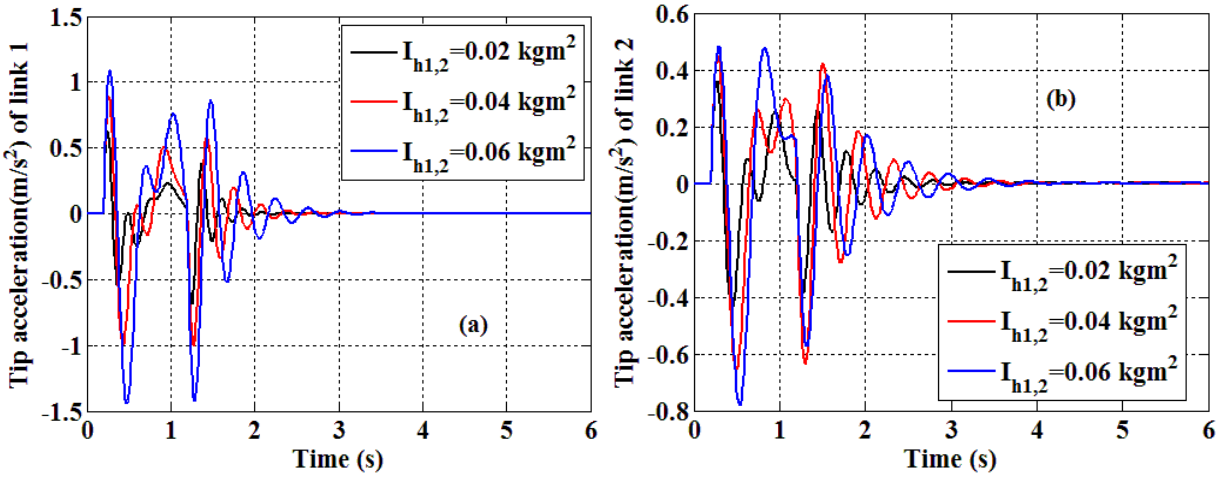

Fig. 4.53: Effect of joint inertia $\left(I_{h1,2}\right)$ on the angular positions and tip accelerations of (a) first link and (b) second link.

Further, in Fig. 4.54, the effect of variation of material of the manipulator links on the system responses is demonstrated. The cases have been presented when the manipulator links are made of three different materials usually employed to manufacture the manipulator links i.e. steel, grey cast iron and aluminum. It is evident from the figure that the angular positions of the links made of aluminum are much larger than those of steel and grey CI. And also the tip accelerations significantly decreases as the material of the links is changed from aluminum to steel or grey CI.

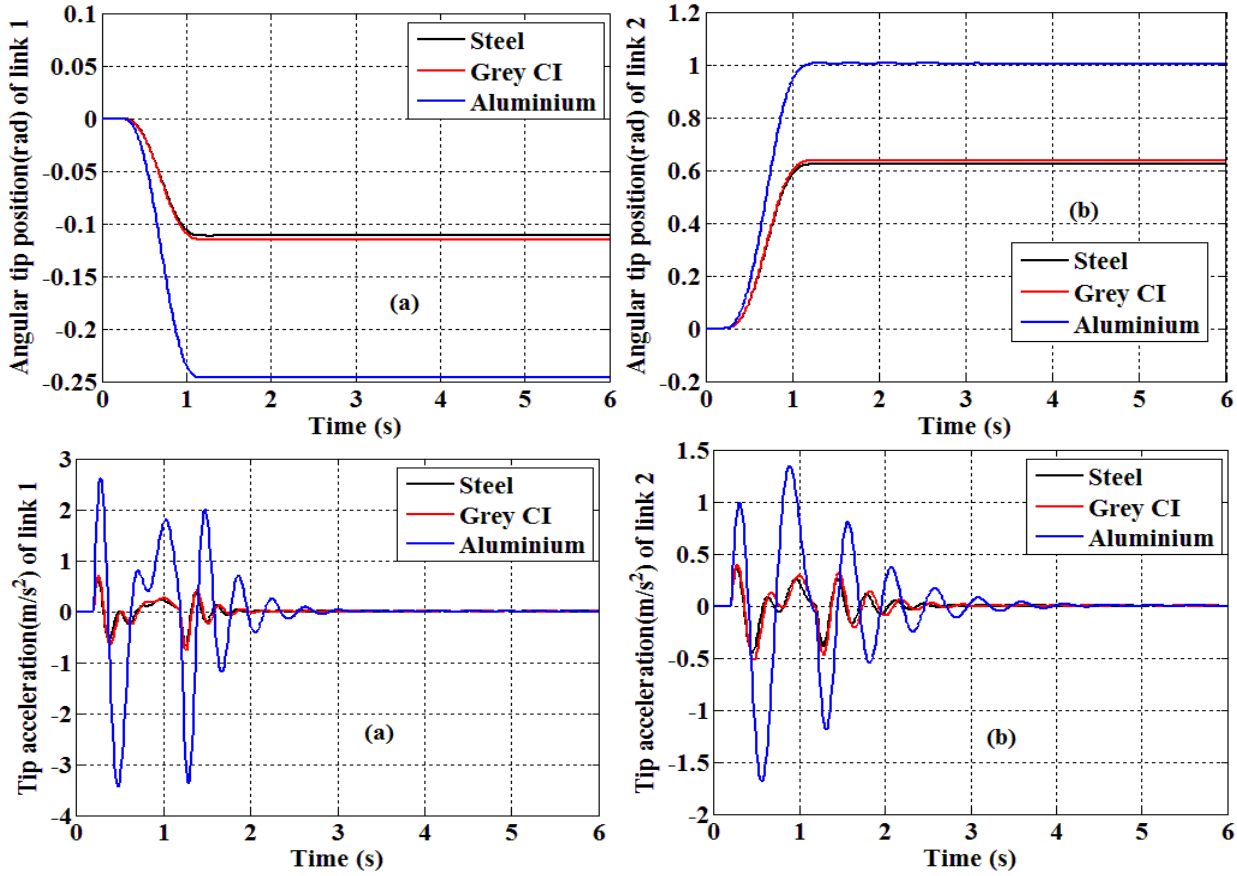

Fig. 4.54: Effect of material of the links on the angular positions and tip accelerations of (a) first and (b) second link.

These results will be very helpful and shall contribute significantly in development of effective control algorithms for a flexible two-link robot manipulator incorporating an extended

payload. The present analysis have demonstrated that the system attributes such as system inertia, link parameters and payload variables plays a very important role in the dynamic behavior and system characteristics of flexible manipulator and should be considered while modeling and controlling such systems. Subsequently, the eigenspectrums can be further used to analyze such models under different forcing conditions in order to achieve a satisfactory and safe design of manipulators with attenuations and to avoid catastrophic failures.

d) *Performance analysis: control parameters*

The procedure of inverse dynamics of the system is exploited to design and determine the open-loop torque accounting of the rigid body motion of the joints for the accurate positioning of the links of manipulator. Here to conduct the simulations, the geometrical and physical characteristics for both links have been considered similar to the previous subsection. The K_p and K_d are taken as (100, 150) and (500,600), respectively. A sinusoidal torque profile is used to position the first link at 60 deg and second link at 30 deg, respectively in 4 seconds. The influence of payload on the angular position, input torque and modal displacement is demonstrated in Fig. 4.55. It can be observed that both links achieve the desired positions and the error (of order 0.001) reduces with increase in payload mass from no payload condition to 0.5 kg. The required input torque and the amplitude of the tip displacements also increases significantly with the increase in payload mass. It can also be observed that the tip of first link have smaller amounts of residual vibrations as compared to the second link, even after the required torque is removed. Hence, while lifting a larger amount of payload will require increased amount of torque. The increased end-point vibrations due to larger payloads have to be suppressed for accurate positioning. A negligible effect on the input torque of the second hub is noticed with the increase in second joint mass in Fig. 4.56, however the torque input of the first joint increases due to the increase in overall inertia of the system driven by first joint.

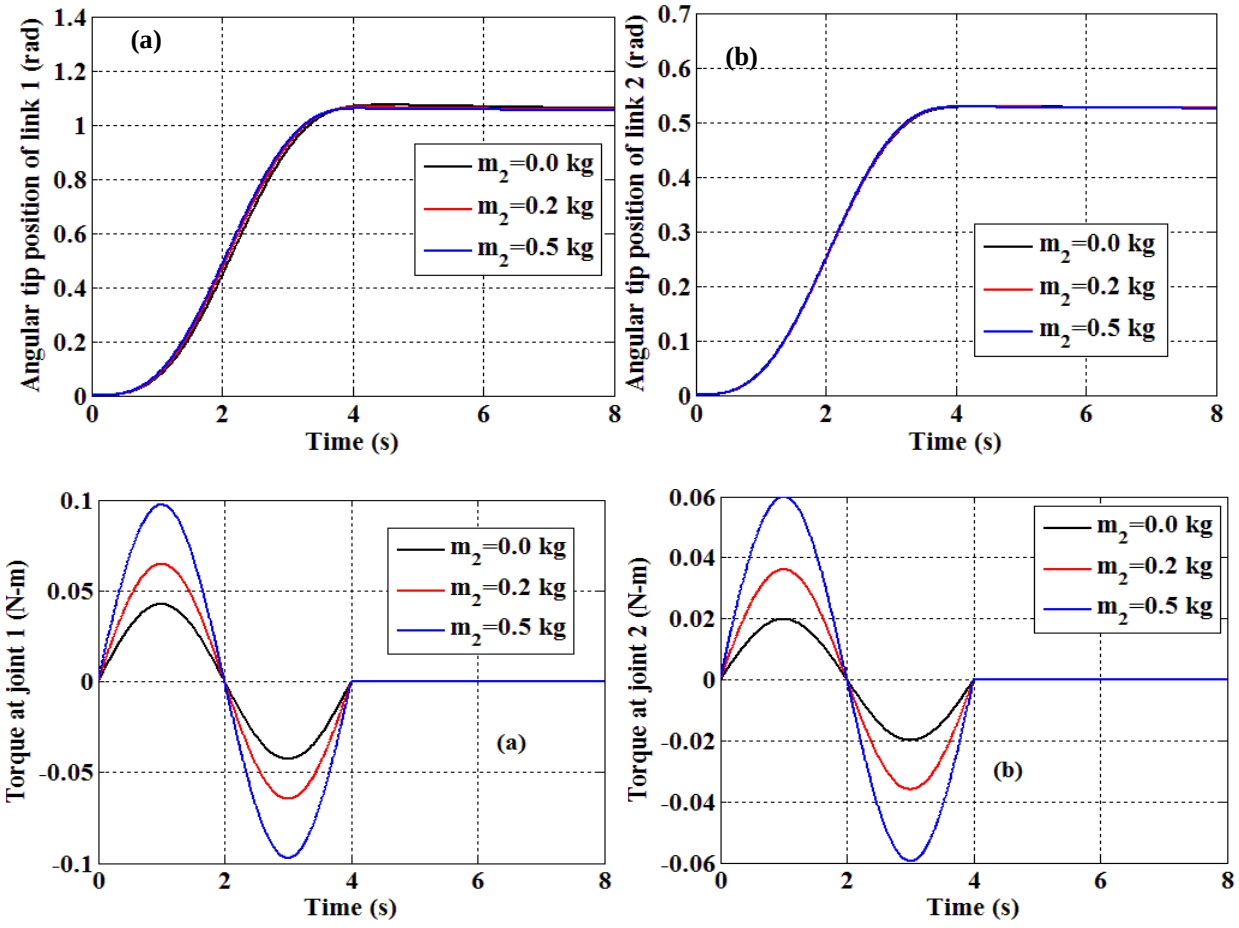

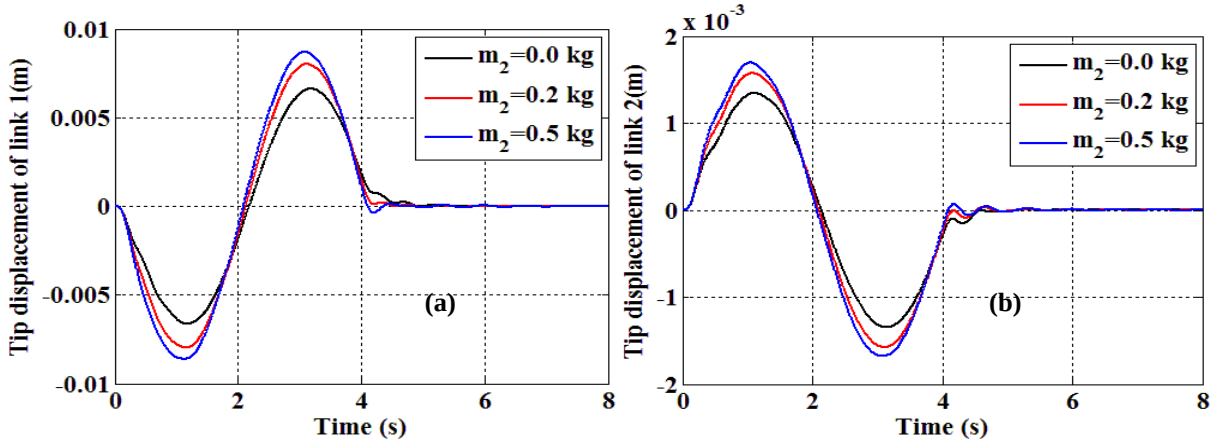

Fig. 4.55: Effect of variation of payload mass (m_2) on the angular positions, input torques, and tip displacements of (a) first link and (b) second link.

An increase in joint inertias increases the power consumption of the actuators due to increased input torques which can be inferred from Fig. 4.57 and it also increases the amplitude of the residual vibrations of the end-effector which may result in increased error in trajectory tracking of the manipulator. The end-effector vibrates at significantly higher amplitudes for larger joint inertias after reaching the desired set angular positions.

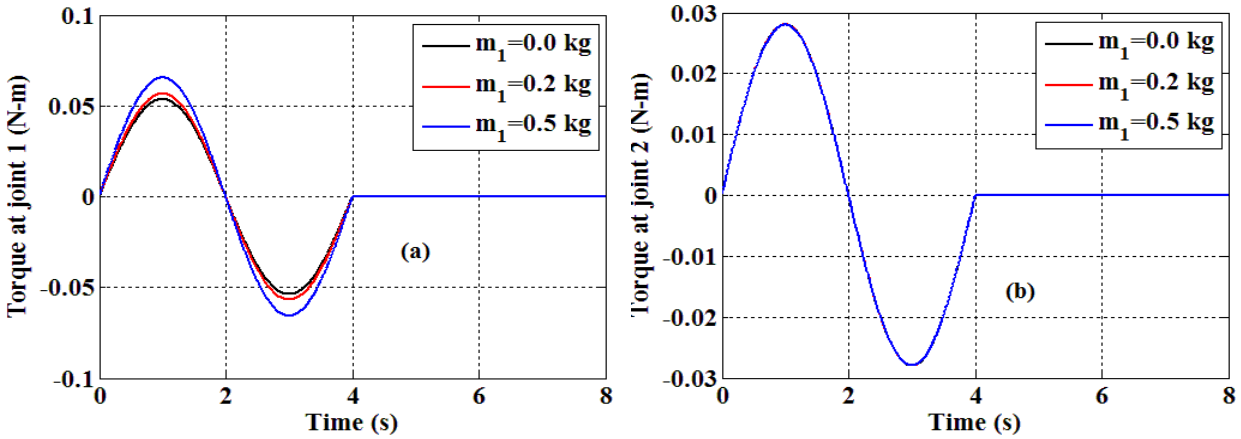

Fig. 4.56: Effect of variation of second joint mass on the input torques of (a) first link and (b) second link.

An increase in length of the first link increases the required amount of torque for both the joints however the rigid motion of the end point of the second link increases significantly which is evident from the Fig. 4.58. While the end point vibrations of the first link damp out after some time for the larger link length but the tip of the second link continues oscillating for a larger duration.

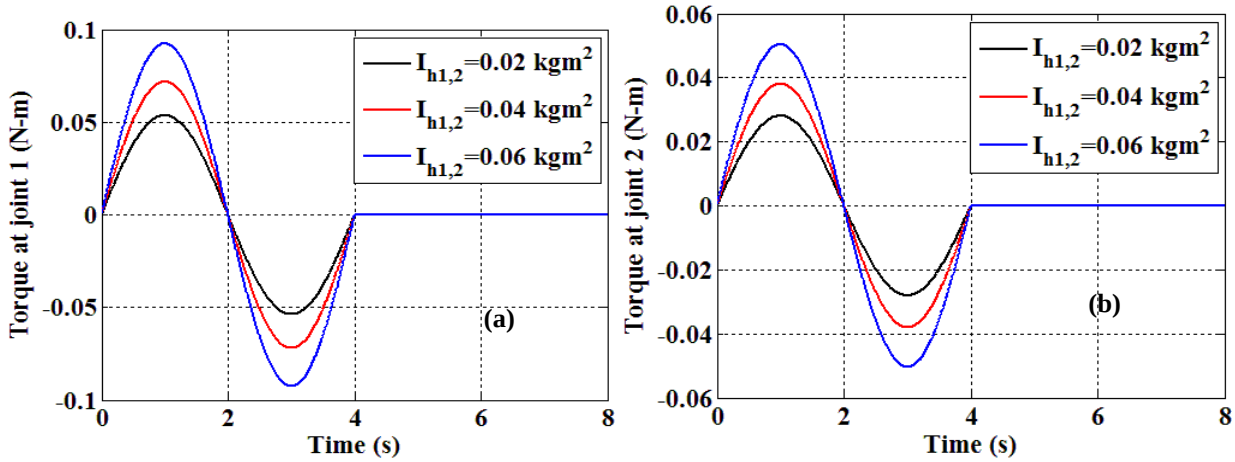

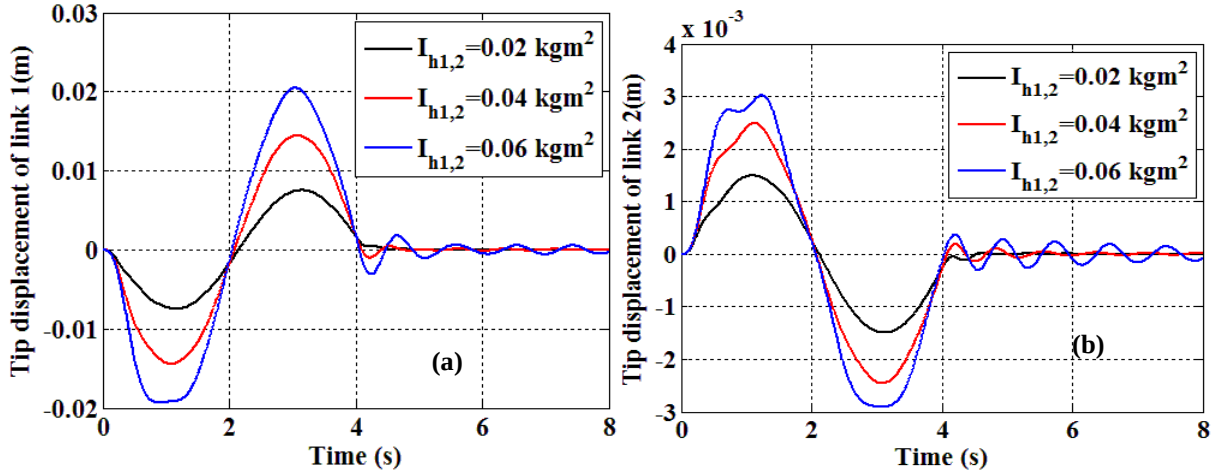

Fig. 4.57: Variation of joint inertia $\left(I_{h1,2}\right)$ on the input torques, and tip displacements of (a) first and (b) second link.

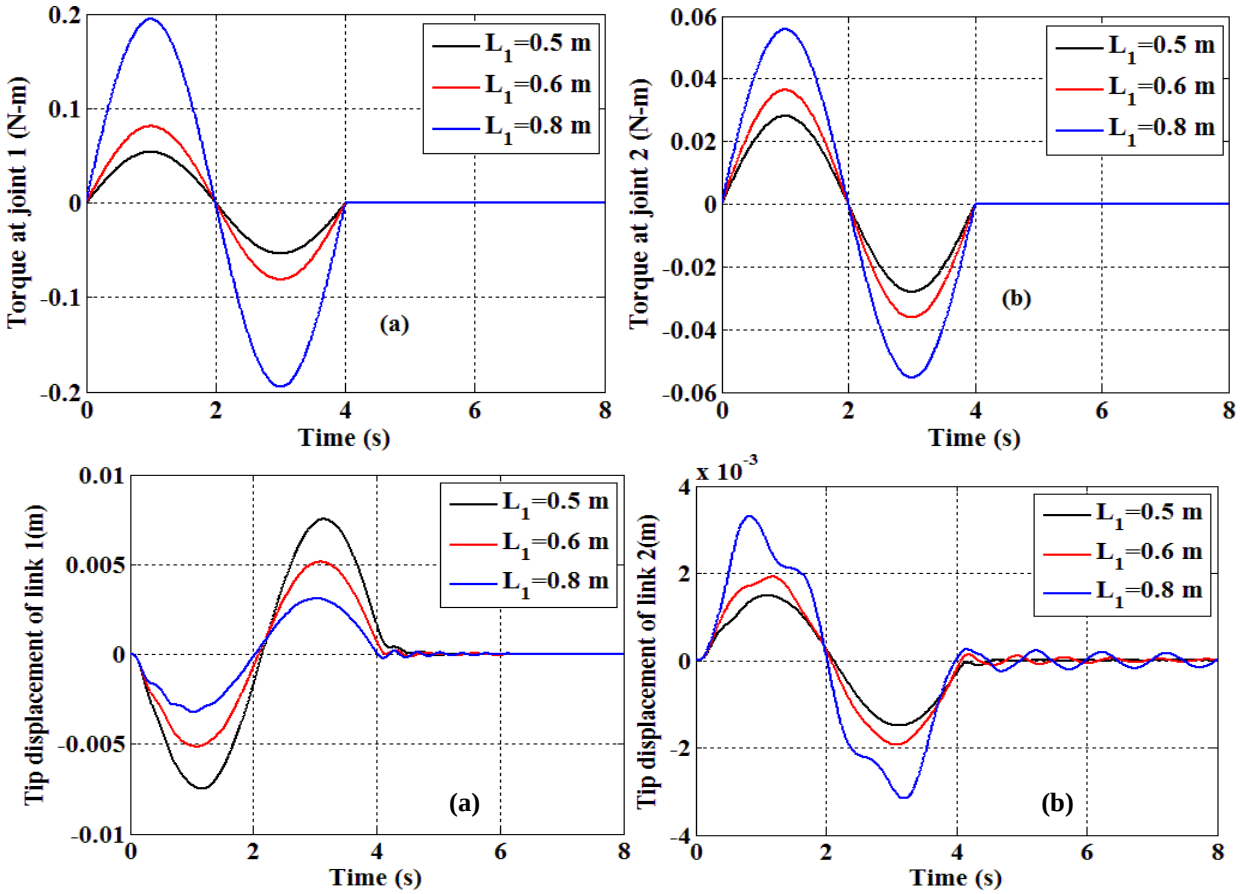

Fig. 4.58: Variation of first link length $\left(L_1\right)$ on input torques, and tip displacements of (a) first and (b) second link.

It is observed from Fig. 4.59 that as the material of the links is changed from steel to aluminum, the input torque reduces but the tip of the manipulator links still vibrates with large amplitudes. The residual vibrations are prominent in the case of the aluminum. Thus, while the use of aluminum shall reduce the power consumption of the manipulator system significantly, the design engineer will have to reduce the end point vibrations for accurate trajectory tracking. Hence, based on the present results, the design engineer must find a strategy which optimizes

both the power consumption and residual vibrations while operating manipulators under parametric variations.

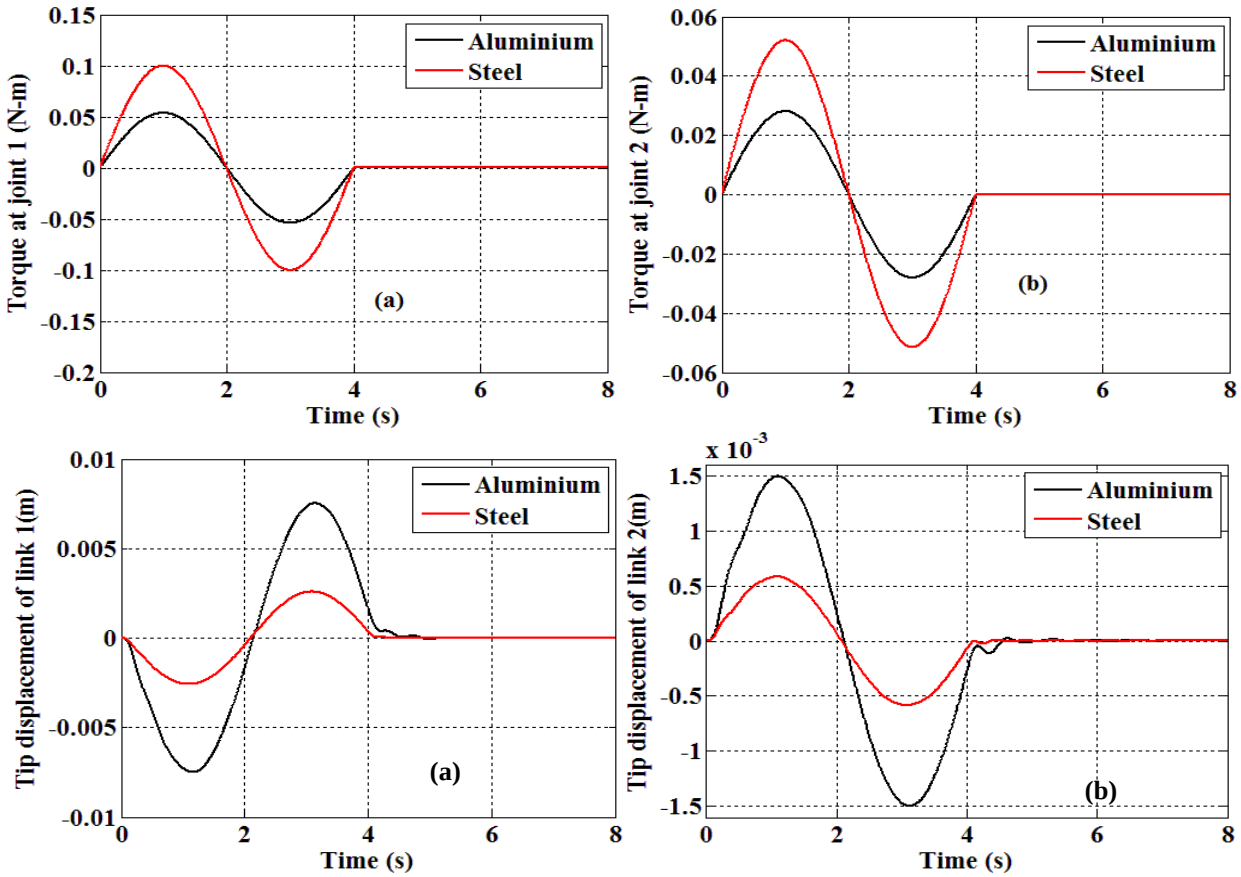

Fig. 4.59: Variation of material on the input torques, and tip displacements of (a) first link and (b) second link.

4.6 TWO-LINK FLEXIBLE MANIPULATOR WITH PRISMATIC AND REVOLUTE JOINTS

A schematic diagram of a two-link planar flexible manipulator is considered where first link is attached to a prismatic joint while revolute joint is used to hold the second link as shown in Fig. 4.60. The first link of the manipulator is being provided time dependent vertical motion (ϑ) at the actuator having mass (m_a) and linear stiffness (k_a) representing the actuator and v_a is the vertical displacement of actuator from the equilibrium position. The second link is being driven by revolute joint having mass (m_1), inertia (I_h) and torsional spring stiffness (k_θ) at one end and payload of mass (m_2) at other end.

The expressions for the total kinetic energy (T_{total}) and potential energy (U_{total}) of the system, respectively are given by:

$$T_{total} = 0.5\left[\sum_{i=1}^{2}\int_{0}^{L_i}\rho_i \dot{\bar{P}}_i^T \dot{\bar{P}}_i dx + \sum_{i=1}^{2} m_i \dot{\bar{P}}_{iL}^T \dot{\bar{P}}_{iL} + I_h\left(\dot{\theta}+\dot{w}'_{1L}\right)^2 + m_a\left\{\dot{w}_{1(x=0)}+\dot{\vartheta}(t)+\dot{v}_a(t)\right\}^2\right]. \quad (4.117)$$

$$U_{total} = 0.5\left[\sum_{i=1}^{2}\int_{0}^{L_i} E_i I_i\left(w_i''\right)^2 dx + \sum_{i=1}^{2}\int_{0}^{L_i} E_i A_i\left((1/2)w_i'^2\right)^2 dx + k_a\left\{\vartheta(t)+v_a(t)\right\}^2 + k_\theta\left(\theta+w'_{1L}\right)^2\right]. \quad (4.118)$$

Here, T_{total} constitutes the kinetic energy associated with masses of the links, masses at the link terminals, actuator mass, and joint inertia, while U_{total} represents the bending strain energy of links, energy due to axial stretching, strain energy of the actuator and revolute joints.

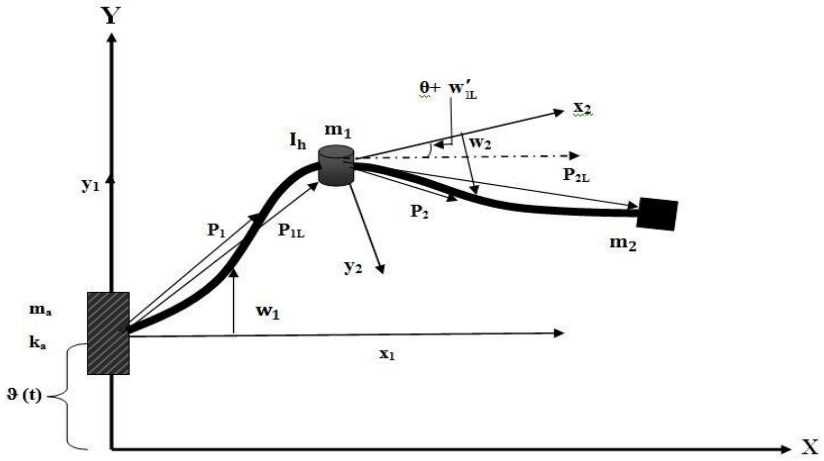

Fig. 4.60: Schematic diagram of a planar two-link flexible robotic manipulator with prismatic and revolute joint incorporating a payload.

4.6.1 Free vibration analysis

The governing equations of link motions along with joint dynamics obtained for the two-link flexible manipulator with prismatic and revolute joint by employing extended Hamilton's principle are expressed here as:

The governing equation of motion for first link is expressed as:

$$\{w_1\}:\ \rho_1 A_1\left(\ddot{w}_1+\ddot{\vartheta}+\ddot{v}_a\right)+E_1I_1w_1''''-(3/2)E_1A_1w_1'^2w_1''=0. \tag{4.119}$$

The associated boundary conditions for the first link are:

$$\left\{E_1I_1w_1''+m_a\left(\ddot{w}_1+\ddot{\vartheta}+\ddot{v}_a\right)\right\}_{(0,t)}+k_a\left(w_1+\vartheta+v_a\right)_{(0,t)}=0,\ \ \{\mathrm{E_1I_1w_1'}\}_{(0,t)}=0,$$

$$\int_0^{L_1}\rho_2A_2\begin{pmatrix}x\ddot{w}_2+x\ddot{\vartheta}+x\ddot{v}_a+x^2\ddot{w}_{1L}'+x^2\ddot{\theta}+2w_2\dot{w}_2\dot{\theta}+2w_2\dot{w}_2\dot{w}_{1L}'+w_2^2\ddot{\theta}+w_2^2\ddot{w}_{1L}'-\theta\dot{\vartheta}^2-\theta\dot{v}_a^2-\\2\theta\dot{\vartheta}\dot{v}_a-w_{1L}'\dot{\vartheta}^2-w_{1L}'\dot{v}_a^2-2w_{1L}'\dot{\vartheta}\dot{v}_a-\theta\dot{w}_2\dot{\vartheta}-w_{1L}'\dot{w}_2\dot{\vartheta}-\theta\dot{w}_2\dot{v}_a-w_{1L}'\dot{w}_2\dot{v}_a-\\w_2\theta\ddot{\vartheta}-w_2w_{1L}'\ddot{\vartheta}-w_2\theta\ddot{v}_a-w_2w_{1L}'\ddot{v}_a\end{pmatrix}dx$$

$$m_2\begin{pmatrix}L_2\ddot{w}_{2L}+L_2\ddot{\vartheta}+L_2\ddot{v}_a+L_2^2\ddot{w}_{1L}'+L_2^2\ddot{\theta}+2w_{2L}\dot{w}_{2L}\dot{\theta}+2w_{2L}\dot{w}_{2L}\dot{w}_{1L}'+w_{2L}^2\ddot{\theta}+s_{2L}^2\ddot{w}_{1L}'-\theta\dot{\vartheta}^2-\\\theta\dot{v}_a^2-2\theta\dot{\vartheta}\dot{v}_a-w_{1L}'\dot{\vartheta}^2-w_{1L}'\dot{v}_a^2-2w_{1L}'\dot{\vartheta}\dot{v}_a-\theta\dot{w}_{2L}\dot{\vartheta}-w_{1L}'\dot{w}_{2L}\dot{\vartheta}-\theta\dot{w}_{2L}\dot{v}_a-w_{1L}'\dot{w}_{2L}\dot{v}_a\\-w_{2L}\theta\ddot{\vartheta}-w_{2L}w_{1L}'\ddot{\vartheta}-w_{2L}\theta_2\ddot{v}_a-w_{2L}w_{1L}'\ddot{v}_a\end{pmatrix}$$

$$+E_1I_1w_{1L}''+J\left(\ddot{\theta}+\ddot{w}_{1L}'\right)+k_\theta\left(\theta+w_{1L}'\right)-E_2I_2w_{2(0,t)}''=0,$$

$$\left(m_1+m_2\right)\left(\ddot{w}_{1L}+\ddot{\vartheta}+\ddot{v}_a\right)+\int_0^{L_2}\rho_2A_2\left(\ddot{w}_{1L}+\ddot{\vartheta}+\ddot{v}_a\right)dx-E_1I_1w_{1L}''+E_2I_2w_{2(0,t)}'''+(1/2)E_1A_1w_{1L}'^2=0. \tag{4.120}$$

The governing equation of motion for second link is expressed as:

$$\{w_2\}:\ \begin{matrix}\rho_2A_2(\ddot{w}_2+\ddot{\vartheta}+\ddot{v}_a+x\ddot{w}_{1L}'+x\ddot{\theta}+\theta\dot{\vartheta}\dot{\theta}+\theta\dot{\vartheta}\dot{w}_{1L}'+\theta\dot{v}_a\dot{\theta}+\theta\dot{v}_a\dot{w}_{1L}'+w_{1L}'\dot{\vartheta}\dot{\theta}+w_{1L}'\dot{\vartheta}\dot{w}_{1L}'\\+w_{1L}'\dot{v}_a\dot{\theta}+w_{1L}'\dot{v}_a\dot{w}_{1L}'-w_2\dot{\theta}^2-w_2\dot{w}_{1L}'^2-2w_2\dot{\theta}\dot{w}_{1L}')+E_2I_2w_2''''-(3/2)E_2A_2w_2'^2w_2''=0.\end{matrix} \tag{4.121}$$

The associated boundary conditions for the second link are:

$$\{\mathrm{E_2I_2w_2}\}_{(0,t)}=\mathrm{E_1I_1w_{1L}},\ \{\mathrm{E_2I_2w_2'}\}_{(x=0)}=\mathrm{E_1I_1w_{1L}'},\ \{\mathrm{E_2I_2w_2''}\}_{(\mathrm{L_2},t)}=0,$$

$$m_2(\ddot{w}_{2L}+\ddot{\vartheta}+\ddot{v}_a+L_2\ddot{w}'_{1L}+L_2\ddot{\theta}+\theta\dot{\vartheta}\dot{\theta}+\theta\dot{\vartheta}\dot{w}'_{1L}+\theta\dot{v}_a\dot{\theta}+\theta\dot{v}_a\dot{w}'_{1L}+w'_{1L}\dot{\vartheta}\dot{\theta}+w'_{1L}\dot{\vartheta}\dot{w}'_{1L}+$$
$$w'_{1L}\dot{v}_a\dot{\theta}+w'_{1L}\dot{v}_a\dot{w}'_{1L}-w_{2L}\dot{\theta}^2-w_{2L}w'^2_{1L}-2w_{2L}\dot{\theta}\dot{w}'_{1L})-E_2I_2w'''_{2L}+(1/2)E_2A_2{w'_{2L}}^3=0. \quad (4.122)$$

Equation of motion of joint dynamics is expressed as:

$$I_h\left(\ddot{\theta}+\ddot{w}'_{1L}\right)+k_\theta\left(\theta+w'_{1L}\right)+\int_0^{L_2}\rho_2A_2\begin{pmatrix}2w_2\ddot{w}_2\dot{w}'_{1L}+2w_2\dot{w}_2\dot{\theta}+w_2^2\ddot{\theta}+w_2^2\ddot{w}'_{1L}+x\ddot{w}_2+\\ x\ddot{\vartheta}+x\ddot{v}_a+x^2\ddot{w}'_{1L}+x^2\ddot{\theta}-\theta\dot{\vartheta}^2-w'_{1L}\dot{\vartheta}^2-\theta\dot{v}_a^2\\ -w'_{1L}\dot{v}_a^2-\theta\dot{w}_2\dot{\vartheta}-w'_{1L}\dot{w}_2\dot{\vartheta}-\theta\dot{w}_2\dot{v}_a-w'_{1L}\dot{w}_2\dot{v}_a\\ -\theta w_2\ddot{\vartheta}-w'_{1L}w_2\ddot{\vartheta}-\theta w_2\ddot{v}_a-w'_{1L}w_2\ddot{v}_a\end{pmatrix}dx$$

$$\{\theta\}: \quad (4.123)$$

$$m_2\begin{pmatrix}2w_{2L}\ddot{w}_{2L}\dot{w}'_{1L}+2w_{2L}\dot{w}_{2L}\dot{\theta}+w_{2L}^2\ddot{\theta}+w_{2L}^2\ddot{w}'_{1L}+L_2\ddot{w}_{2L}+L_2\ddot{\vartheta}+L_2\ddot{v}_a+L_2^2\ddot{w}'_{1L}\\ +L_2^2\ddot{\theta}-\theta\dot{\vartheta}^2-w'_{1L}\dot{\vartheta}^2-\theta\dot{v}_a^2-w'_{1L}\dot{v}_a^2-\theta\dot{w}_{2L}\dot{\vartheta}-w'_{1L}\dot{w}_{2L}\dot{\vartheta}-\theta\dot{w}_{2L}\dot{v}_a-w'_{1L}\dot{w}_{2L}\dot{v}_a\\ -\theta w_{2L}\ddot{\vartheta}-w'_{1L}w_{2L}\ddot{\vartheta}-\theta w_{2L}\ddot{v}_a-w'_{1L}w_{2L}\ddot{v}_a\end{pmatrix}=0$$

In this section the eigenfunction and eigenfrequencies are sought for the dynamic model derived earlier through free vibration analysis. The coupled nonlinear terms from Eqs. (4.119)-(4.123) are neglected and the transverse deflections of first and second links are expressed in terms of new functions in space and time as $r_1(\eta,t)=w_1(\eta,t)+\vartheta(t)+v_a(t)$ and $r_2(\eta,t)=w_2(\eta,t)+\vartheta(t)+v_a(t)+x(\theta+w'_{1L})$. The new deflection functions and the joint motion are expressed as explicit function of time and space similar to those in section 4.5.1 and substituted in the governing equations of motion of the links to obtain the respective mode shapes for the nth mode of vibration as:

$$W_1^n(\bar{\eta})=R_1^n\cos\left(\bar{\delta}^n\bar{x}\right)+R_2^n\left\{\sin\left(\bar{\delta}^n\bar{x}\right)-\sinh\left(\bar{\delta}^n\bar{x}\right)\right\}+R_3^n\cosh\left(\bar{\delta}^n\bar{x}\right). \quad (4.124)$$

$$W_2^n(\bar{\eta})=S_1^n\cos\left(\lambda\bar{\delta}^n\bar{x}\right)+S_2^n\sin\left(\lambda\bar{\delta}^n\bar{x}\right)+S_3^m\cosh\left(\lambda\bar{\delta}^n\bar{x}\right)+S_4^m\sinh\left(\lambda\bar{\delta}^n\bar{x}\right). \quad (4.125)$$

The constants $(R_1\cdots R_3,\ S_1\cdots S_4)^n$ are calculated by substituting the mode shapes obtained in Eqs. (4.124)- (4.125) in the boundary conditions. The resulting equations are arranged in the matrix form similar to Eq. (4.12) whose coefficients are expressed in terms of nondimensional system parameters as:

$K_{11}=-\alpha_{ma}\bar{\delta}^n\left(1-\Omega_a^2\right)$, $K_{12}=-2$, $K_{13}=-\alpha_{ma}\bar{\delta}^n\left(1-\Omega_a^2\right)$,

$K_{21}=-\sin\left(\bar{\delta}^n\right)-\left(\alpha_{m1}+\alpha_{m2}+\alpha_M\alpha_L\right)\bar{\delta}^n\cos\left(\bar{\delta}^n\right)$,

$K_{22}=\cos\left(\bar{\delta}^n\right)+\cosh\left(\bar{\delta}^n\right)-\left(\alpha_{m1}+\alpha_{m2}+\alpha_M\alpha_L\right)\bar{\delta}^n\left\{\sin\left(\bar{\delta}^n\right)-\sinh\left(\bar{\delta}^n\right)\right\}$,

$K_{23}=-\sinh\left(\bar{\delta}^n\right)-\left(\alpha_{m1}+\alpha_{m2}+\alpha_M\alpha_L\right)\bar{\delta}^n\cosh\left(\bar{\delta}^n\right)$, $K_{25}=\chi\kappa^3$, $K_{27}=-\chi\kappa^3$, $K_{31}=-\cos\left(\bar{\delta}^n\right)$,

$K_{32}=-\sin\left(\bar{\delta}^n\right)-\sinh\left(\bar{\delta}^n\right)$, $K_{33}=\cosh\left(\bar{\delta}^n\right)$, $K_4=\chi\kappa^2$, $K_{36}=-\chi\kappa^2$, $K_{41}=\cos\left(\bar{\delta}^n\right)$,

$K_{42}=\sin\left(\bar{\delta}^n\right)-\sinh\left(\bar{\delta}^n\right)$, $K_{43}=\cosh\left(\bar{\delta}^n\right)$, $K_{44}=-\chi$, $K_{46}=-\chi$, $K_{51}=\alpha_{Ih}\left(1-\Omega_h^2\right)\bar{\delta}^n\sin\left(\bar{\delta}^n\right)$,

$K_{52}=-\alpha_{Ih}\left(1-\Omega_h^2\right)\bar{\delta}^n\left\{\cos\left(\bar{\delta}^n\right)-\cosh\left(\bar{\delta}^n\right)\right\}$, $K_{53}=-\alpha_{Ih}\left(1-\Omega_h^2\right)\bar{\delta}^n\sinh\left(\bar{\delta}^n\right)$,

$K_{54}=\left\{\alpha_M\chi/\left(\mu\bar{\delta}^n\right)^2\right\}\left\{\cos\left(\lambda\bar{\delta}^n\right)+\mu\bar{\lambda}^m\alpha_L\sin\left(\lambda\bar{\delta}^n\right)-1\right\}+\alpha_{m2}\alpha_L\chi\cos\left(\lambda\bar{\delta}^n\right)$,

$K_{55}=\alpha_{Ih}\bar{\delta}^n\chi\mu\left(1-\Omega_h^2\right)+\left\{\alpha_M\chi/\left(\mu\bar{\delta}^n\right)^2\right\}\left\{\sin\left(\lambda\bar{\delta}^n\right)-\mu\bar{\delta}^n\alpha_L\cos\left(\lambda\bar{\delta}^n\right)\right\}+\alpha_{m2}\alpha_L\chi\sin\left(\lambda\bar{\delta}^n\right)$,

$K_{56}=\left\{\alpha_M\chi/\left(\mu\bar{\delta}^n\right)^2\right\}\left\{\mu\bar{\delta}^n\alpha_L\sinh\left(\lambda\bar{\delta}^n\right)-\cosh\left(\lambda\bar{\delta}^n\right)+1\right\}+\alpha_{m2}\alpha_L\chi\cosh\left(\lambda\bar{\delta}^n\right)$,

$K_{57}=\alpha_{J2}\bar{\delta}^n\mu\chi\left(1-\Omega_2^2\right)+\left\{\alpha_M\chi/\left(\mu\bar{\delta}^n\right)^2\right\}\left\{\mu\bar{\delta}^n\alpha_L\cosh\left(\lambda\bar{\delta}^n\right)-\sinh\left(\lambda\bar{\delta}^n\right)\right\}+\alpha_{m2}\alpha_L\chi\sinh\left(\lambda\bar{\delta}^n\right)$,

$K_{64}=\cos\left(\lambda\bar{\delta}^n\right),\ K_{65}=\sin\left(\lambda\bar{\delta}^n\right),\ K_{66}=-\cosh\left(\lambda\bar{\delta}^n\right),\ K_{67}=-\sinh\left(\lambda\bar{\delta}^n\right),$

$K_{74}=\alpha_{m2}\bar{\delta}^n\cos\left(\lambda\bar{\delta}^n\right)+\chi\mu^3\sin\left(\lambda\bar{\delta}^n\right),\ K_{75}=\alpha_{m2}\bar{\delta}^n\sin\left(\lambda\bar{\delta}^n\right)-\chi\mu^3\cos\left(\lambda\bar{\delta}^n\right),$

$K_{76}=\alpha_{m2}\bar{\delta}^n\cosh\left(\lambda\bar{\delta}^n\right)+\chi\kappa^3\sinh\left(\lambda\bar{\delta}^n\right),\ K_{77}=\alpha_{m2}\bar{\delta}^n\sinh\left(\lambda\bar{\delta}^n\right)+\chi\mu^3\cosh\left(\lambda\bar{\delta}^n\right),$

$K_{14},K_{15},K_{16},K_{17},K_{24},K_{26},K_{35},K_{37},K_{45},K_{47},K_{61},K_{62},K_{63},K_{71},K_{72},$ and $K_{73}=0.$

The integration constants and the eigenfrequency equation are computed as explained in section 4.5.1. In addition to the system parameters given in Eq. **Error! Reference source not found.**, at the same time above elements are expressed in terms of: $\Omega_h=\left(k_\theta/I_h\right)/\omega_m^2$, $\Omega_a=\left(k_a/m_a\right)/\omega^2$, $\alpha_J=Ih/\rho_1A_1{L_1}^3$, and $\alpha_{m1}=m_a/\rho_1A_1L_1$.

4.6.2 Nonlinear forced vibration analysis

The nonlinear behaviors and stability characteristics of the two-link flexible manipulator with harmonically driven prismatic and revolute motion of frequency $\bar{\omega}_{1,2}$ have been analyzed. The nonlinear coupled terms and the cubic nonlinearity arising due to geometric stretching have been retained in the governing equations of motions of the links expressed in Eqs. (4.119) & (4.121) and viscous damping $\left(c_{d1,2}\right)$ is included in both links. Similar to section 4.5.2 the governing equations of motion are nondimensionalized, discretized using the mode shapes obtained in previous sub-section and after appropriate ordering of the nonlinear terms are expressed here as:

$$\ddot{p}_1(\tau)+\bar{\Omega}_1^2p_1(\tau)+2\varepsilon\xi_1\dot{p}_1-\varepsilon\beta_1\bar{\omega}_1^2\cos(\bar{\omega}_1\tau)-\varepsilon^2\beta_2p_1^3(\tau)=0. \tag{4.126}$$

$$\begin{aligned}&\ddot{p}_2(\tau)+\bar{\Omega}_2^2p_2(\tau)+2\varepsilon\xi_2\dot{p}_2(\tau)-\varepsilon\left\{\beta_3\omega_1^2\cos(\bar{\omega}_1\tau)+\beta_{11}\bar{\omega}_2^2\cos(\bar{\omega}_2\tau)\right\}+\\&\varepsilon^2\begin{Bmatrix}\beta_4\bar{\omega}_1\bar{\omega}_2\sin(\bar{\omega}_1\tau)\sin(\bar{\omega}_2\tau)\cos(\bar{\omega}_2\tau)-\beta_5\bar{\omega}_1\dot{p}_1(\tau)\sin(\bar{\omega}_1\tau)\cos(\bar{\omega}_2\tau)+\beta_{12}\ddot{p}_1(\tau)+\\\beta_6\bar{\omega}_1\bar{\omega}_2p_1(\tau)\sin(\bar{\omega}_1\tau)\sin(\bar{\omega}_2\tau)-\beta_7\bar{\omega}_1p_1(\tau)\dot{p}_1(\tau)\sin(\bar{\omega}_1\tau)-\beta_8\bar{\omega}_2^2p_2(\tau)\sin^2(\bar{\omega}_1\tau)\\-\beta_9p_2(\tau)\dot{q}_1^2(\tau)+\beta_{10}\bar{\omega}_2p_2(\tau)\dot{p}_1(\tau)\sin(\bar{\omega}_2\tau)-\beta_{13}p_2^3(\tau)\end{Bmatrix}=0\end{aligned} \tag{4.127}$$

The approximate solutions of Eqs. (4.126)- (4.127) are determined by using second order method of multiple scales similar to section 4.5.2 and $p_{1,2}$ are expressed in terms of fast $\left(T_0=\tau\right)$ and slow time $\left(T_1=\varepsilon\tau,T_2=\varepsilon^2\tau\right)$ scales. Equating the coefficients of the same powers of ε the governing equations of motion of the first link in different time scales are obtained as:

$$O\left(\varepsilon^1\right):\ \partial^2p/\partial{T_0}^2+\bar{\Omega}_1^2p_{10}=0\,. \tag{4.128}$$

$$O\left(\varepsilon^2\right):\ \partial^2p_{11}/\partial{T_1}^2+\bar{\Omega}_1^2p_{11}+2\xi_1\left(\partial p_{10}/\partial T_0\right)+2\left(\partial^2p_{10}/\partial T_0\partial T_1\right)-\beta_1\bar{\omega}_1^2\cos\left(\bar{\omega}_1T_0\right)=0. \tag{4.129}$$

$$O\left(\varepsilon^3\right):\ \begin{aligned}&\partial^2p_{12}/\partial{T_2}^2+\bar{\Omega}_1^2p_{12}+2\xi_1\left(\partial p_{11}/\partial T_0+\partial p_{10}/\partial T_1\right)+2\left(\partial^2p_{10}/\partial T_0\partial T_2\right)+\\&2\left(\partial^2p_{11}/\partial T_0\partial T_1\right)-\beta_2p_{10}^3=0.\end{aligned} \tag{4.130}$$

The equations for the second link are obtained in a similar manner as:

$$O\left(\varepsilon^1\right):\ \partial^2p_{20}/\partial{T_0}^2+\bar{\Omega}_2^2p_{20}=0 \tag{4.131}$$

$$O\left(\varepsilon^2\right):\ \begin{aligned}&\partial^2p_{21}/\partial{T_1}^2+\bar{\Omega}_2^2p_{21}+2\xi_2\left(\partial p_{20}/\partial T_0\right)+2\left(\partial^2p_{20}/\partial T_0\partial T_1\right)-\beta_3\bar{\omega}_1^2\cos\left(\bar{\omega}_1T_0\right)-\\&\beta_{11}\bar{\omega}_1^2\cos\left(\bar{\omega}_2T_0\right)=0.\end{aligned} \tag{4.132}$$

$$O(\varepsilon^3): \begin{aligned} &\partial^2 p_{22}/\partial T_2{}^2 + \bar{\Omega}_2^2 p_{22} + 2\xi_2(\partial p_{21}/\partial T_0 + \partial p_{20}/\partial T_1) + 2\left(\partial^2 p_{20}/\partial T_0 \partial T_2\right) + \\ &2\left(\partial^2 p_{21}/\partial T_0 \partial T_1\right) + \partial^2 p_{20}/\partial T_1{}^2 + \beta_{12}\partial^2 p_{10}/\partial T_0{}^2 - \beta_3 \omega_1^2 \cos(\bar{\omega}_1 T_0) - \\ &\beta_{11}\bar{\omega}_2^2 \cos(\bar{\omega}_2 T_0) + \beta_4 \bar{\omega}_1 \bar{\omega}_2 \sin(\bar{\omega}_1 T_0)\sin(\bar{\omega}_2 T_0)\cos(\bar{\omega}_2 T_0) - \\ &\beta_5 \bar{\omega}_1 (\partial p_{10}/\partial T_0)\sin(\bar{\omega}_1 T_0)\cos(\bar{\omega}_2 T_0) + \beta_6 \bar{\omega}_1 \bar{\omega}_2 p_{10}\sin(\bar{\omega}_1 T_0)\sin(\bar{\omega}_2 T_0) - \\ &\beta_7 \bar{\omega}_1 p_{10}(\partial p_{10}/\partial T_0)\sin(\bar{\omega}_1 T_0) - \beta_8 \bar{\omega}_2^2 p_{20}\sin^2(\bar{\omega}_1 T_0) - \beta_9 p_{20}(\partial p_{10}/\partial T_0)^2 + \\ &\beta_{10}\bar{\omega}_2 p_{20}(\partial p_{10}/\partial T_0)\sin(\bar{\omega}_2 T_0) - \beta_{13} p_{20}^3 = 0. \end{aligned} \tag{4.133}$$

The general solution of differential equations Eqs. (4.128)- (4.131) can be expressed as:

$$p_{10} = \bar{Q}_1(T_1, T_2)\exp(i\bar{\Omega}_1 T_0) + \bar{Q}_1(T_1, T_2)\exp(-i\bar{\Omega}_1 T_0). \tag{4.134}$$

$$p_{20} = \bar{Q}_2(T_1, T_2)\exp(i\bar{\Omega}_2 T_0) + \bar{Q}_2(T_1, T_2)\exp(-i\bar{\Omega}_2 T_0). \tag{4.135}$$

Now, it can be observed that any solution of Eqs. (4.129)- (4.132) will contain secular or small divisor terms if the frequency of prismatic $(\bar{\omega}_1)$ and revolute joint $(\bar{\omega}_2)$ motion become equal or nearly equal to link's normalized frequencies $(\bar{\Omega}_{1,2})$. In order to have bounded solutions of the respective equations these secular or small divisor terms should be removed. Also, it has been numerically found that the normalized link frequencies $(\bar{\Omega}_{1,2})$ are nearly equal for same link parameters which results in the existence of internal resonance between the links of the manipulator.

4.6.3 Primary resonance in the first and second link: $(\bar{\omega}_1 \approx \bar{\Omega}_1)$ and $(\bar{\omega}_2 \approx \bar{\Omega}_2)$

In case of the first link, a simple resonance condition exits when the frequency of prismatic joint motion $(\bar{\omega}_1)$ becomes equal or nearly equal to the normalized frequency $(\bar{\Omega}_1)$ and in the second link when the frequency of revolute joint motion $(\bar{\omega}_2)$ becomes equal or nearly equal to the normalized frequency $(\bar{\Omega}_2)$. Now, for simple resonance case, the nearness of $\bar{\omega}_1$ to $\bar{\Omega}_1$ and $\bar{\omega}_2$ to $\bar{\Omega}_2$ are respectively expressed as, $\bar{\Omega}_1 + \varepsilon\sigma_1$, and $\bar{\Omega}_2 + \varepsilon\sigma_2$, here σ_1 and σ_2 are known as detuning parameters. Following a similar procedure as adopted in sub-section 4.4.2, the governing equations for the vibration for both the links in terms of original time variable τ are obtained as:

$$\begin{aligned} &2i\bar{\Omega}_1(\partial Q_1/\partial\tau) + 2i\bar{\Omega}_1\varepsilon\xi_1 Q_1 + \left\{\left(\beta_1\varepsilon^2\bar{\omega}_1^2\sigma_1/4\bar{\Omega}_1\right) - \left(\beta_1\varepsilon\bar{\omega}_1^2/2\right)\right\}\exp(i\sigma_1 T_1) - \\ &\left(i\beta_1\varepsilon^2\bar{\omega}_1^2\xi_1/4\bar{\Omega}_1\right)\exp(i\sigma_1 T_1) - 3\beta_2\varepsilon^2 Q_1^2\bar{Q}_1 - \varepsilon^2\xi_1{}^2 Q_1 = 0. \end{aligned} \tag{4.136}$$

$$\begin{aligned} &2i\bar{\Omega}_2(\partial Q_2/\partial\tau) + 2i\bar{\Omega}_2\varepsilon\xi_2 Q_2 + \left\{\left(\beta_{11}\varepsilon^2\bar{\omega}_2^2\sigma_2/4\bar{\Omega}_2\right) - \left(\beta_{11}\varepsilon\bar{\omega}_2^2/2\right)\right\}\exp(i\sigma_2 T_1) - \\ &2\beta_9\varepsilon^2\bar{\Omega}_1^2 Q_1\bar{Q}_1 Q_2 - \left(i\beta_{11}\varepsilon^2\bar{\omega}_2^2\xi_2/4\bar{\Omega}_2\right)\exp(i\sigma_2 T_1) - \left(\beta_8\varepsilon^2\bar{\omega}_2^2/2\right)\left(Q_2 - \bar{Q}_2\exp(2i\sigma_2 T_1)/2\right) \\ &-3\beta_{13}\varepsilon^2 Q_2^2\bar{Q}_2 - \varepsilon^2\xi_2{}^2 Q_2 = 0. \end{aligned} \tag{4.137}$$

Substituting the polar form of $Q_1(\tau)$ and $Q_2(\tau)$ as $Q_1(\tau)=(1/2)r_1(\tau)e^{i\phi_1(\tau)}$ and $Q_2(\tau)=(1/2)r_2(\tau)e^{i\phi_2(\tau)}$ and separating real and imaginary parts, the following differential equations are obtained by letting $\lambda_1 = \sigma_1 T_1 - \varphi_1$ and $\lambda_2 = \sigma_2 T_1 - \phi_2$ as:

$$\begin{aligned} &\bar{\Omega}_1(\partial r_1/\partial\tau) + \bar{\Omega}_1\varepsilon\xi_1 r_1 + \left\{\beta_1\varepsilon^2\bar{\omega}_1^2\sigma_1/4\bar{\Omega}_1 - \beta_1\varepsilon\bar{\omega}_1^2/2\right\}\sin(\lambda_1) - \left(\beta_1\varepsilon^2\bar{\omega}_1^2\xi_1/4\bar{\Omega}_1\right)\cos(\lambda_1) = 0, \\ &r_1\bar{\Omega}_1(\partial\lambda_1/\partial\tau) - \varepsilon\sigma_1 r_1\bar{\Omega}_1 + \left\{\beta_1\varepsilon^2\bar{\omega}_1^2\sigma_1/4\bar{\Omega}_1 - \beta_1\varepsilon\bar{\omega}_1^2/2\right\}\cos(\delta_1) + \left(\beta_1\varepsilon^2\bar{\omega}_1^2\xi_1/4\bar{\Omega}_1\right)\sin(\delta_1) \\ &-\varepsilon\xi_1^2 r_1/2 - (3/8)\beta_2\varepsilon^2 r_1^3 = 0. \end{aligned} \tag{4.138}$$

$$\bar{\Omega}_2\left(\partial r_2/\partial\tau\right)+\bar{\Omega}_2\varepsilon\xi_2 r_2+\left\{\beta_{11}\varepsilon^2\bar{\omega}_2^2\sigma_2/4\bar{\Omega}_2-\beta_{11}\varepsilon\bar{\omega}_2^2/2\right\}\sin\left(\lambda_2\right)-\left(\beta_{11}\varepsilon^2\bar{\omega}_2^2\xi_2/4\bar{\Omega}_2\right)\cos\left(\lambda_2\right)$$
$$+\left(\beta_8\varepsilon^2\bar{\omega}_2^2/8\right)r_2\sin\left(2\lambda_2\right)=0,$$
$$r_2\bar{\Omega}_2\left(\partial\lambda_1/\partial\tau\right)+\left\{\beta_{11}\varepsilon^2\bar{\omega}_2^2\sigma_2/4\bar{\Omega}_2-\beta_{11}\varepsilon\bar{\omega}_2^2/2\right\}\cos\left(\lambda_2\right)+\left(\beta_{11}\varepsilon^2\bar{\omega}_2^2\xi_2/4\bar{\Omega}_2\right)\sin\left(\lambda_2\right)-$$
$$\varepsilon\sigma_2 r_2\bar{\Omega}_2+\left(\beta_8\varepsilon^2\bar{\omega}_2^2/8\right)r_2\cos\left(2\lambda_2\right)-\left\{\varepsilon\xi_2^2/2+\varepsilon^2\beta_8\bar{\omega}_2^2/2+\beta_9\varepsilon^2\bar{\Omega}_1^2r_1^2/8\right\}r_2-\left(3/8\right)\beta_{13}\varepsilon^2r_2^3=0. \tag{4.139}$$

The solutions of the first and second link up to the second order approximations in terms of original time variable τ, are expressed as:

$$p_1=\left(1/2\right)r_1\cos\left(\bar{\omega}_1\tau-\lambda_1\right)+O\left(\varepsilon^2\right),$$
$$p_2=\left(1/2\right)r_2\cos\left(\bar{\omega}_2\tau-\lambda_2\right)+\varepsilon\left\{\beta_3\bar{\omega}_1^2/2\left(\bar{\Omega}_2^2-\bar{\omega}_1^2\right)\right\}\cos\left(\bar{\omega}_1\tau\right)+O\left(\varepsilon^2\right). \tag{4.140}$$

The steady-state response of Eqs. (4.138)- (4.139) can be obtained by equating $\left(\partial r_j/\partial\tau\right)$ and $\left(\partial\lambda_j/\partial\tau\right)$ (*j=1, 2*) to be zero which results in a set of two equations for the links. Further, the respective frequency response equations of the links in terms of r_j and σ_j can be obtained by eliminating λ_j from the resultant equations obtained earlier. Similar to the sub-section 4.5.3, for the first link, in order to determine the stability of the steady-state solutions, a small perturbation is introduced in Eqs. (4.138) and r_1, and λ_1 are replaced with $r_1=r_{10}+r_{11}$, and $\lambda_1=\lambda_{10}+\lambda_{11}$. The stability of the steady-state solutions is determined by investigating the eigenvalues of following Jacobian matrix:

$$J=\begin{bmatrix} -\varepsilon\mu_1 & -\left\{\beta_1\varepsilon^2\bar{\omega}_1^2\sigma_1/4\bar{\Omega}_1^2-\beta_1\varepsilon\bar{\omega}_1^2/2\bar{\Omega}_1\right\}\cos\left(\lambda_{10}\right)- \\ & \left(\beta_1\varepsilon^2\bar{\omega}_1^2\mu_1/4\bar{\Omega}_1^2\right)\sin\left(\lambda_{10}\right) \\ \varepsilon\sigma_1/r_{10}+9\varepsilon^2\beta_2 r_{10}/8+\varepsilon\mu_1^2/2a_{10}\lambda_1 & \left\{\beta_1\varepsilon^2\bar{\omega}_1^2\sigma_1/4r_{10}\bar{\Omega}_1^2-\beta_1\varepsilon\bar{\omega}_1^2/2r_{10}\bar{\Omega}_1\right\}\sin\left(\lambda_{10}\right)- \\ & \left(\beta_1\varepsilon^2\bar{\omega}_1^2\mu_1/4r_{10}\bar{\Omega}_1^2\right)\cos\left(\lambda_{10}\right) \end{bmatrix}$$

The steady-state solutions will be stable if and only if the real parts of the eigenvalues are negative. The steady-state solutions stability for the second link can also be determined in a similar manner.

4.6.4 Internal resonance in the second link: $\left(\bar{\omega}_1\approx\bar{\Omega}_1\right)$ and $\left(\bar{\Omega}_1\approx\bar{\Omega}_2\right)$

Numerically, it was found that the normalized frequency of the first link $\left(\bar{\Omega}_1\right)$ is nearly equal to the normalized frequency of the second link $\left(\bar{\Omega}_2\right)$ leading to the existence of internal resonance. Here, the primary resonance occurs in first link $\left(\bar{\omega}_1\approx\bar{\Omega}_1\right)$ and the second link vibrates due to the internal resonance between the links $\left(\bar{\Omega}_1\approx\bar{\Omega}_2\right)$. The nearness of $\bar{\Omega}_1$ to $\bar{\Omega}_2$ is expressed as, $\bar{\Omega}_2+\varepsilon\sigma_3$ and σ_3 is the detuning parameter for internal resonance. The governing equation of motion for the first link remains the same as Eq. (4.126) and hence the equation for the vibrating amplitude and phase are given by Eq. (4.138). However, for the second link the reduced equations for vibration amplitude and phase after following the procedure explained earlier are expressed as:

$$\bar{\Omega}_2\left(\partial r_3/\partial\tau\right)+\bar{\Omega}_2\varepsilon\xi_2 r_3+\left\{\beta_3\varepsilon^2\bar{\omega}_1^2\left(\sigma_1+\sigma_3\right)/4\bar{\Omega}_2-\beta_3\varepsilon\bar{\omega}_1^2/2\right\}\sin\left(\lambda_3+\lambda_1\right)-\left(\beta_{12}\varepsilon^2\bar{\Omega}_1^2r_1/2\right)\sin\left(\lambda_3\right)$$
$$-\left(\beta_3\varepsilon^2\bar{\omega}_1^2\xi_2/4\bar{\Omega}_2\right)\cos\left(\lambda_3+\lambda_1\right)+\left(\beta_9\varepsilon^2\bar{\Omega}_1^2r_1^2/8\right)r_3\sin\left(2\lambda_3\right)+\left(\beta_7\varepsilon^2\bar{\Omega}_1\bar{\omega}_1r_1^2/8\right)\sin\left(\lambda_3-\lambda_1\right)=0$$

$$r_3\bar{\Omega}_2\left(\partial\lambda_1/\partial\tau+\partial\lambda_3/\partial\tau\right)-\varepsilon\left(\sigma_3+\sigma_1\right)r_3\bar{\Omega}_2+\left\{\beta_3\varepsilon^2\bar{\omega}_1^2\left(\sigma_1+\sigma_3\right)/4\bar{\Omega}_2-\beta_3\varepsilon\bar{\omega}_1^2/2\right\}\cos\left(\lambda_3+\lambda_1\right)$$
$$+\left(\beta_3\varepsilon^2\bar{\omega}_1^2\xi_2/4\bar{\Omega}_2\right)\sin\left(\lambda_3+\lambda_1\right)+\left(\beta_9\varepsilon^2\bar{\Omega}_1^2r_1^2/8\right)r_3\cos\left(2\lambda_3\right)+\left(\beta_7\varepsilon^2\bar{\Omega}_1\bar{\omega}_1r_1^2/8\right)\cos\left(\lambda_3-\lambda_1\right)$$
$$-\left(\beta_{12}\varepsilon^2\bar{\Omega}_1^2r_1/2\right)\cos\left(\lambda_3\right)-\left\{\varepsilon\xi_2^2/2+\varepsilon^2\beta_8\bar{\omega}_2^2/2+\beta_9\varepsilon^2\bar{\Omega}_1^2r_1^2/8\right\}r_3-\left(3/8\right)\beta_{13}\varepsilon^2r_3^3=0. \tag{4.141}$$

Here, $\lambda_1=\sigma_1T_1-\varphi_1$, $\lambda_3=\sigma_3T_1-\phi_3+\phi_1$, and second order solution for the second link motion is $q_3=\left(1/2\right)r_3\cos\left(\bar{\Omega}_1\tau-\lambda_3\right)+\varepsilon\left\{\beta_{11}\bar{\omega}_2^2/2\left(\bar{\Omega}_2^2-\bar{\omega}_2^2\right)\right\}\cos\left(\bar{\omega}_2\tau\right)+O\left(\varepsilon^2\right)$. The frequency response equation and the stability of the steady-state solutions can be determined by following the methodology as explained in earlier section.

4.6.5 Numerical Results and Discussion

a) *Modal analysis: eigenspectrums*

The eigenspectrums of a system are the essential parameters whose comprehension is crucial for its safe operation and acceptable performance as well. The system vibrates at inadmissible amplitudes leading to its failure or catastrophic injuries to the operator involved when the system is operated at a frequency equal or nearly equal to one of its natural frequencies. The variation of the eigenfrequencies with the system parameters provides a better understanding of the operational territory of the system in order to avoid such occurrences.

The variation of system parameters has been accomplished by altering the nondimensional parameters and thus apprehending its effect on the eigenspectrums of the two-link flexible manipulator with prismatic and revolute joints. The variation of payload mass $\left(\alpha_{m2}\right)$ corresponds to the different payload masses being lifted by the terminal end of the link, the influence of change in flexibility and masses of the links can be achieved respectively by varying the flexural rigidity $\left(\chi\right)$ of the system and the beam mass density ratio $\left(\alpha_M\right)$. A similar interpretation can be sought for the variation of other system parameters.

The variation of eigenfrequencies of flexible two-link manipulator with prismatic and revolute motion with actuator mass $\left(\alpha_{ma}\right)$ and actuator joint frequency parameter $\left(\Omega_a\right)$ is shown in Fig. 4.61. It is evident that the system eigenfrequencies decrease as the inertia is added to the system $\left(\omega_n\propto\sqrt{K/M}\right)$ by increasing the actuator mass. The actuator frequency parameter $\left(\Omega_a\right)$ represents the stiffness of the actuator if other parameters are kept constant. In the case of actuator frequency parameter, there is a gradual increase in lower eigenfrequencies but the higher eigenfrequencies increase with the actuator frequency $\left(\Omega_a\right)$ up to unit magnitude $\left(\Omega_a=1.0\right)$ and witness a sudden jump thereafter. Similar to section 4.5.6, it has also been observed that the system eigenfrequencies decrease with increasing mass of the payload lifted by the manipulator $\left(\alpha_{m2}\right)$, mass of the actuator $\left(\alpha_{ma}\right)$, mass of joint $\left(\alpha_{m1}\right)$ or beam mass density $\left(\alpha_M\right)$. Also, adding stiffness to the system either, by increasing the flexural rigidity ratio $\left(\chi\right)$ or by increasing the stiffness of the joint, resulted in increase in eigenfrequency of the system.

Also, the unit magnitude of the joint frequency $\left(\Omega_h\right)$ represents the condition when the natural frequency of the manipulator system becomes equal to the natural frequency of the torsional spring-inertia system depicting the flexible joint. At unit magnitude, Eq. becomes void and joint dynamics gets decoupled from the manipulator system limiting the joint to behave as a point mass. It has also been observed that the system eigenfrequency experience a sudden jump at unit magnitude $\left(\Omega_h=1.0\right)$ of the joint frequency parameter. Hence, beyond this value

the system starts oscillating at a higher mode of vibration. Similar to Fig. 4.28, it is also observed that a lower eigenfrequency generates around $\Omega_h = 1.5$, and due to which the system again tends to vibrate at lower eigenfrequency.

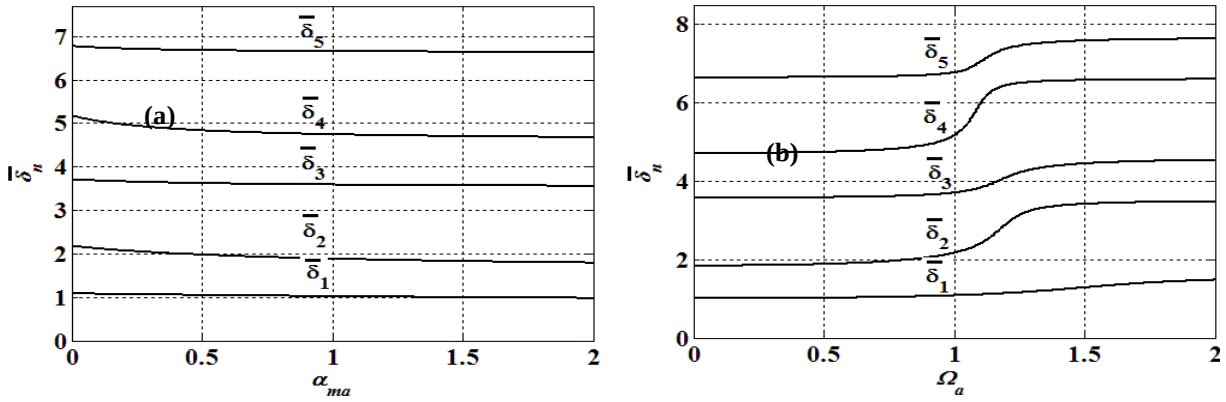

Fig. 4.61: Influence of (a) actuator mass (α_{ma}) and (b) frequency parameter (Ω_a) on eigenfrequencies of flexible two-link manipulator with prismatic and revolute joints for $\alpha_{m1,2}$ =1.0, α_{Ih} =1.0, Ω_a =0.5, and (α_M) =1.0.

In order to develop efficient control strategies and have a better understanding of nonlinear response of flexible robots, the development of accurate eigenspectrums is perquisite requirement. The effect of system parameters on the manipulator response is apprehended through the eigenfunction which has been used to discretize the infinite dynamic model of the manipulator governed by the partial differential equations. Therefore, a brief investigation to understand the influence of system parameters on the eigenfunctions of the two-link flexible manipulator has been presented.

The payload (α_{m2}) being lifted by the manipulator has a significant effect on the deflection of manipulator system which is visible in Fig. 4.62. In comparison to the no load condition, the deflection of the lower modes of vibration decreases as the mass of the payload (α_{m2}) at the terminal end of the manipulator is increased. However, the influence of payload (α_{m2}) is observed to be negligible on the higher modes of vibration and mode shapes tend to clutter along the length of the manipulator.

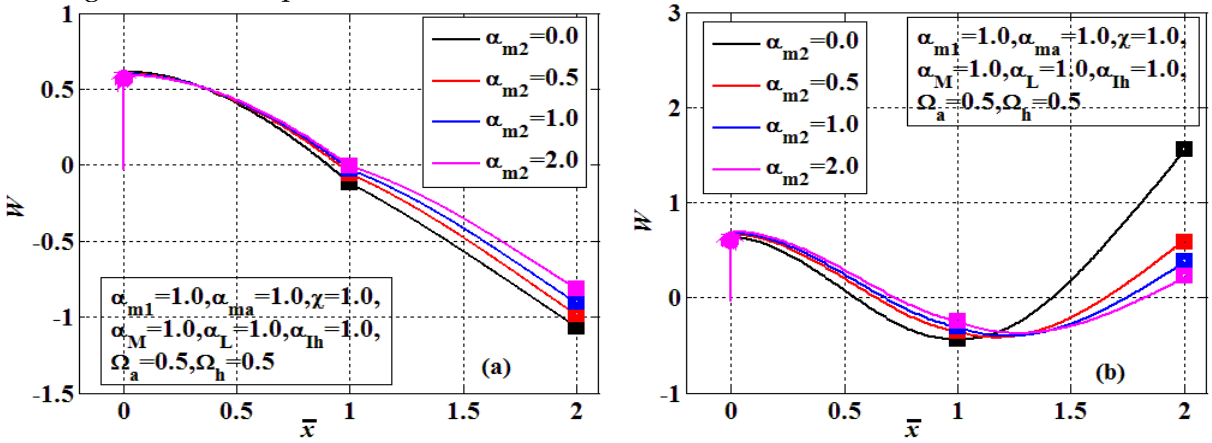

Fig. 4.62: Influence of payload mass parameter (α_{m2}) on mode shapes of flexible two-link manipulator with prismatic and revolute joints (a) mode 1 (b) mode 2.

The mass of the actuator (α_{ma}) majorly affects the deflection of the roller supported end of the manipulator which is evident from Fig. 4.63. The deflection of the roller supported end decreases with the increase in actuator mass (α_{ma}) with a negligible effect on the terminal end of the manipulator. The flexural rigidity ratio (χ) represents the flexibility of the links which

can be varied by manipulating the cross-sectional area of the links. The influence of flexural rigidity ratio (χ) is significant on the lower modes of vibration as shown in Fig. 4.64. The deflection of the manipulator decreases as the flexural rigidity ratio(χ) is increased and the mode shapes tend spread out along the length of the manipulator.

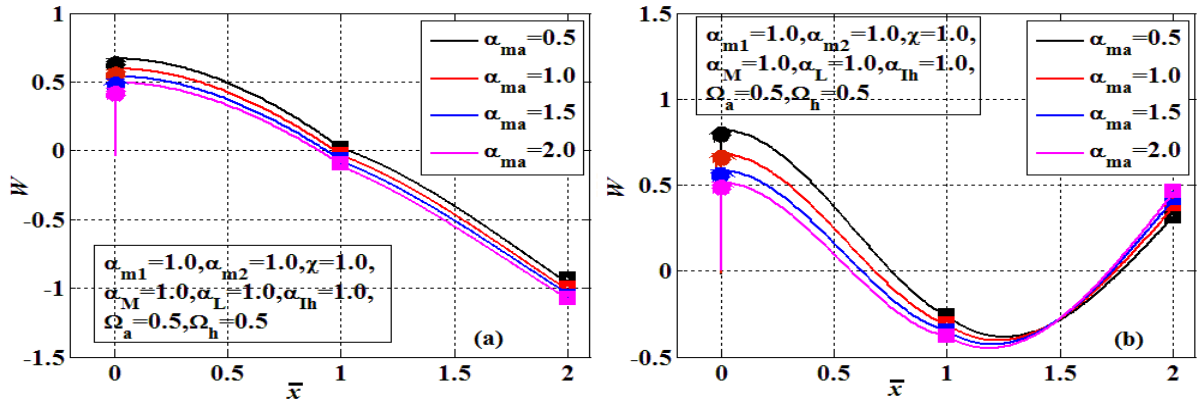

Fig. 4.63: Influence of actuator mass parameter (α_{ma}) on mode shapes of flexible two-link manipulator with prismatic and revolute joints (a) mode 1 (b) mode 2.

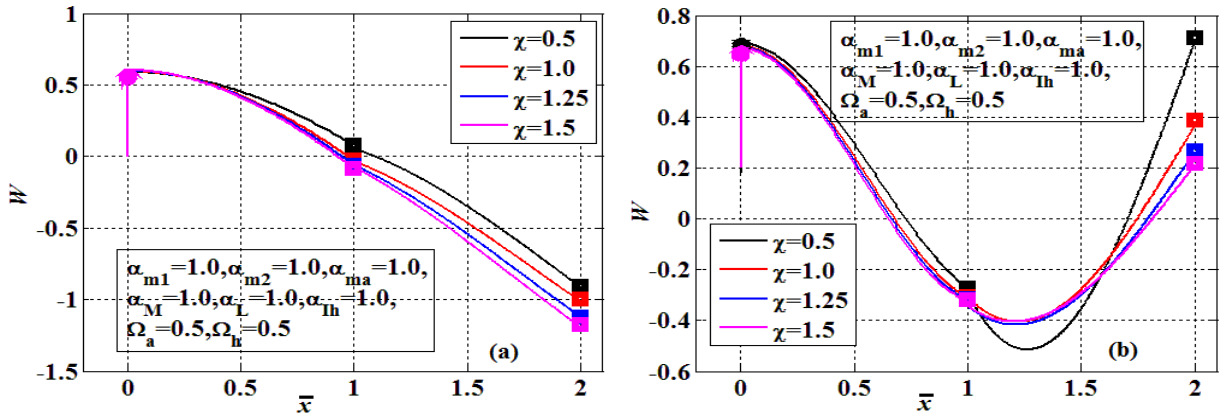

Fig. 4.64: Influence of flexural rigidity ratio (χ) on mode shapes of flexible two-link manipulator with prismatic and revolute joints (a) mode 1 (b) mode 2.

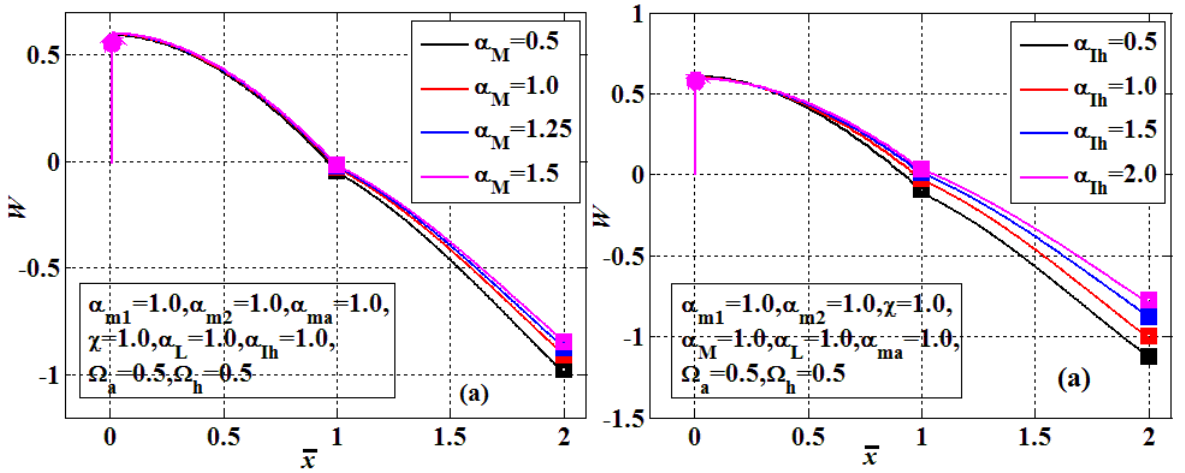

Fig. 4.65: Influence of (a) beam density parameter (α_M) and (b) joint inertia parameter (α_{Ih}) on mode shapes of flexible two-link manipulator with prismatic and revolute joints.

The influence of beam mass density(α_M) ratio and the joint inertia parameter (α_{Ih}) on the mode shapes of the flexible two-link manipulator is demonstrated in Fig. 4.65. The beam mass density ratio (α_M) of the manipulator can be manipulated by varying the thickness of the

links. The manipulator deflection decreases with increase in beam density ratio (α_M) as well as the joint inertia (α_{Ih}) and mode shapes for higher modes of vibrations are observed to clutter together.

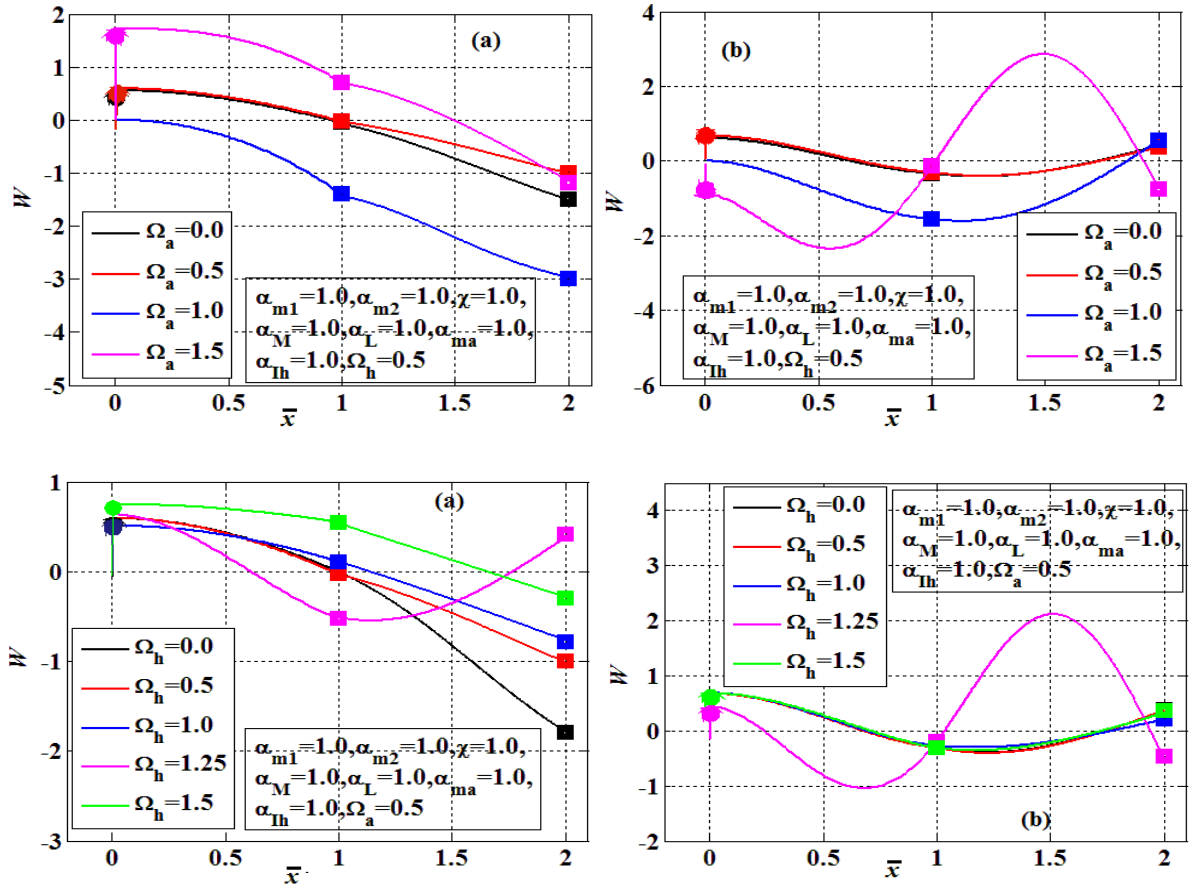

Fig. 4.66: Influence of joint frequency parameter (Ω_h) on mode shapes of flexible two-link manipulator with prismatic and revolute joints (a) mode 1 (b) mode 2.

The variation of mode shapes of the manipulator with the actuator frequency (Ω_{ma}) and joint frequency (Ω_h) parameter is shown in Fig. 4.66. The actuator stiffness has a significant influence on the roller supported end of the manipulator. For the second mode of vibration, the system starts vibrating at amplitude corresponding to the third natural frequency for $\Omega_a \geq 1.0$ which has also been shown in Fig. 4.61 where the system's eigenfrequencies experience the jump for higher modes of vibration. It is observed that the eigenfrequencies experience a sudden jump at unit magnitude of the joint frequency $(\Omega_h = 1)$ and hence the system vibrates at a higher mode of vibration. Also, as the joint frequency (Ω_h) is increased beyond 1.5, the system again tends to vibrate at a lower mode of vibration. A sudden jump in values of eigenfrequency is noticed for $1.0 < \Omega_h < 1.5$. The amplitude of the manipulator at roller supported end as well as the terminal ends are significantly affected by the change in actuator and joint frequency parameters $(\Omega_{a,h})$. The presented results furnish vital information regarding eigen-parameters of two-link flexible manipulator with prismatic and revolute joint which shall enable the identification of resonance conditions when operating frequency becomes equal or nearly equal to the system natural frequency and hence, facilitate the proper attenuation of system to avoid the inadmissible vibrations.

b) *Nonlinear analysis: bifurcation and stability*

In the literature, the nonlinear behavior of prismatic single-link manipulator has been extensively studied and the research has been confined to the development of control strategies of two-link manipulator having prismatic joints and rigid links. When the manipulator is subjected to a prismatic motion, the system experiences a forced vibration and undergoes relatively large vibrations causing undesirable vibrations due to its low stiffness which is a major concern. The adequate familiarity with the manipulator behavior under parametric variation of system attributes enables the operator to avoid catastrophic failure under such circumstances. In the present analysis, the geometrical and physical characteristics are the same as considered in section 4.6.5 and the other parameters are stated in the figures itself. For primary resonance condition in both the links, the internal resonance has been avoided by considering the length ratio (α_L) of 1.1. While for internal resonance in the second link, the links are assumed to be of the same length, i.e., α_L =1.0. The amplitude ratio for Cartesian motion $(\bar{\vartheta}_0)$ and revolute joint motion $\bar{\theta}_0$ are chosen as 0.0005 while the nondimensional damping coefficients $(\xi_{1,2})$ are taken as 0.01. In all numerical simulations, book-keeping parameter (ε) and scaling factor (r) are selected as 0.1 and 0.005, respectively.

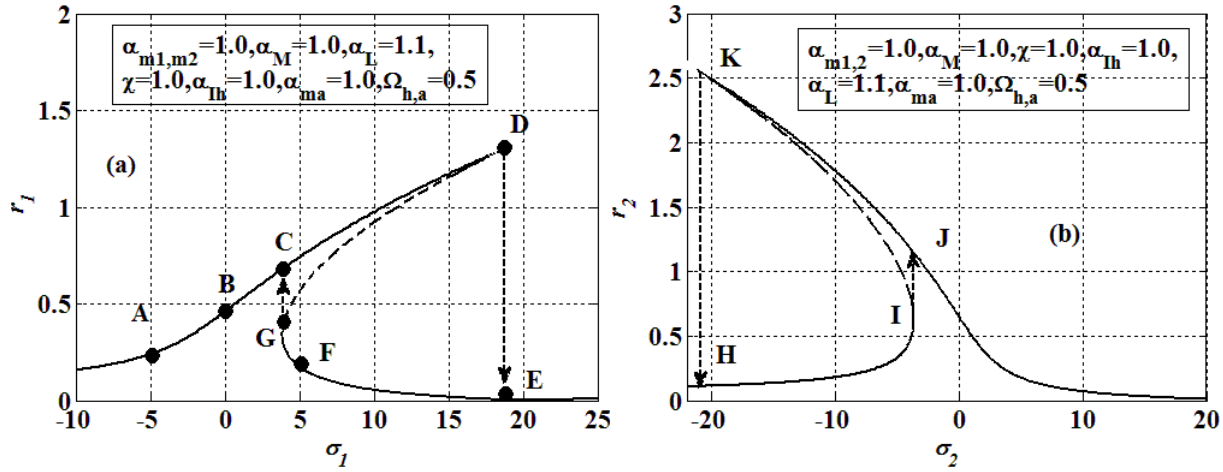

Fig. 4.67: Frequency response curve of the (a) first and (b) second link of flexible two-link manipulator with prismatic and revolute joint for primary resonance case.

The frequency response curves representing the amplitude $(r_{1,2})$ of manipulator with respect to the respective motor speeds $(\sigma_{1,2})$ obtained for the steady-state conditions of Eqs. **Error! Reference source not found.-Error! Reference source not found.** for primary resonance cases in both the links are shown in Figs. 4.67-4.75. While the solid lines represent the stable solutions, the dashed lines depict the unstable solutions in all figures. The representative frequency response curves of the first and second link for the primary resonance due to the harmonic motion imparted to the actuator and revolute joints are shown in Fig. 4.67. The presence of geometric nonlinearities induces the multivalued solutions and jump phenomenon in the frequency response curves of both links. It is observed that while the first link exhibits the spring hardening behavior with the bending of curve towards right, the second link illustrates spring softening behavior with bending towards the left. In case of first link the jump down phenomenon is observed at point D while increasing the motor speed and a sudden increase in amplitude of vibration is witnessed at point G as the motor speed is decreased. The numerical and the corresponding analytical time response, phase portrait and FFTs have been presented in Fig. 4.68 and results are found to be in good agreement.

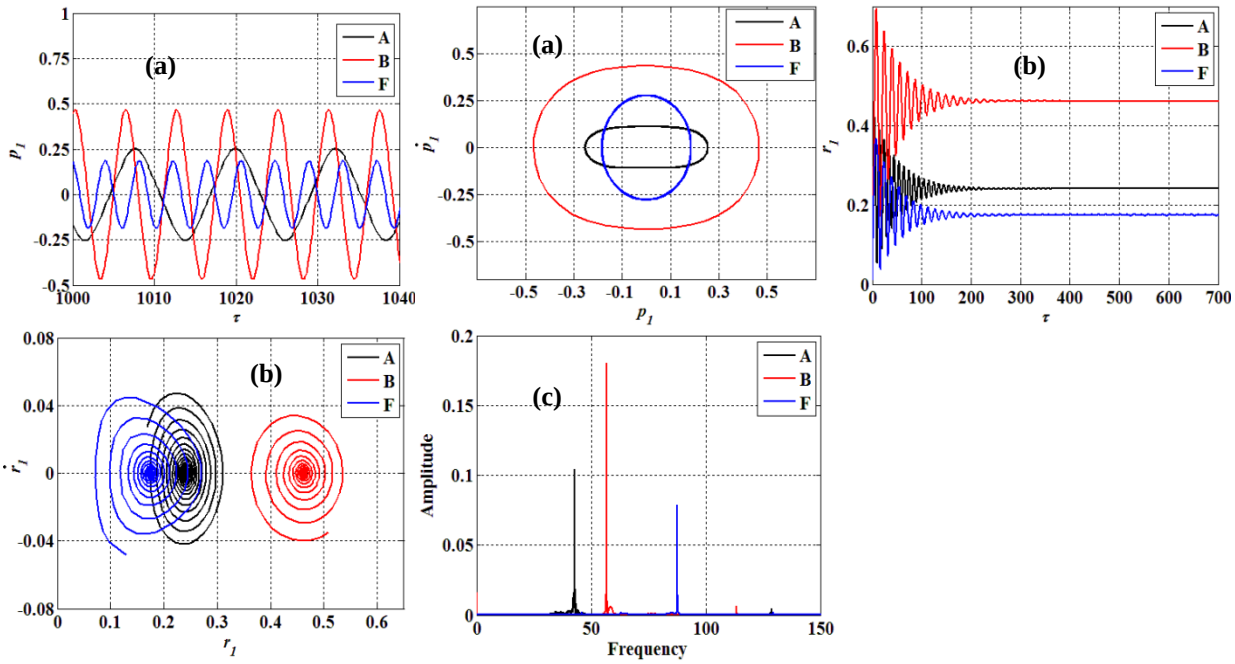

Fig. 4.68: (a) Numerical and (b) analytical time history, phase portrait, and (c) FFT at critical points A, B, and F identified in Fig. 4.67.

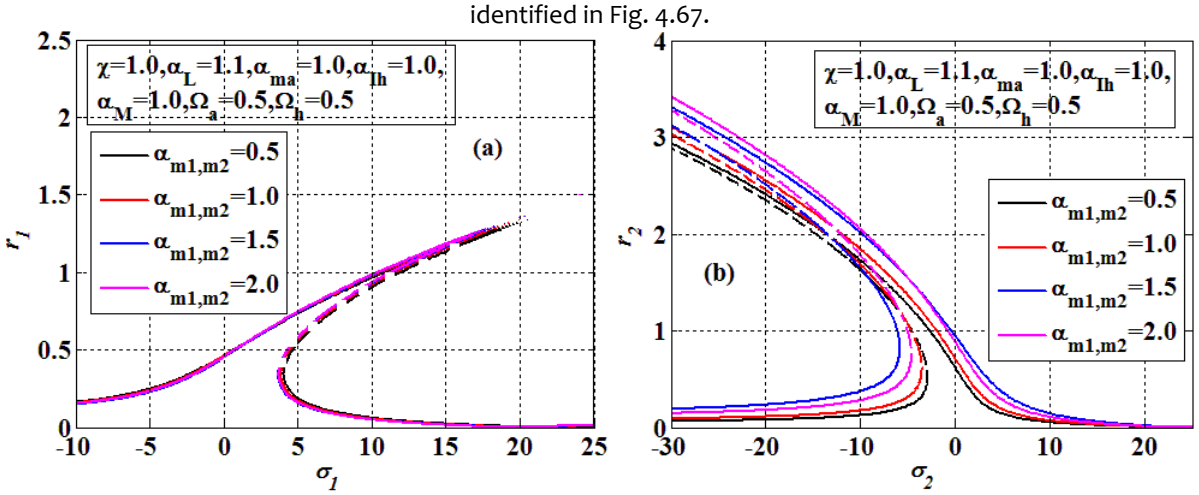

Fig. 4.69: Variation of frequency response curve of (a) first and (b) second link with of mass parameters $(\alpha_{m1,2})$

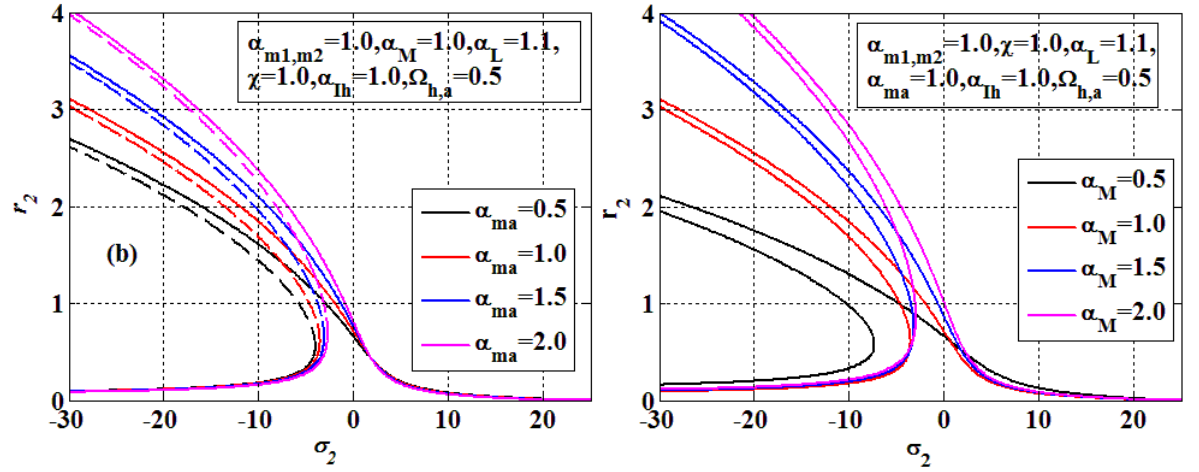

Fig. 4.70: Variation of frequency response curve of second link with (a) actuator mass parameter (α_{ma}) and (b) beam mass density ratio (α_M).

The variation in the configuration of manipulator can be accomplished by altering the system attributes such as payload mass parameter (α_{m2}) representing payload lifted by manip-

ulator, flexural rigidity ratio (χ) and beam mass density ratio (α_M) by manipulating the cross sectional area, joint inertia (α_{Ih}) and their stiffness $(k_{h,\theta})$ etc. It is observed that the payload mass (α_{m2}), actuator mass (α_{ma}), and beam density ratio (α_M) have a negligible effect on the amplitude of the first link for primary resonance case. While the maximum amplitude of second link increases with increase in payload mass parameter (α_{m2}), actuator mass (α_{ma}), and beam mass density ratio (α_M) which is evident from Fig. 4.69-Fig. 4.70.

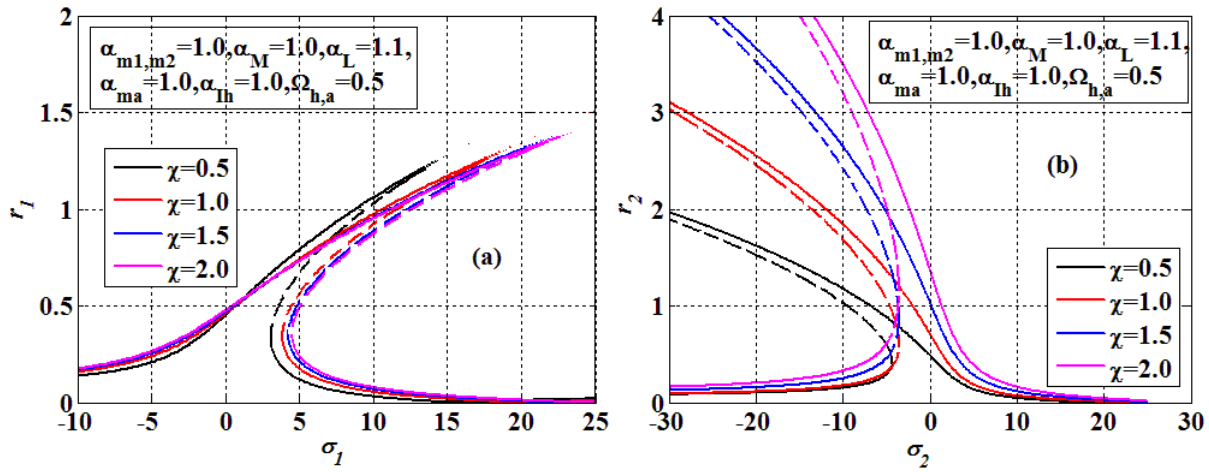

Fig. 4.71: Variation of frequency response curve of (a) first and (b) second link with flexural rigidity ratio (χ).

The influence of flexural rigidity ratio on the frequency response curves is shown in Fig. 4.71 and it is seen that as the flexibility ratio (χ) increases the amplitude of the first link decreases for $0.5 \le \chi \le 1.5$ and with a further increase in flexural rigidity ratio (χ) the amplitude experiences a marginal change. However, the jump length of the second link witnesses a significant increase with the increase in flexural rigidity ratio (χ).

It is evident from Fig. 4.72 that the amplitude at a particular frequency for the first link increases marginally with increase in joint inertia (α_{Ih}). It is also noticed that the jump length and the unstable region of frequency response curve of the second link decreases significantly with increase in joint inertia (α_{Ih}). The results presented here are in contrast with those of section 4.5.6, where the first link experiences an alteration in vibration behavior from spring hardening to spring softening or vice-verse for payload mass, beam density ratio and joint inertia. Thus, it can be concluded that the nonlinear system behavior is a critical function of the joint dynamics.

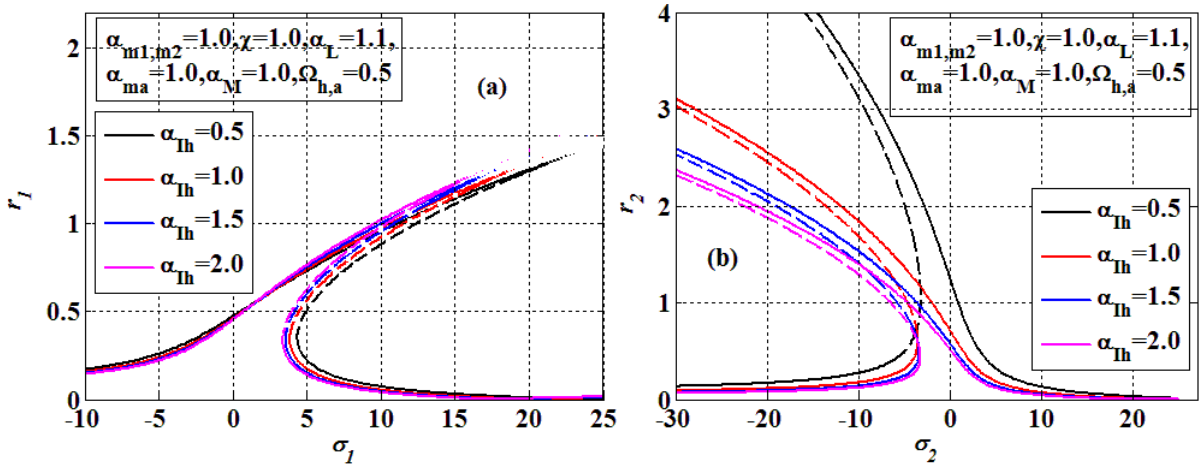

Fig. 4.72: Variation of frequency response curve of (a) first and (b) second link joint inertia parameter (α_{Ih}).

The actuator frequency parameter (Ω_a) and joint frequency parameter (Ω_h) respectively represents the actuator spring stiffness (k_a) and joint torsional spring stiffness (k_θ) if other parameters are kept constant. It is observed in Fig. 4.73 that the variation of the actuator frequency parameter (Ω_a) witness a transformation of behavior of first link from spring hardening to spring softening and a sudden increase in amplitude of second link at the unit magnitude of (Ω_a). However, with further increase in actuator frequency parameter (Ω_a), the jump length of the nonlinear response for both the links decreases. In case of joint frequency parameter (Ω_h), the second link alternates its behavior from spring softening to spring hardening and first link experiences a sudden increase in amplitude at unit magnitude of (Ω_h).The behavior alteration of system with joint stiffness may result in sudden change in jump length during starting or stopping of prime mover. Thus, trend of spring hardening or softening in the frequency response can be maintained by the appropriate selection of the joint stiffness.

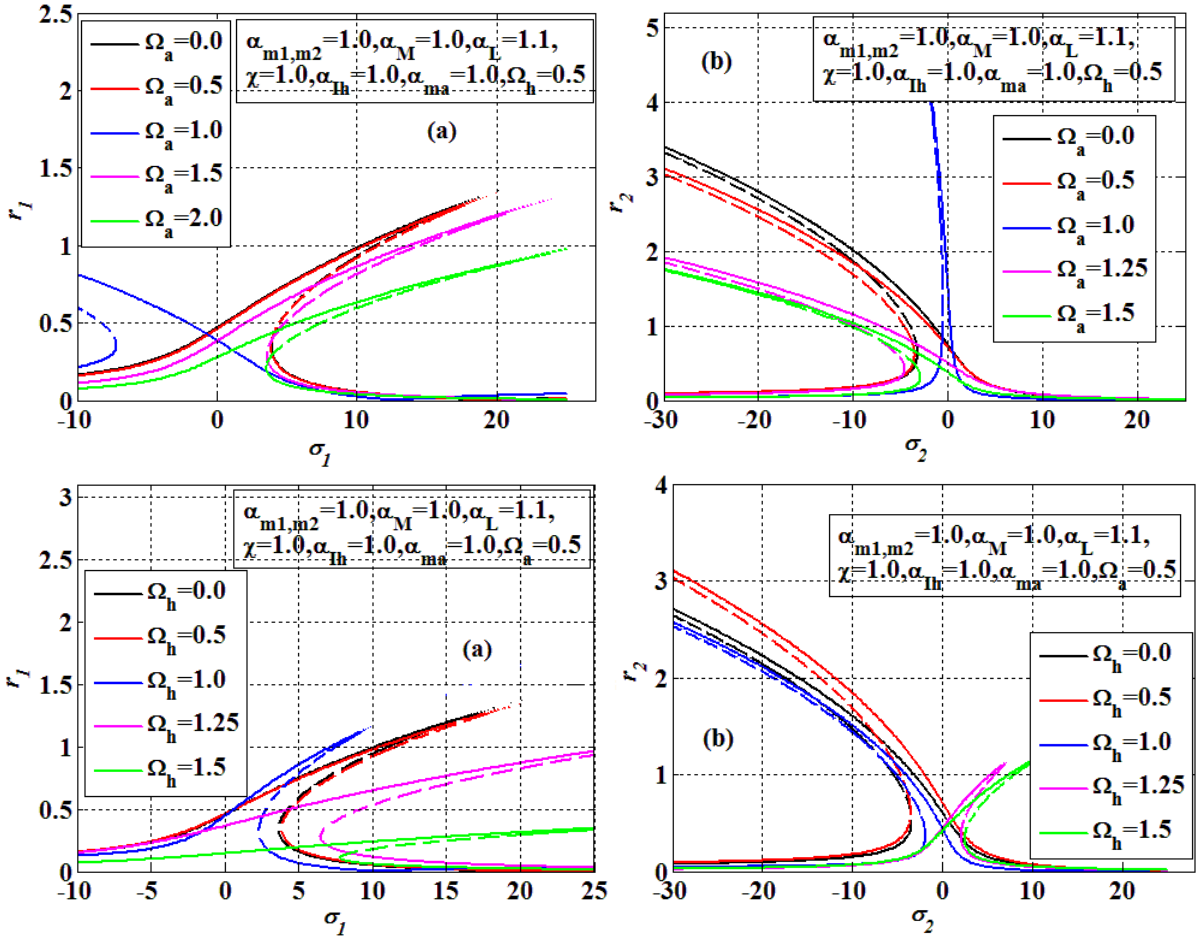

Fig. 4.73: Variation of frequency response curve of (a) first and (b) second link with actuator frequency parameter (Ω_a) and joint frequency parameter (Ω_h).

The influence of critical system parameters on the manipulator link responses has been shown in Fig. 4.74-Fig. 4.75 for the existence of internal resonance in the second link of the manipulator. In the present case, the amplitude generated in first link due to the primary resonance excites the second link. In Fig. 4.74, a comparison has been made between the response of second link for simple resonance and internal resonance case. It is observed that the amplitude of the second link for internal resonance at a particular detuning parameter (σ_3) is significantly larger as compared to the primary resonance case. Also, the amplitude of second link (r_3), and hence the jump length experienced by the second link, considerably increase with the increase

in excitation amplitude of first link (r_1). As the links of the manipulator are dynamically coupled leading to internal resonance, the system may experience large vibrations even without the presence of external excitations. Again, the amplitude of the second link increases and decreases respectively with increase in payload mass parameter (α_{m2}) and joint inertia (α_{Ih}) parameter as illustrated in Fig. 4.75.

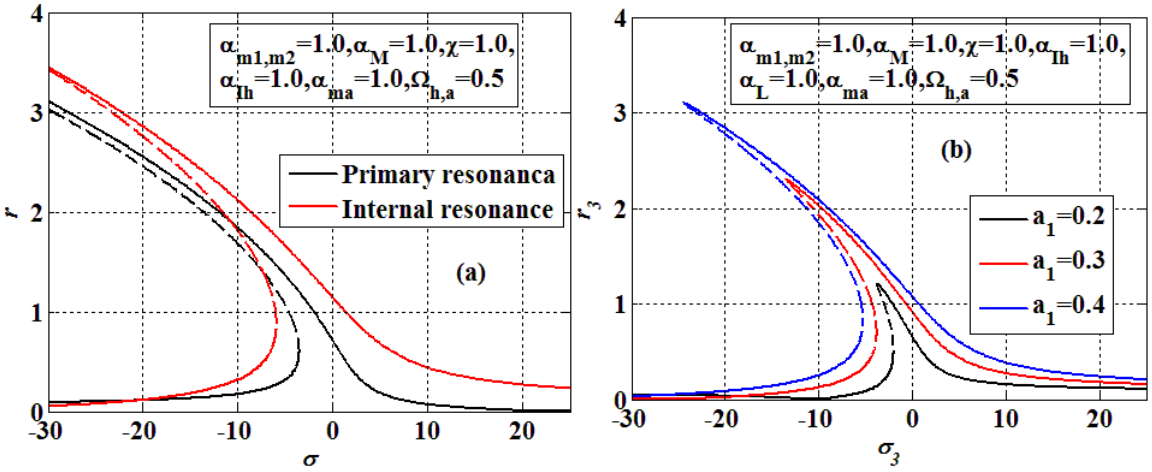

Fig. 4.74: Comparison of frequency response curve of second link for (a) primary and internal resonance and (b) effect of amplitude of first link (a_1).

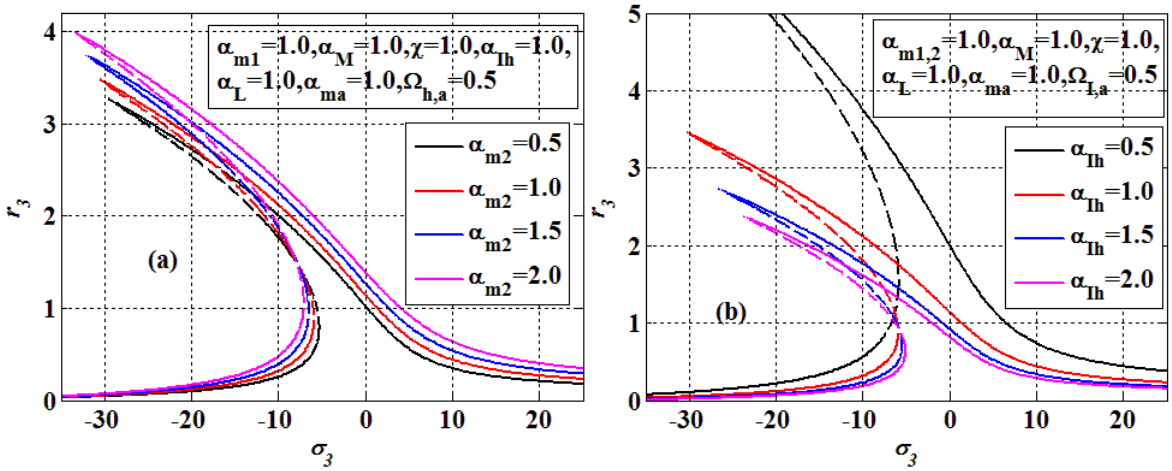

Fig. 4.75: Variation of frequency response curve of second link with (a) payload mass parameter (α_{m2}) and (b) joint inertia parameter (α_{Ih}) for internal resonance case.

The present analysis can be satisfactorily applied to long reach robot manipulators involved in pick and drop operations. The derived eigenspectrums can be adopted in developing control schemes for end point vibration suppressions and nonlinear analysis of manipulators undergoing large deformations. Nowadays, manipulators are being used in different adverse conditions where the end-effector is subjected to various forcing conditions with different joint conditions and also, end-effector move along the link to perform various operations. The presented linear and nonlinear approach can be employed for the analysis of such manipulators dynamics.

4.7 SUMMARY

The present work introduces a theoretical analysis to understand the modal parameters of a two-link flexible manipulator with prismatic and revolute joint incorporating a generic payload. Due to the extensive utilization of long reach manipulator in industries under different working environments, it becomes essential to study the modal-parameter and their variations

with system attributes of such manipulators to gain an insight on their behavior in resonance conditions. Further, the nonlinear flexural vibrations when the flexible robotic system is subjected to a harmonic motion at the flexible joints and pulsating axial constraint force have been studied. In an attempt to understand the influence of the system attributes on the dynamic characteristics of subject manipulator the forward and inverse dynamics of the manipulator is studied. A summary of the precise and distinct outcomes obtained as follows.

The quantitative decrease in eigenfrequencies with increase in payload mass, payload inertia, actuator mass, actuator inertia, joint inertias and increasing the beam mass density of second link with respect to first link, has been graphically reported and tabulated. However, an increase in flexibility of second link with respect to the first link and stiffness of joint and actuator has witnessed an increase in eigenfrequencies. The payload parameters especially payload inertia and offset length have distinctive affect on the fundamental eigenfrequencies. The payload mass, payload inertia, joint inertia and beam mass density ratio have a significant influence on the lower modes of vibration and mode shapes tend to spread out along the length of the manipulator. The amplitude of roller supported and terminal ends decreases respectively with the increase of actuator and payload masses. The system started functioning at higher modes of vibration for the frequency parameters greater than unity. When the natural frequency of joint is equal to the system frequency, the joint motions get decoupled from the transverse motion of the manipulator and joints started acting like point masses.

The joint dynamics has a significant influence on the existence of the internal resonance in the links of the two-link flexible manipulator. 3:1 internal resonance has been found for point payload condition when the manipulator joints are considered as point masses and as soon as the joint dynamics is considered in the analysis, the links are found to be 1:1 internally resonated. The nonlinearity coefficients associated with second link tend to decrease the peak amplitude of steady-state response of the system. A large reduction in peak amplitude of second link vibration has been noticed with the slight increase in damping parameter. It is noticed that the amplitude of the links at a particular frequency for subharmonic resonance case increases with the payload mass and offset and the unstable region increases with the payload parameters. The variation of payload mass, joint inertia and beam mass density parameter have noticed a fluctuation of system behavior from spring softening to spring hardening or vice-versa only in the first link for manipulator with revolute joints. A negligible influence of the payload mass, actuator mass and beam density is noticed on the frequency response of roller supported link. However, both links have observed this phenomenon of behavior alteration when the natural frequency of the second joint increases beyond the system natural frequency.

The angular tip position of both the links decreases with increase in payload mass, length of second link, and joint inertias. The response of the first link remains unaltered with the payload parameters such as payload inertia and payload offset length. Large residual vibrations are noticed for the increase in joint inertia even after the completion of duty cycle of input torque and power consumption by the joints significantly reduce as the material of the links is changed from steel to aluminum. In case of inverse dynamics, while reaching the desired angular position, the increase in mass of payload, mass of joints, inertia of the joints and link length increases the required torque input significantly The increase in link length and the joint inertia witness an adverse effect on the end point vibrations and the tip of the link vibrates at large amplitudes during the operation. The present framework enables an efficient theoretical model of two-link manipulator with prismatic and revolute joints and shall contribute in better understanding of its vibration attenuation and development of the effective control techniques for suppression of residual oscillations.